Modelling and Simulation of a Hip Abduction–Adduction Assistive Exoskeleton to Improve Elderly Stability

Thomas Burton

A thesis submitted to the University of Ottawa
in partial fulfilment of the requirements for the degree of
Master of Applied Science in Biomedical Engineering

Ottawa–Carleton Institute for Biomedical Engineering
Department of Mechanical Engineering
Faculty of Engineering
University of Ottawa

ABSTRACT

Walking Assist Exoskeletons are wearable devices that can allow individuals with mobility impairments to maintain their autonomy. The growing elderly population has benefited from these devices by receiving assistance at joints where their muscle function has declined. Typically, the primary objective of these exoskeletons has been to reduce the metabolic cost of walking, allowing users to walk for extended periods of time while reducing fatigue. However, this strategy does not directly address the growing concern that seniors are at an increased risk of falling and sustaining severe injuries due to falls. Gait and balance disorders are among the most common causes of falls in the elderly. As the Canadian population ages, it is increasingly important to investigate the musculoskeletal changes contributing to frontal-plane instability, as mediolateral and posterolateral falls are correlated with higher incidences of severe injuries. Specifically, the hip abductor and hip adductor muscles are essential in maintaining balance in the frontal plane, yet little research has been conducted on the effect of hip abduction–adduction exoskeleton assistance on the stability of elderly individuals.

This thesis investigates the effect of introducing an assistive torque with a specific magnitude, timing, and location (i.e. applied to one or both legs) on the margin of stability of elderly individuals using the OpenSim biomechanics software. Simulations of four elderly subjects were conducted while the subjects stood in a quiet standing position with both feet on the ground. A lateral perturbation force of magnitude 5%, 10% or 15% of bodyweight was applied to the pelvis of each subject. The simulations were designed to provide elderly subjects with contralateral (i.e. the limb on the opposite side of the body as the perturbation), ipsilateral (i.e. the limb on the same side as the perturbation), or bilateral hip abduction–adduction assistive torque from a hip

exoskeleton device after a perturbation force was applied to the pelvis. The simulated actuators mounted at the hip joints were massless, applied torque in the frontal plane, and could generate torque instantaneously based on user-defined inputs. The change in margin of stability was used to measure the effectiveness of each assistive strategy and for comparison across all subjects.

The results of this study suggest that, as the perturbation magnitude increases, the hip abduction–adduction assistive exoskeleton should prioritize assistance applied to the contralateral limb. Regardless of the perturbation magnitude, each assistive strategy that was simulated (i.e. contralateral, ipsilateral and bilateral assistance) was able to improve the margin of stability. The greatest mean improvement on the margin of stability compared to the unassisted condition occurred when using the contralateral assistance strategy. For the 5%, 10% and 15% bodyweight perturbations, a contralateral assistance of 0.75 N·m/kg (torque normalized by the subject's mass) resulted in an improvement in the margin of stability of 13.1 ± 0.987 mm, 13.0 ± 0.946 mm and 13.1 ± 0.816 mm, respectively. The simulations also suggested that similar improvements on the margin of stability were experienced at smaller assistive torque magnitudes when the actuators provided torque to the body quicker following a perturbation. The results of this study can be used by exoskeleton designers to guide their decisions when developing abduction–adduction assistive exoskeletons that target mediolateral stability assistance in the elderly population.

ACKNOWLEDGEMENTS

I would like to acknowledge many for their support in this journey to complete my graduate studies. It would not have been possible without their endless amounts of support and understanding. First, Dr. Marc Doumit and Dr. Thomas Uchida for their guidance and encouragement throughout the entire process. For sharing their time and knowledge to develop this project and continue to push me every day. Without their positive encouragement and time invested in me throughout the process it would not have been possible. I am grateful for the opportunity that I have had to work and learn from both of my supervisors and cannot express how much it has impacted my motivation and experience throughout this research.

Second, to the University of Ottawa, the Faculty of Mechanical and Biomedical Engineering for their contributions to my academic career. My undergraduate and graduate studies experiences have been amazing. A special thank you to my fellow graduate students and research group for their support and assistance throughout our graduate studies.

Third, to Dan Blocka and the team at Boundless Biomechanical Bracing. Their investments have made it possible for me to complete my graduate studies, along with the team's vast knowledge of biomechanics and assistive technologies.

Finally, to my parents John and Mary Clare, my sister Samantha, and my girlfriend Courtney, for their continuous encouragement, patience and understanding. This has been a team effort all around and the strength that they have given me to push towards this goal cannot be described. You have always inspired me to explore higher education and have been my motivation throughout the entirety of this degree.

This chapter of my life has been exciting, stressful, thrilling, exhausting and everything in between. Thank you for continued support from my family, friends, and that everyone close to me has provided over the past few years. It has allowed me to continue working towards accomplishing this goal.

Table of Contents

List of Tables

List of Figures

Nomenclature

Acronym	Description
AP	Anterior–posterior
BMI	Body mass index
BoS	Base of support
CMC	Computed muscle control
CNS	Central nervous system
CoM	Center of mass
CoP	Center of pressure
EMG	Electromyography
FWD	Forward dynamics
GRF	Ground reaction force
HAA	Hip abduction–adduction
HFE	Hip flexion–extension
IK	Inverse kinematics
ML	Mediolateral
MoS	Margin of stability
MOT	Motion file
OA	Osteoarthritis
ROM	Range of motion
RRA	Residual reduction algorithm
SEA	Series-elastic actuator
STL	Stereolithography
TRC	Track row column file
Txt	Text file
$vCoM$	Velocity of the center of mass
WAE	Walking assist exoskeleton
XcoM	Extrapolated center of mass

Chapter 1: Introduction

In this chapter, the prevalence of balance disorders in the elderly will be reviewed. The current state of the art in Walking Assist Exoskeletons (WAEs) and the lack of devices that address a loss of balance in the elderly will be highlighted. The thesis objectives, contributions to research and organization will also be discussed.

1.1 Background

In July 2021, Statistics Canada reported that there were approximately 7.1 million individuals living in Canada over the age of 65, forming 18% of the population, and that this proportion is expected to reach 30% by 2068 [1]. The prevalence of gait and balance disorders increases from 10% in individuals between the ages of 60 and 69 to more than 90% in individuals over 80 years of age [2]. As a result, falling becomes more common and is estimated to affect 28% of adults over the age of 65 annually [3], [4]. Falls can be detrimental to the elderly population and lead to chronic disability, reduced independence, and ultimately a reduced quality of life [2], [5]. Traumatic brain injuries and bone fractures of the wrist, arm, ankle and hip are the most common injuries [6]. Moreover, falls in the mediolateral (ML) and posterolateral directions are particularly dangerous, contributing to approximately 95% of hip fractures due to falling [4], [6]–[9]. Even in the absence of severe injury, the fear of falling alone can limit the activities people are willing to participate in, leading to negative impacts on physical and mental health while increasing the risk of future falls [10].

As a person ages, many factors can reduce their ability to maintain balance, such as visual impairments, unstable joints, muscle weakness, loss of sensory function and unreliable postural reflexes. Gait disorders such as Trendelenburg Gait can increase postural sway velocities that

contribute to fall risk. Degenerative joint diseases such as knee osteoarthritis (OA) can cause pain, leading to the improper weight transfer of the body and a less stable gait pattern. Each of these conditions has been linked to weakened hip abductor and hip adductor muscles, as they play a vital role in proper foot placement to maintain balance while controlling the ML loading patterns of the lower limbs. Individuals with reduced hip abductor muscle strength are at an increased risk of falling as they cannot use their typical stabilization strategies as effectively [11], [12].

Assistive devices such as wheelchairs, canes, walkers, and crutches have been commonly used to counteract gait impairments and muscular degradation associated with ageing. While effective in some respects, these devices also have their limitations. In each case, the user's walking ability and autonomy can be compromised, or the assistive devices may heavily rely on upper body strength. As an alternative to these technologies, WAEs have offered a potential solution for enhancing the mobility of elderly individuals, returning gait function, reducing the metabolic cost of walking and providing stabilization forces to the body.

WAEs are wearable devices designed to improve, restore, or augment a person's mobility. In recent years, exoskeleton technology has been applied to gait rehabilitation training following a stroke, walking assistance for individuals with spinal cord injuries, children with cerebral palsy and performance augmentation in the military [12]–[15]. WAEs are designed to provide external forces to the body using batteries, actuators and sensors ("active" devices) or through springs and clutches to store and release elastic energy to the body ("passive" devices).

As walking is primarily a sagittal-plane motion, WAEs have traditionally targeted flexion–extension assistance at the hip, knee and ankle joints to reduce the metabolic cost of locomotion. For these exoskeletons, lateral stability generally relies on the user's existing muscle function or

external devices like crutches. For elderly individuals, this design approach is insufficient. A literature search revealed a lack of WAEs designed for ML stability assistance in the elderly population.

1.2 Objective

The purpose of this thesis is to investigate the effects of hip abduction–adduction (HAA) exoskeleton assistance strategies on the ML stability of elderly individuals. Computational simulations performed in OpenSim allow for the analysis of margin of stability (MoS) in elderly individuals with and without an assistive torque applied by a hip exoskeleton following a perturbation force. Short-duration forward dynamics simulations are conducted to provide insight into how the MoS of elderly individuals is affected by exoskeleton assistance in terms of key design parameters represented by actuator timing, magnitude and location. These results can be used by exoskeleton designers when developing assistance strategies, hardware components and control strategies for exoskeletons targeting stability assistance in elderly individuals.

1.3 Contributions

The contributions of this thesis are as follows:

1. A thorough literature review was conducted to highlight differences in the biomechanics of gait between young adults and elderly individuals, specifically the differences that lead to reduced stabilizing capabilities and an increased risk of falling. The literature review was also used to identify the current state of the art in walking assistive hip exoskeleton technology for the elderly.

2. A detailed methodology was developed and implemented through the OpenSim biomechanics software to evaluate the MoS of elderly individuals after being subjected to a perturbation force applied at the pelvis. This methodology was used to investigate HAA assistive exoskeleton devices and their predicted effects on MoS.
3. The effect of adding assistive actuators in the frontal plane on the contralateral (the opposite side of the body as the perturbation), ipsilateral (same side of the body as the perturbation), and bilateral hip joints was examined. The MoS was analyzed while the subject was unassisted and assisted by several magnitudes of assistive torques.
4. The effect of actuator timing was investigated by changing the control input of the actuators to be 5%, 10% and 15% faster than the nominal activation time. The MoS was analyzed for each actuator timing during each perturbation condition.

1.4 Thesis Outline

This thesis contains five chapters. In Chapter 1, the motivation for improving elderly stability and mitigating fall risk has been outlined. The subsequent goals and research objectives have also been discussed. In Chapter 2, the relevant biomechanics of gait, anatomy and coordination of stabilization strategies will be investigated. Changes to the balance control system that are observed with increasing age and reasons why elderly individuals experience an increased risk of falling will be explained. A model of MoS will also be outlined. MoS is the primary outcome measure used throughout the thesis to determine the effectiveness of each assistance strategy under various simulated conditions. Chapter 3 explains the methodology implemented to explore changes in elderly stability with and without assistance from a HAA assistive exoskeleton. This chapter will describe the musculoskeletal models, motion data, subjects, actuator characterization

and tools used in OpenSim to produce the results in support of the research objectives. Chapter 4 presents and discusses the results obtained from the unassisted simulations and the contralateral, ipsilateral and bilateral assistive conditions. It will also present and discuss the results from simulations with contralateral assistance when actuator time delay is decreased. Chapter 5 concludes the thesis by outlining the contributions, limitations of the study and the recommended directions for future work.

Chapter 2: Literature Review

2.1 Biomechanics of Gait

A gait cycle is composed of cyclical movements of the upper and lower extremities to propel the center of mass (CoM) forward and to maintain balance in both the anteroposterior (AP) and ML directions. Throughout gait, a precise sequence of muscle activations is regulated by the central nervous system (CNS) to generate motion. A healthy gait cycle requires proper coordination of neural networks, application of muscle force and processing of sensory information [16], [17]. Gait analysis is the study of locomotion and provides insight into the coordination of muscles, how to improve physical performance, the diagnosis of movement disorders or injuries, and the evaluation of rehabilitation programs [18]. Cadence, step width, step length and walking speed are commonly used to quantify gait abnormalities and deficiencies [18].

A walking gait cycle is defined as the period between two consecutive foot contact events on the same leg, with foot contact of the opposite limb occurring approximately halfway through the gait cycle. The gait cycle can be divided into two phases: stance and swing. These phases comprise approximately 60% and 40% of the gait cycle, respectively. The stance phase can be further divided into three sub-phases: double support, single support, and a second double support phase, making up approximately 10%, 40% and 10% of the gait cycle, respectively, as shown in Figure 2-1. During the swing phase, the foot is in the air while the contralateral limb supports the individual’s bodyweight (BW).

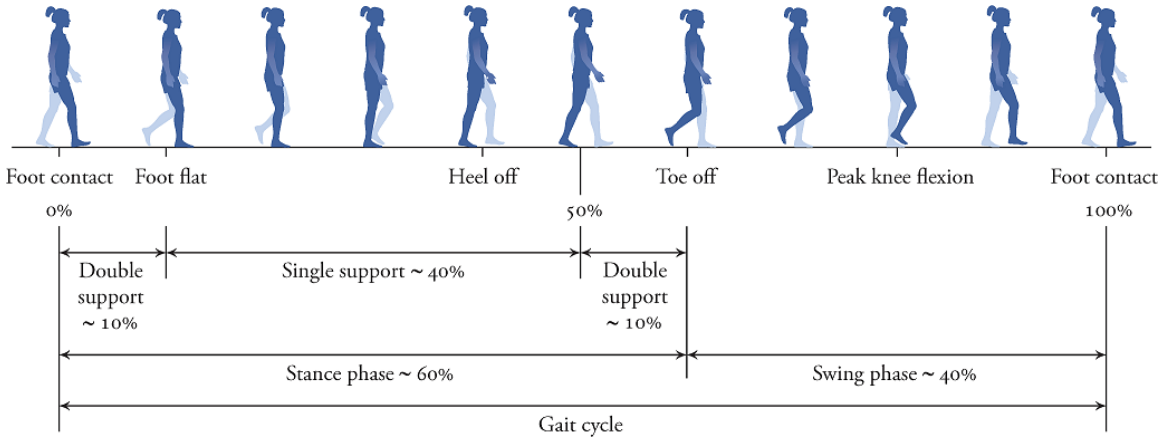

Figure 2-1. The walking gait cycle and its related events and phases. Image © 2020 David Delp, from Biomechanics of Movement: The Science of Sports, Robotics, and Rehabilitation by Thomas K. Uchida and Scott L. Delp (Cambridge, MA: The MIT Press, 2020). All rights reserved [19].

2.2 Anatomy and Physiology

To initiate voluntary movement, an excitation signal is sent from the CNS to the motor neurons that innervate the muscles. The motor neuron joins to each muscle fiber at a synapse known as the neuromuscular junction [19]. A muscle fiber contains several specialized structures to receive excitatory signals from the CNS and propagate them to the rest of the muscle cell [19]. The amount of force generated to accomplish a particular task is regulated by the CNS through modulation of the frequency of electrical stimulation delivered to the motor neurons, and the number of motor units (motor neurons and muscle fibers) that are activated. These modulation strategies are referred to as rate encoding and motor unit recruitment, respectively [19], [20]. Motor units are typically recruited according to “Henneman’s size principle” to prevent muscle fatigue [21], [22]. During gait, it has been widely accepted in biomechanics research that the CNS generates muscle forces to produce forward progression in a metabolically inexpensive way [19], [21], [23]. However, coordination of balance, specifically in the frontal plane, is associated with an increase in metabolic energy expenditure [3]. It is important to identify the muscles that are

essential to maintaining balance during gait and the recruitment patterns of these muscles when balance is disturbed.

The muscles of the lower limb can be categorized by the primary degree of freedom about which they produce moments. The muscles that produce motion about a joint can also be described in agonist–antagonist pairs. The agonist muscles generate joint moments in one direction when they produce force, while the antagonist muscles generate joint moments in the opposite direction [19]. The following sections describe each muscle group and their main roles throughout the gait cycle.

2.2.1 Ankle Plantarflexors and Dorsiflexors

During healthy gait, the ankle plantarflexor muscles generate a substantial amount of torque about the ankle joint for support and forward progression of the CoM. The ankle plantarflexors have been described as the main engines of the lower limbs to advance the swing leg and stabilize the trunk in the AP direction [24], [25]. During late stance, the plantarflexor muscles generate approximately 23 J of energy and 1.5 to 2 N·m/kg of torque (normalized by subject mass) about the ankle joint at comfortable walking speeds to propel the stance limb into swing [19], [26]. The muscles belonging to the ankle plantarflexor group primarily consist of the medial and lateral gastrocnemius and the soleus (known colloquially as the calf muscles).

The main ankle dorsiflexor muscles are the tibialis anterior, extensor digitorum longus and extensor hallucis longus. These muscles ensure that the foot clears the floor during swing by dorsiflexing the ankle immediately after push-off and control ankle plantarflexion at foot contact [27]. The dorsiflexor and plantarflexor muscle groups also contribute to maintaining AP stability throughout locomotion. To improve AP stability in response to an external perturbation, various

levels of agonist–antagonist activity will occur in the two muscle groups to increase the stiffness of the ankle joint [27].

2.2.2 Ankle Invertors and Evertors

In the frontal plane, the muscles surrounding the ankle are primarily responsible for controlling the ML stability of the joint and contributing to whole-body ML stability. The evertor muscle group consists of the peronei and the extensor digitorum muscles. In contrast, ankle inversion is controlled by the tibialis anterior, tibialis posterior, extensor hallucis, flexor digitorum and flexor hallucis. Similarly, for ML stability of the ankle joint, the invertor and evertor muscles experience co-contraction during tasks that require increased stability, which effectively increases the stiffness of the joint in the frontal plane [28], [29].

2.2.3 Knee Flexors and Extensors

The knee flexor group is composed of the hamstrings (biceps femoris, semitendinosus and semimembranosus) and the gracilis, sartorius, gastrocnemius and popliteus muscles [30]. The knee extensors are composed of the rectus femoris, vastus lateralis, vastus medius and vastus intermedius (the quadriceps muscle group) [30]. At initial loading response, the knee extensors contract eccentrically (length of muscle increases as tension is being produced) to control knee flexion and to prevent buckling of the knee joint [31]. The knee flexors are primarily active in decelerating the leg during terminal swing; the hamstring muscles are also active during loading response to control hip flexion [31]. MacKinnon et al. concluded that knee joint moments are not generated to regulate balance in the frontal plane but are contributors to performing stabilization tasks in the sagittal plane [32].

2.2.4 Hip Flexors and Extensors

In the sagittal plane, the muscles surrounding the hip joint are responsible for propelling the CoM forward while maintaining AP pelvic tilt and stability of the upper body [33]. The iliopsoas, sartorius, tensor fasciae latae, adductor longus and rectus femoris muscles are the main muscles that generate hip flexion moments [33]. The gluteus maximus, biceps femoris, adductor magnus, and semitendinosus are the primary muscles that generate hip extension moments [33].

2.2.5 Hip Abductors and Adductors

In the frontal plane, the muscles surrounding the hip joint assist in controlling the ML position of the CoM during stance, while allowing for proper foot placement after swing [4]. Hip abduction moments are primarily generated by the gluteus medius, gluteus minimus and tensor fascia lata; hip adduction moments are generated by the adductor longus, adductor brevis, gracilis and adductor magnus [33]. These muscles belong to the hip abductor and hip adductor groups, respectively.

2.3 Muscle Coordination and Stabilization

Regulating balance and posture during gait is a highly complex motor control problem [32]. It requires precise communication between the somatosensory system, the musculoskeletal system and the CNS to coordinate the motion of the limbs and trunk so that the body remains stable [3]. The mechanoreceptors of the somatosensory system capture sensory information such as touch, position in space and joint movements. The vestibular system provides information about the direction and speed of the body. Visual, vestibular, and mechanoreceptor inputs are essential in providing timely, accurate information for the CNS to coordinate stabilization strategies [3], [24], [32], [34], [35]. These systems allow the body to regulate foot placement, detect surface changes,

and anticipate perturbations. Mediolateral stability is constantly challenged during walking due to the narrow base of support (BoS) and balancing on one leg during the single-limb support phase of gait [32].

2.4 Elderly Gait

As individuals age, muscular, neurological, and visual changes affect their balance and ability to generate power for forward progression. In contrast to younger healthy adults, healthy elderly individuals adopt a more cautious gait strategy centered around the hip joint to compensate for a loss of strength in the ankle plantarflexors [24]. This gait strategy requires the hip joint musculature to generate significant power in the sagittal plane, provide step width control, stabilize the trunk, and resist pelvic drop on the side of the swinging limb in the frontal plane [19], [24]. Some researchers have hypothesized that these changes are adopted naturally to improve dynamic gait stability, whereas others suggest that they result from underlying pathologies [24], [32]. Nevertheless, it is widely accepted that the elderly are more prone to falling due to changes in several systems of the body [3], [4].

The cautious gait pattern adopted by elderly individuals is characterized by an increase in step width variability, slower walking speeds, shorter step length, increased double support time, a reduced range of motion (ROM) at the knee and ankle joints, and an increased ROM at the hip joint [3]. The elderly also have a 40% wider walking base and an increased peak HAA joint power, suggesting an increased reliance on HAA muscles to control step width [36]. Increased step width has been seen as a compensatory strategy to increase the BoS, however the corresponding increase in ML velocity of the CoM during weight shifting can decrease the overall MoS [37].

2.4.1 Changes to the Balance Control System

A fall occurs when an individual fails to recover from a loss of balance resulting in the body coming to rest on the ground, or when another body part breaks the fall [17], [38], [39]. Due to complex interactions between the CNS and the musculoskeletal system, it is difficult to definitively determine why balance is reduced as people age. However, several factors contribute to an increased risk of falling: previous falls, decreased muscle strength, medications, cognitive and visual impairments, arthritis, pain, reduced proprioception and high blood pressure, among others [2], [40], [41]. Though falls can occur in the AP or ML direction, elderly fall risk is highly dependent on the muscular and neurological changes that directly affect ML balance [3], [32], [35], [39], [42]. Though ML stability decreases with ageing, AP and vertical gait stability remain unchanged [3]. The following sections present an overview of the changes that affect an elderly individual's ability to maintain balance.

2.4.1.1 Somatosensory System

Changes in the somatosensory system can inhibit the body's timely and accurate sensory feedback for balance control. Loss of vision impairs the ability to predict surface changes or obstacles, contributing to slower reaction times [42], [43]. In addition, the number of mechanoreceptors in the muscles and the sensitivity of these receptors both decrease with age [44]. A reduction of mechanoreceptors results in inaccurate feedback being provided to the brain, thus diminishing one's ability to regulate ML foot position [3], [44]. A decrease in the number of mechanoreceptors on the plantar surface of the foot increases the threshold required to perceive center of pressure (CoP) changes, disrupting the speed and accuracy of sensory feedback [44]. Moreover, the loss of neurons and neural connections in the brain results in delayed processing of

information and delays in executing stabilization strategies [44]. Thus, more time is required to adapt to situations that challenge one's stability.

2.4.1.2 Muscle–Tendon Dynamics

In the elderly, longer onset timing of muscle activations decreases stability, which is likely due to a combination of the following: muscle weakness, more compliant tendons, slower processing of sensory information, and a reduced number of fast motor units in the muscles [20], [21], [44], [45].

Muscle strength determines the amount of torque that can be generated about the joints to resist the forces acting on the CoM throughout gait. Many studies have focused on HAA muscle strength as a determinant for fall risk due to the role of the HAA muscles in maintaining ML stability. A study conducted by Johnson et al. found significant age-related declines in HAA peak isometric strength and activation rate [46]. The negative impact of weakened hip abductor muscles generally correlates with increased lateral sway amplitudes during walking and is observed in elderly individuals with a high risk of falling [39]. As a result of hip abductor weakness, an individual may have a reduced ability to slow down the center of mass during the single-limb support phase of gait, negatively impacting the individual's mediolateral balance [39]. In addition, the primary factors determining fall risk in the elderly are hip abduction torque and trunk rotation ROM [4], [7].

The mechanical properties of the muscle–tendon units also affect the speed at which the elderly can generate muscle forces. The tendons surrounding the hip joint become more compliant with age, delaying force transmission and slowing down the body's ability to activate muscles in response to different walking surfaces, obstacles, or gait speeds [34], [47], [48]. Moreover, healthy

elderly individuals generally lack precision during walking and while maintaining ML stability [44], [49].

2.4.1.3 Elevated Metabolic Cost

As muscles fatigue during movement, motor control variability increases and individuals may have a reduced capacity to respond to balance challenges [44], [50]. Experimental studies have demonstrated that subjects walking at a higher metabolic cost are at a 25% increased risk of falling [51] and that subjects in their 70s walk at a 15–30% higher metabolic cost than individuals in their 20s [52]. Fatigue in the muscles of the lower limb generally decreases walking speed and AP stability, while also resulting in more significant stride-to-stride variability [53]. In the frontal plane, fatigue in the lower-limb muscles is generally correlated with increased stride-width variability and a reduced capacity to regulate the ML sway of the CoM [3].

While responding to a perturbation, the elderly commonly activate muscles in a proximal-to-distal sequence by first recruiting the muscles surrounding the hip joint to control the CoM [3], [24]. In contrast, younger adults tend to activate muscles in a distal-to-proximal sequence, initially relying on the ankle invertor and evertor muscles to control ML balance [3].

The muscle–tendon units at proximal locations in the body, such as the hip joint, generally have long, parallel muscle fibers that connect to little or no tendon [14], [47]. Thus, the tendons have little ability to reduce the velocity and length changes that a muscle undergoes throughout motion. Therefore, the mechanical work produced relies more on muscle work than on tendon elastic energy [14]. Hence, the proximal-to-distal sequence of recruiting muscles experienced by elderly individuals is metabolically expensive compared to the younger ankle plantarflexor gait strategy due to the different muscle–tendon properties at the two joints [14], [47]. Studies have

also shown greater co-activation of muscles in the elderly, likely in an attempt to enhance joint stability while walking [36]. ML balance requires more active control from the musculoskeletal system [4], suggesting a corresponding increase in metabolic cost [3].

2.5 Modelling Balance

The ability of an individual to maintain balance is determined by their ability to keep their CoM within their base of support. Biomechanics researchers have widely used the MoS to relate the body's CoM location to the BoS [43].

In 2005, Hof et al. introduced the extrapolated CoM (XcoM) model to describe AP and ML gait stability. This model uses an inverted pendulum and defines the MoS as the distance between the BoS and the extrapolated CoM [54]. The following equations characterize the XcoM model:

$$MoS = BoS - XcoM \tag{1}$$

where BoS and XcoM are position vectors with originating from the CoM, and

$$XcoM = CoM + \frac{vCoM}{\sqrt{g/\ell}} \tag{2}$$

where $vCoM$ is the velocity of the CoM, ℓ is the effective pendulum length, and g is the gravitational acceleration, as shown in Figure 2-2.

The XcoM model represents a stable condition when the MoS is positive, where the inverted pendulum would return to its upright position. If the XcoM is located beyond the BoS, as illustrated in Figure 2-2, the MoS is negative and represents an unstable gait pattern: the pendulum in the XcoM model would not return to its original position [43]. The stability limits depend on the individual's kinematics, range of motion, muscle strength, the type of walking surface and the complexity of the motor control required for a specific activity that is being performed. Increased

variability in the location of the CoM increases the demand on muscles that maintain balance [3], [4].

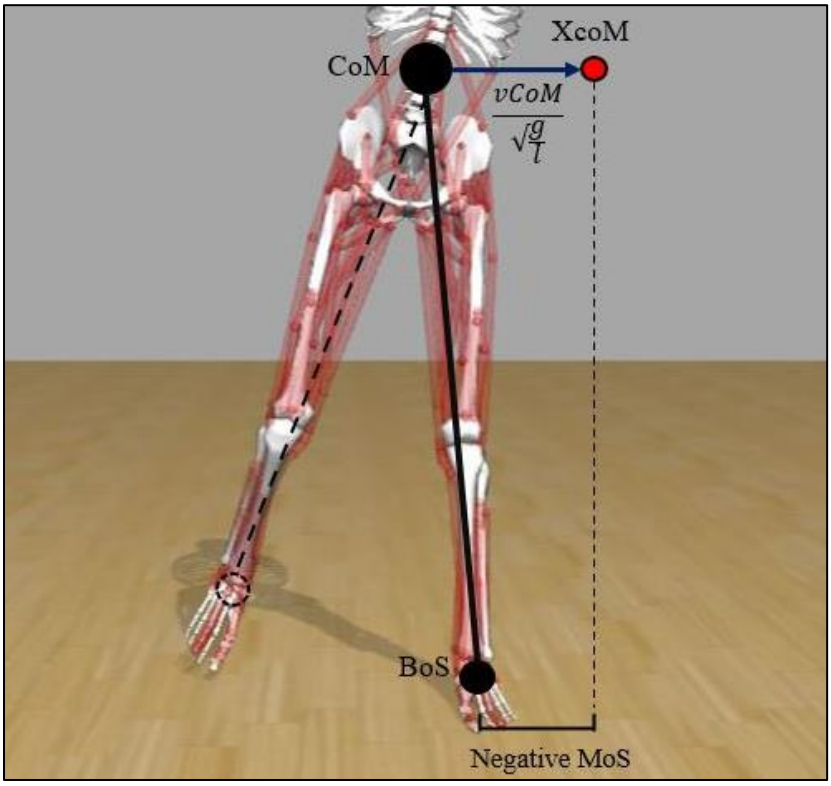

Figure 2-2. The XcoM inverted pendulum model described by Hof et al. for calculating the MoS in the AP and ML directions.

2.5.1 Frontal-Plane Stability

To maintain frontal-plane stability, the CoM must remain within the lateral BoS. Muscle coordination to maintain balance throughout gait is regulated by consistently producing a horizontal CoM acceleration towards the body's midline [32]. During the swing phase of gait, the CNS regulates the placement of the heel at foot contact by analyzing the state of the CoM in space [32]. A corresponding signal is sent to the HAAs to control the position of the contralateral limb, which regulates the lateral acceleration of the CoM [32]. Proper foot placement is the most fundamental aspect of controlling frontal-plane balance. Subsequently, inaccuracies in foot placement that produce an unintended acceleration of the CoM are corrected by the HAA and

ankle invertor/evertor muscles [32]. Moreover, Mackinnon et al. hypothesized that minor errors in foot placement are corrected by the ankle invertors/evertors, while significant errors are generally corrected by the HAA muscle groups [32].

The contribution of the HAA muscles to ML stability is described in three phases. From initial contact to mid-double support, a concentric contraction of the hip adductors creates a lateral pelvic tilt in response to the lateral acceleration of the CoM [32]. During the single-limb support phase, balance of the torso and upper extremities is achieved by the generation of an ipsilateral hip abduction torque and a passive medial acceleration of the hip joint [11], [32], [34]. As the contralateral foot leaves the ground, the external adduction torque about the hip dramatically increases due to gravity applying a downward force at the CoM. Healthy hip abductors counteract this motion by acting eccentrically from the mid-double support phase to the late stance phase, stabilizing the pelvis relative to the femur and preventing the pelvis from dropping on the side of the contralateral limb. This eccentric contraction of the hip abductors effectively controls the amount of pelvic tilt experienced during gait. In the late stance phase, the abductors contract to elevate the pelvis to its neutral position and initiate pelvic tilt towards the contralateral limb for heel contact [32]. Specifically, the gluteus medius muscles are strongly involved in ML weight shifting motions and can provide significant forces to stabilize the body in the frontal plane [34]. The HAAs are essential in maintaining ML balance throughout the gait cycle and regaining balance when it is lost [3], [32].

When responding to an external perturbation, placing the foot at a new location does not necessarily counteract a loss of balance [55]. The CNS implements four main strategies when a perturbation is experienced which can be characterized as the stepping strategy, the ML ankle

strategy, the inertial strategy, and the braking strategy [55]. The stepping strategy involves placing the foot contact leg in the most appropriate ML position to regulate the acceleration of the CoM. This is the most important strategy to recover balance following a perturbation [32], [55].

The ML ankle strategy is defined by rapid generation of ankle invertor and evertor torques to move the CoP mediolaterally from the midline of the foot. This strategy can be applied rapidly and has been hypothesized to be a reflex reaction rather than requiring active control from the CNS [55]. In addition, control of the CoP in the lateral direction has been observed to be accompanied by a displacement of the CoP in the sagittal direction, suggesting that counteracting lateral perturbations requires active control in all motion planes [55].

The inertial strategy defines the generation of a lateral ground reaction force by rotating the body segments of the lower limbs to induce an angular acceleration about the whole-body CoM. The HAAs are particularly effective at generating this moment about the hip joint to control the angular acceleration of the CoM [3], [43]. Braking of movement in the plane of progression is also used to balance the CoM, while applying an external force such as leaning against a wall, holding onto handrails, or using canes or walkers may be effective as a last resort [3], [17], [38], [55].

2.6 Walking Assist Exoskeletons

Walking has many health benefits, including reducing the risk of stroke, heart disease and diabetes; improving mental health; enhancing circulatory function; and improving weight fluctuation, blood pressure and overall energy levels [56]. Experience with falling, the fear of falling, and reduced confidence while walking prevent many elderly individuals from performing walking activities. Balance training is often proposed to improve stability and it has been

moderately successful [40]. Oddsson et al. proposed a training regimen that improved postural stability in elderly fallers using a combination of stretching, strength training and conditioning, and sit-to-stand exercises [57]. Oddsson et al. also concluded that these exercises can enhance strength, flexibility, and endurance but do not necessarily correlate with a more efficient and stable gait pattern [40], [57].

Biomechanically, the ankle invertors/evertors and the hip abductors/adductors are the major muscle groups that contribute to ML balance. Because adding the mass of a device more distally results in a greater increase in the metabolic cost of walking, the hip joint has been determined to be a more viable location for exoskeleton assistance as the device mass is added closer to the body's CoM [45], [58]. It is essential to consider the mass of the device as elderly individuals typically have reduced muscle strength and are more affected by added weight on the body [51], [58], [59]. Furthermore, the hip abductors and hip adductors are crucial in maintaining ML stability by regulating foot placement and providing joint torques to regulate the position and velocity of the CoM during the stance phase of gait. Nevertheless, research on providing elderly individuals with hip abduction/adduction assistance is lacking, while hip exoskeleton technology has focused on providing sagittal-plane assistance to improve the metabolic cost of walking. Mitigating the risk of falling in the elderly through ML stability assistance strategies from an exoskeleton device has been scarcely explored in the existing literature.

Walking-assist hip exoskeletons such as the Honda Stride Management Assist, The Gait Enhancing and Motivating System, and The Active Pelvis Orthosis have been designed to assist hip flexion and extension (HFE) in the elderly population. While these devices have found recent success in the sagittal plane, they cannot provide ML stability for their users. The NREL-Exo is

the only hip exoskeleton developed to date that actively controls HFE and HAA motion. The following sections briefly summarize the design of these untethered devices, their effectiveness, and their restrictions.

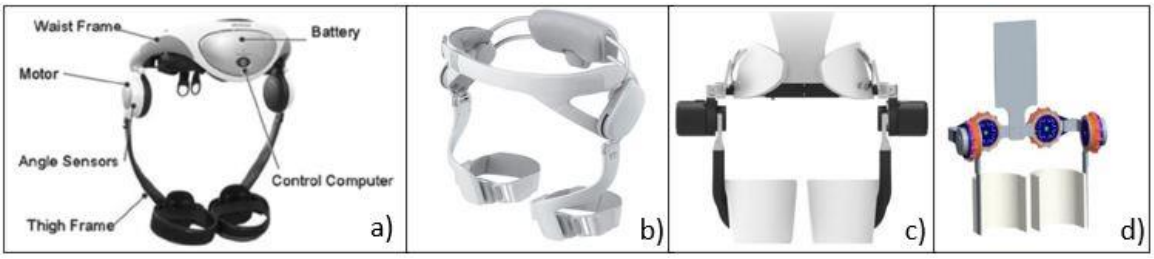

Figure 2-3. Powered hip exoskeleton designs: (a) Honda Stride Management Assist [60], (b) The Gait Enhancing and Motivating System [61], (c) The Active Pelvis Orthosis [62], and (d) The NREL-EXO [45]. Images © 2015, Buesing et al., © 2016 IEEE, © 2017 Monaco et al., © 2018 IEEE, respectively, and reproduced with permission.

2.6.1 The Honda Stride Management Assist

The Honda Stride Management Assist (SMA) system shown in Figure 2-3(a) was designed in 2008 as a wearable robotic device for elderly patients and individuals with atypical gait [60]. The SMA system incorporates brushless DC motors and a planetary gear at the hip joints that extend from the pelvis, attaching at the upper thigh using a strapping system. As a result, the SMA cannot be used for patients with extensive reductions in mobility in their lower limbs as it does not provide the necessary support. The device assists HFE with maximum assistive torques of 6 N·m. Angle and current sensors monitor the user's HFE and apply the appropriate assistive torques to the upper thighs based on the sensor signals [60]. The device is battery powered and has a mass of 2.8 kg. The SMA relies on the cyclic motion of the user's gait cycle to initiate the assistive torque but can modify assistive patterns based on user feedback [60]. Use of the device in healthy young adults aged 21 to 35 has been shown to reduce the metabolic cost of the user by 7.06% at a comfortable walking speed and by 10.52% at their maximum walking speed [63]. This device has not been evaluated for stability assistance in the elderly population. Although it allows for free

rotation in the frontal and transverse planes, it is limited to sagittal-plane assistance and does not apply torques to assist hip abduction or adduction.

2.6.2 The Gait Enhancing and Motivating System

The Gait Enhancing and Motivating System (GEMS) shown in Figure 2-3(b) was developed by Samsung Electronics to improve gait function in the elderly population. The exoskeleton is mainly composed of carbon fiber reinforced plastic and has a mass of 2.1 kg. Two 75-Watt brushless DC motors produce a maximum torque of 12 N·m for HFE assistance [61]. Hinges mounted inferior to the motors allow for free HAA movement but no assistive torques are applied to the hip joints in the frontal plane. An on-board microcontroller regulates the actuators with sensor feedback to apply the appropriate torques about the user's hip joints. The device was tested at 0%, 5%, and 10% inclines during treadmill walking trials for five healthy young adults aged 34 to 46 years. The results demonstrated mean net reductions in metabolic cost of 14.5%, 15.5%, and 9.8%, respectively, compared to walking without the exoskeleton. Previously, the GEMS exoskeleton was tested with 30 elderly adults and resulted in a mean metabolic reduction of 7% at self-selected treadmill walking speeds [64]. However, the GEMS has not been tested for balance control in the elderly population and provides neither passive nor active HAA assistance.

2.6.3 The Active Pelvis Orthosis

The Active Pelvis Orthosis (APO) shown in Figure 2-3(c) was designed by Giovacchini et al. to assist elderly users by applying HFE torques. The APO uses series elastic actuators (SEA) mounted to a carbon fiber frame with custom thermo-shaping orthoses that attach to the waist and thighs [62]. The device includes a mechanical structure that permits passive motion in HAA and pelvic tilt. The APO has a target assistance of 50% of the muscle torque required, yielding a maximum actuator torque of 35 N·m. A torsional spring and a sensor aligned with the biological

HFE axis enable measurement of the hip joint angle. The device has a total mass of 6.5 kg, most of which is mounted to the waist frame to minimize the inertia added to the lower limbs [65]. After a 4-week training period, healthy elderly individuals experienced an average reduction in metabolic cost of 4.24 ± 2.57% compared to walking without using the APO [65]. The APO has been shown to improve AP balance in elderly individuals by applying coordinated bursts of hip flexion and hip extension torques after a slip [66].

2.6.4 The NREL-Exo

Zhang et al. developed the NREL-Exo to improve lateral stability and eliminate the need for crutches (see Figure 2-3(d)) [45]. The NREL-Exo's HAA assistance allows for the adaptation of step width based on a lateral shift of the users' COM. A "guidance force" is applied to the user through SEAs to maintain balance in the sagittal and frontal planes [45]. Zhang et al. designed the device as a research prototype to assist individuals experiencing hip muscular weakness. The actuators were designed to provide a maximum torque of 80 N·m to the user. Without the battery unit, the NREL-Exo has a mass of 9.2 kg, which is similar to other exoskeletons that incorporate lateral stability mechanisms [45]; however, the added mass exceeds the 4 kg threshold suggested by Browning et al. to avoid substantial negative impacts on metabolic cost and the kinematics of walking [58]. It was found that the device was able to adjust the step width of a healthy 30-year-old male to maintain the gait stability of the human–exoskeleton system while walking [45]. The device's effectiveness on the elderly population has not yet been reported.

2.7 Biomechanics Simulations

The development of WAEs relies on the accurate and repeatable analysis of gait and the identification of underlying pathologies. The current gold-standard for collecting gait data is

through optical motion capture for kinematics, force plates for kinetics and electromyography (EMG) sensors to measure the activity of selected muscles throughout the gait cycle [67]. The physical testing of WAEs typically requires a lengthy process to design and manufacture several prototypes while improving upon design parameters. Collecting experimental motion capture data is also time consuming, and it is difficult to measure several variables in the laboratory setting, including the forces, timing, and activity of muscles, as well as full-body and muscle-level energy consumption. Understanding the causal relationship between muscular dynamics, gait kinematics and kinetics, and assistive device properties is essential [68]. While experimental testing and evaluation of exoskeleton prototypes is necessary, the cost and time associated with developing multiple prototypes can be reduced by using biomechanical simulations early in the design process [69].

Computational musculoskeletal modelling is an important tool that complements experimental research by providing predictive and parametric models. Simulation and modelling software that are commonly used by researchers include Visual 3D (C-Motion Inc.), AnyBody (AnyBody Technology) and OpenSim (Stanford University) [70], [71]. Visual 3D is a robust biomechanics software used to analyze joint angles, moments, center of pressure, signal filtering and inverse dynamics from imported marker data [72]. However, Visual 3D does not allow the user to analyze the individual muscle forces that contribute to generating the observed movement.

AnyBody is a biomechanics software that allows for the analysis and simulation of the body working with its environment [73]. In addition to calculating multibody dynamics, it is also capable of analyzing the muscle forces and energetics that are required to produce movement. The anatomical properties of the model can be modified for each test subject, including the height,

weight, anthropometric dimensions, and bone geometries. The software also allows for the evaluation of assistive devices by importing computer-aided design files to create a human–machine system. Additionally, when evaluating exoskeleton devices, mass, inertia, damping factors and the interactions between the exoskeleton and the user will influence the control and effectiveness of the device. AnyBody allows for the analysis of these parameters in one biomechanics software package; however, it must be purchased.

OpenSim provides an open-source platform to analyze the musculoskeletal dynamics of movement. It can compute inverse kinematics, inverse dynamics, and muscle forces like AnyBody. Researchers have developed and validated several musculoskeletal models that are free to download and can be scaled to match the height, weight, anthropometric dimensions, and specific muscle properties of test subjects. OpenSim also provides researchers with a platform to analyze muscle excitations that produce coordinated movement through the computed muscle control (CMC) algorithm. The Forward Dynamics (FWD) tool allows the user to predict the movement that will result from the application of specified muscle excitations and control parameters, using Newton's laws to integrate the model's governing dynamic equations forward in time. This tool is particularly useful when one wishes to predict the kinematics of a model when a given set of forces and torques are applied to it [70], [71]. Assistive devices have been investigated in OpenSim by adding ideal (massless) actuators to a model to analyze their effect on kinematics, muscle activity and metabolic cost [23], [74], [75]. The main relationship of interest in this study is the effect of the assistive torque on the MoS of the model, and therefore the FWD tool is required.

2.7.1 Forward Dynamics Studies

One FWD modelling approach in OpenSim was used in a study conducted by DeMers et al., which allowed the researchers to investigate the effects of ankle invertor and evertor muscle

co-activation on ankle inversion injuries [28]. Throughout their investigation, the researchers conducted short forward dynamics simulations where the Gait2392 model (released with OpenSim) was dropped onto a landing surface (tilted at 30˚) from a height of 0.3 m. The model's initial position was determined based on experimental kinematics. The muscle excitations were modelled using stretch feedback controllers and were used to excite the muscles in the leg prior to coming into contact with the ground. When the model was dropped to the ground, the researchers could modify the level of co-activation between the ankle invertors and evertors to investigate their effects on the inversion angle of the ankle after landing. Once the model had landed, the simulation results were only evaluated prior to reflexes generating stabilizing forces approximately 62 ms after landing [28]. The researchers highlighted the usefulness of their presented modelling workflow to investigate simulated changes in kinematics away from experimentally captured results.

Chapter 3: Methods

This chapter outlines the methodology used to generate and analyze the biomechanics simulations in OpenSim. The musculoskeletal model that was created, the data that were used and the procedures that were employed to compute the model's motion will be described. The simulation workflow comprised five OpenSim tools: Scaling, Inverse Kinematics (IK), Residual Reduction Algorithm (RRA), Computed Muscle Control (CMC) and Forward Dynamics (FWD). Assistive devices added to the hip joint in the frontal plane were characterized and used to simulate assistive torques generated by an exoskeleton device.

3.1 Overview

A hip exoskeleton must regulate the ML state of the CoM with respect to the BoS to provide ML stability assistance. The current study investigates the effects of actuator placement, actuator torque magnitude and actuator timing of a HAA assistance strategy on the MoS of elderly subjects.

Musculoskeletal models of elderly individuals were generated in OpenSim from the base "Gait2392" model released with the software [76], [77]. Once the model was scaled to match each subject's body dimensions and modified with the appropriate actuator specifications, the pose was set to the subject's initial position during quiet standing. This process will be detailed in Section 3.3.6. A lateral perturbation force was then applied to the pelvis of the model to simulate an unexpected disturbance to the musculoskeletal system. Forward dynamics simulations were completed without assistance from the exoskeleton device and with HAA assistance on the contralateral limb (the limb on the opposite side of the body as the perturbation force), the ipsilateral limb (the limb on the same side of the body as the perturbation) and bilaterally. The

forward dynamics simulations allowed for the MoS to be evaluated for each exoskeleton assistance condition. As a result, the relationship between exoskeleton torque magnitude, timing and location was analyzed as these factors directly impact exoskeleton designers' decision-making when designing hardware, control strategies and structures that interact with the body to achieve stability assistance.

3.2 Experimental Motion Capture Data

Publicly available motion capture data were used as input data for the simulations. OpenSim-compatible files were generated based on the published results from Dos Santos et al. [78]. In their study, motion capture data were collected from 49 subjects, including 27 subjects between 18 and 40 years of age and 22 subjects who were 60 years of age or older. To evaluate elderly balance strategies, the younger cohort was omitted from this data set, leaving 11 male and 11 female subjects 60 years of age or older [78]. Three-dimensional kinematics for each subject were collected using 12 infrared cameras (Raptor-4, Motion Analysis, Santa Rosa, CA, USA) during quiet bipedal standing. The subjects were evaluated standing still during four conditions for 60 seconds each: on a rigid surface with their eyes open, on a rigid surface with eyes closed, on an unstable surface with eyes open and on an unstable surface with their eyes closed [78]. The data from the rigid surface, eyes open condition were used for the current study. Ground reaction forces (GRFs) were collected using a dual force platform setup (OPT400600-1000; AMTI, Watertown, MA, USA), which allowed the researchers to capture CoP and GRF data from each foot during double support. Forty-two reflective markers were used to track the subject's kinematics as described by the anatomical landmarks in Table 3-1.

Table 3-1. Anatomical landmarks used for collecting optical motion capture data from [78].

Label	Name	Description
R.Front.Head/L.Front.Head	Right/Left front head	Approximately over the right and left temple
R.Back.Head /L.Back.Head	Right/Left back head	On the back of the head, in a horizontal plane of the front head markers
R.Shoulder /L.Shoulder	Right/Left shoulder	Right/Left acromion-clavicular joint
C7	7th cervical vertebra	Spinous process of the seventh cervical vertebra
T2	2nd thoracic vertebra	Second thoracic vertebra
T7	7th thoracic vertebra	Seventh thoracic vertebra
L1, L3, L5	1st, 3rd, 5th lumbar vertebrae	First, third and fifth lumbar vertebrae
IJ	Incisura jugularis	Deepest point of incisura jugularis
PX	Xiphoid process	Xiphoid process (most caudal point of the sternum)
R.ASIS/L.ASIS	Right/Left anterior superior iliac spine	Anterior superior iliac spine
R.PSIS/L.PSIS	Right/Left posterior superior iliac spine	Posterior superior iliac spine
R.Iliac.Crest/L.Iliac.Crest	Right/Left iliac crest	Iliac crest
R.GRT/L.GRT	Right/Left greater trochanter	Most lateral prominence of the greater trochanter
R.Knee/L.Knee	Right/Left femoral epicondyle	Most lateral prominence of the lateral femoral epicondyle
R.Knee.Medial/L.Knee.Medial	Right/Left medial femoral epicondyle	Most medial prominence of the medial femoral epicondyle
R.HF/L.HF	Right/Left head of the fibula	Proximal tip of the head of the fibula
R.TT/L.TT	Right/Left tibial tuberosity	Anterior border of the tibial tuberosity
R.Ankle/L.Ankle	Right/Left lateral malleolus	Lateral prominence of the lateral malleolus
R.Ankle.Medial/L.Ankle.Medial	Right/Left medial malleolus	Most medial prominence of the medial malleolus
R.Heel/L.Heel	Right/Left heel	Aspect of the Achilles tendon insertion on the calcaneus
R.MT1/L.MT1	Right/Left 1st metatarsal head	Dorsal margin of the first metatarsal head
R.MT2/L.MT2	Right/Left 2nd metatarsal head	Dorsal aspect of the second metatarsal head
R.MT5/L.MT5	Right/Left 5th metatarsal head	Dorsal margin of the fifth metatarsal head

These marker locations represent the experimental anatomical landmarks. For the simulations, a set of virtual landmarks was created to reflect the experimental marker positions used for scaling the base Gait2392 OpenSim model to each subject. This file was created within the OpenSim GUI.

The data were provided as text (.txt) files which were modified to be compatible with OpenSim [78]. OpenSim requires marker trajectory data to be in Track Row Column (.trc) format and ground reaction force data to be in motion (.mot) format. For each test subject, a static marker data set, trial marker data set, and trial GRF data set were extracted and converted to the corresponding OpenSim file types. Custom MATLAB scripts were generated to read the .txt files and convert them into the desired format for each data type.

Each of the 22 subjects within the data set from Dos Santos et al. were viable subjects for the current study; however, due to time constraints, only the subjects listed in Table 3-2 were selected.

Table 3-2. Subjects selected for the study from the open-source database of Dos Santos et al. [78].

Subject	Age (years)	Mass (kg)	Height (m)	Sex	BMI (kg/m^2)
PDS13	70.83	65.35	1.75	M	21.34
PDS18	61.75	70.55	1.50	F	31.28
PDS19	63.25	72.25	1.72	M	24.34
PDS22	62.17	70.50	1.64	M	26.05

3.3 Methodology

A set of forward dynamics simulations was conducted in OpenSim to investigate the contribution of HAA assistance to elderly stability during perturbed stance. The workflow that was used for this study is outlined in Figure 3-1.

First, the Gait2392 model that is released with the OpenSim software was scaled to match each individual subject's body dimensions by comparing the experimental markers from the raw data collection and the virtual markers on the model. Scaling will be described in detail in Section 3.3.2. Next, Inverse Kinematics was used to compare the experimental and virtual markers throughout the time frame of collected experimental data to apply motion to the model. In this study, the static motion was tracked, which will be described in detail in Section 3.3.3. The Residual Reduction Algorithm was then used to reduce dynamic inconsistencies in the experimental data, which will be described in Section 3.3.4. Finally, the Computed Muscle Control Algorithm was used to find the muscle excitations during quiet stance, which provided the initial conditions required to run the forward dynamics simulations. The forward dynamics simulations were then used to investigate the perturbation conditions with and without HAA assistance from the simulated exoskeleton device.

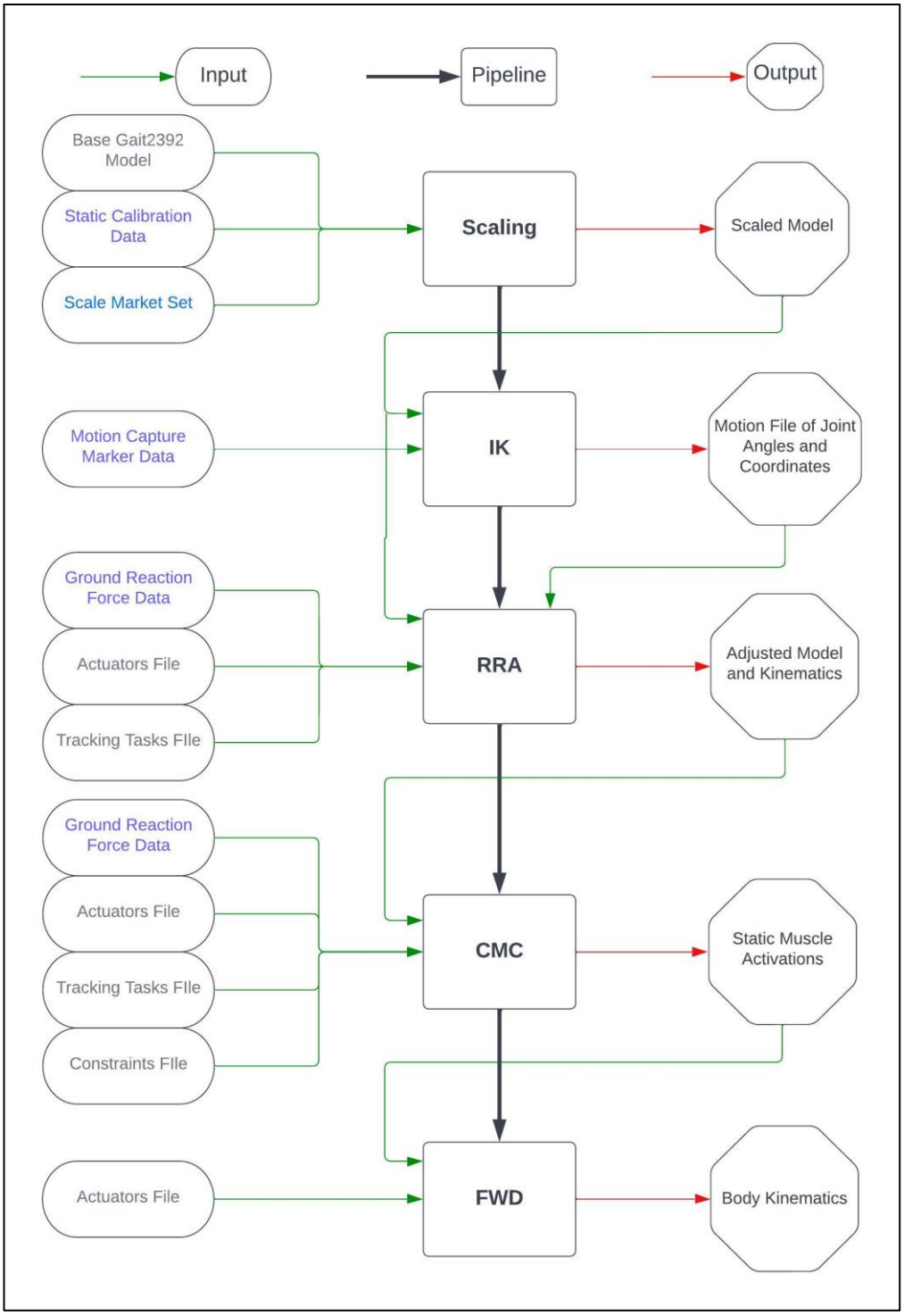

Figure 3-1. Flowchart of the OpenSim methodology used for this study from Scaling to Forward Dynamics. OpenSim tools are depicted in bold letters in square boxes. Green arrows show the input files that are used for the OpenSim tool. Red arrows show the output of the OpenSim tool. Purple font denotes experimental data files. Gray font denotes a setup file from OpenSim. Blue font denotes files created by the user and used as input in the OpenSim tool. (IK = Inverse Kinematics, RRA = Residual Reduction Algorithm, CMC = Computed Muscle Control, FWD = Forward Dynamics.)

3.3.1 OpenSim Model

An OpenSim model defines the dynamics of the system that is to be analyzed during a computer simulation [70], [71]. It consists of rigid bodies, joints, constraints, forces, contact geometry, markers, controllers and reference frames. The models used in this study were modified from the Gait2392 musculoskeletal model. The Gait2392 model consists of 23 degrees of freedom and 92 musculotendon actuators representing 76 muscles in the lower extremities and torso. The Gait2354 model was also a viable option for this simulation; however, it has a reduced number of muscles (to improve simulation speed) and is used primarily for education rather than research purposes [70], [71]. Models that include the upper extremities were not considered for this study because the main outcome of interest relies on lower-body kinematics and the effect on the individual's center of mass. In addition, subjects' upper-extremity kinematics were not collected in the data set from Dos Santos et al. Adding the upper extremities would increase simulation time without adding value to the results. Also note that the upper extremities would not move substantially throughout the duration investigated, which is further discussed in Section 3.3.6.2. The Gait2392 model is the most widely used model within OpenSim and many studies have validated the results of this model during various movements and in various conditions. The Gait2392 model was selected as the base model, representing an individual with a mass of 75.16 kg and a height of 1.8 m, as shown in Figure 3-2. In Figure 3-2, the global coordinate system can be seen in red, green and blue which represent the positive X-direction, the positive Y-direction and the positive Z-direction, respectively.

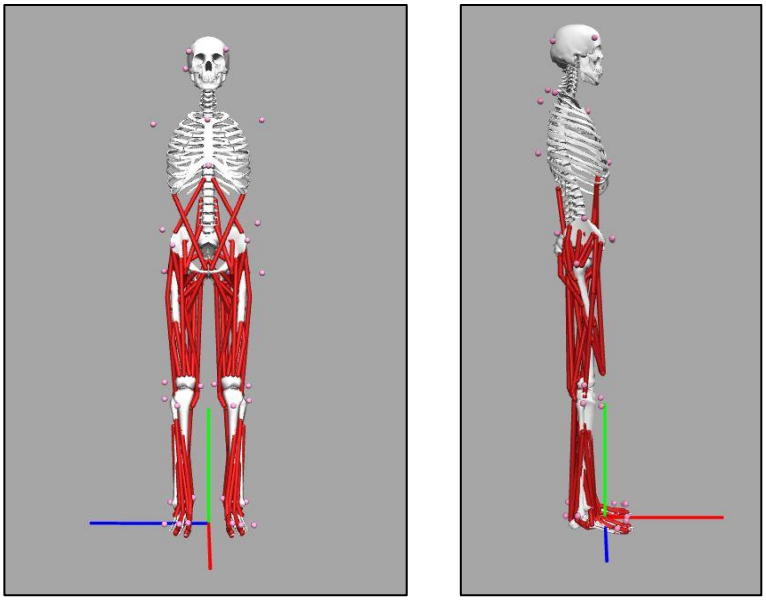

Figure 3-2. OpenSim Gait2392 model frontal-plane view (left) and sagittal-plane view (right). The reference frame at the bottom of the image indicates the positive X (red), Y (green) and Z (blue) directions.

3.3.1.1 Primary Elderly Model

In a previous study, the Gait2392 model was modified to create an elderly gait model that more closely reflects the musculotendon dynamics of an elderly individual [74]. The model was modified based on the recommendations by Thelen to adjust the Hill-type musculotendon parameters [79]. The adjustments made were as follows (described in relation to a model for a healthy younger adult):

- 30% decrease in muscle peak isometric force
- 20% increase in muscle deactivation time
- 20% decrease in maximum contraction velocity
- The passive stress–strain relationship was adjusted to account for the relative increase in passive stiffness
- The maximum normalized force achievable during eccentric contraction was increased from 1.4 in young adults to 1.8 in older adults

This model was referred to as the 'Primary Elderly Model' used during the Scaling, IK, RRA and CMC steps of the simulation workflow to estimate the subjects' muscle excitations during quiet standing. A second model was created to perform the forward dynamics portion of the study, which was generated from the subject-specific primary elderly gait model.

3.3.1.2 Secondary Elderly Model

The forward dynamics simulations required additional features to be added to the Primary Elderly Model described above. The adjusted elderly model from RRA was modified through a custom MATLAB script. This script read the adjusted model and added the components outlined in Table 3-3. The foot–floor contact model that was used represented a rubber-on-rubber interface with a shoe sole thickness of 2 cm, as described by DeMers et al. [28]. Contact geometry was used on the foot to characterize the geometry and dynamics of the interactions between the floor and the foot. The secondary elderly model used for forward dynamics is shown in Figure 3-3.

Table 3-3. OpenSim model components that were added to the primary elderly model to perform the forward dynamics simulations.

Component	Function
Contact Half Space	Provide the modelling environment with a platform ground object that can interact with contact geometry on the musculoskeletal model.
Contact Geometry	Contact nodes at the heel, 1st metatarsal head and 5th metatarsal head to interact with the platform ground object.
Hunt–Crossley Forces	Hunt–Crossley Forces at the contact geometry of the foot to characterize the interaction between the ground platform and contact nodes on the models' feet.
Torque Actuators	Used to apply various magnitudes of assistive hip abduction/adduction torque from the exoskeleton device.
Controllers	Defines the force-generating ability and activation of the torque actuators in the model.
Disturbance (Perturbation) Force	A force applied laterally at the pelvis to simulate a perturbation applied to the model. Various magnitudes of disturbance are characterized and applied to the pelvis.

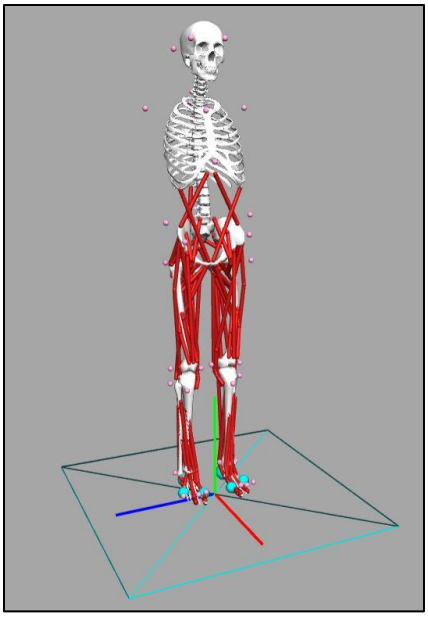

Figure 3-3. Secondary elderly model used for forward dynamics. Contact nodes are depicted as blue spheres at the heel, 1st metatarsal head and 5th metatarsal head. The contact half space is depicted as the blue crossed platform, which represents the ground contact geometry of the simulation environment.

3.3.2 Scaling

The first step of the simulation workflow was to scale the primary elderly model to the patient-specific data from Dos Santos et al. [78]. Scaling changes the dimensions of the model to match a subject by comparing experimental marker data with virtual markers on the model and adjusting the mass properties of the body segments [70], [71]. Static trial marker trajectories were used from the experimental data for each subject. In this trial, the subject stood as still as possible with all anatomical markers present. A "scale marker set" XML file was created to define marker pairs in the experimental data. These marker pairs were used to scale the virtual markers attached to the primary elderly model by attempting to match the distance between the experimental marker pairs with the distance between the corresponding virtual marker pairs. The "static pose weights" were adjusted to determine how strongly the scaling tool must match each marker position. The scaling algorithm matches the virtual and experimental markers more closely if a larger weight is applied to the marker. The static pose weights are outlined in Table 3-4. The weights were

generated by applying the scaling algorithm to the model and adjusting the weights manually depending on the errors outlined in the OpenSim interface.

Table 3-4. Marker weights for the scaling tool.

Marker Name	Weight
IJ	1
R.Shoulder	10
L.Shoulder	10
R.Back.Head	1
R.ASIS	1000
L.ASIS	1000
L5	1
R.Knee	1000
R.Knee.Medial	1000
R.HF	1
R.TT	1
R.Ankle	1000
R.Ankle.Medial	1000
R.Heel	1000
R.MT5	100
R.MT1	100
R.MT2	1000
L.Knee	1000
L.Knee.Medial	1000
L.HF	1
L.TT	1
L.Ankle	1000
L.Ankle.Medial	1000
L.Heel	1000
L.MT5	100
L.MT1	100
L.MT2	1000
R.PSIS	100
R.Front.Head	1
L.Front.Head	1
L.Back.Head	1
L.PSIS	100
C7	1000
T2	1
T7	1
L1	1
L3	1
PX	1000
L.Iliac.Crest	10
R.Iliac.Crest	10
R.GTR	1
L.GTR	1

The scaling tool provided four subject-specific elderly models for the remaining steps of the simulation. Toggling "on" the "Preserve mass distribution during scale" option allowed for the subject's body segment mass to remain proportional to the overall mass of the subject. Each scaling procedure yielded marker errors of less than 2 cm and RMS errors of less than 1 cm, providing acceptable results based on OpenSim's recommended guidelines [70], [71], [80].

3.3.3 Inverse Kinematics

The Inverse Kinematics (IK) tool was used to calculate the joint angles of the subject at each time frame during the experimental trials [70], [71]. The experimental data was extracted using a custom MATLAB script, which also extracted a single time step of experimental marker trajectories and GRF data. The purpose of the "Scaling" to "CMC" steps of the OpenSim workflow (see Figure 4) was to calculate the muscle excitations of the subject during quiet standing. Therefore, during the quiet standing trials, it was desired to eliminate any body sway in the experimental data. The IK tool was configured using the "rigid surface with eyes open" data set for each subject after being converted to .trc format. The weights of the tracking markers were increased if it was desired to track a marker more closely throughout the trial. The IK tool minimized the sum of squared errors between the experimental markers and the corresponding virtual markers on the scaled model, resulting in a .mot file containing the joint angles of the respective anatomical coordinates throughout the trial. All marker error and RMS error was less than 2 cm for each subject, indicating an acceptable IK solution based on the OpenSim guidelines [70], [71], [80].

3.3.4 Residual Reduction Algorithm

The Residual Reduction Algorithm was used to minimize inconsistencies ("residuals") between the GRF data and the skeletal kinematics computed from the marker data [70], [71]. Four

main files were needed to run RRA: inverse kinematics (.mot), tracking tasks (.xml), actuators (.xml) and ground reaction force data (.mot). The inverse kinematics output file contains the model's joint angles and pelvis translations. The tracking tasks file specifies the coordinates to track and their respective weights to determine how strongly the algorithm would track IK joint angles [70], [71]. An external loads file was created to specify the experimental ground reaction forces and apply them to the model's right and left calcaneus bodies. For each subject, residual forces and moments were computed and used to adjust the model's torso mass to correct inaccuracies in the model, since the torso mass and center of mass location are model parameters with substantial uncertainty. This "adjusted" primary elderly model was then used for the CMC portion of the simulation and as the base model to create the secondary elderly model for the forward dynamics simulations. To validate the RRA step, the maximum (MAX) and root-mean-squared (RMS) forces and moments were compared to the thresholds recommended by the OpenSim group, as shown in Table 3-5. An adjusted kinematics file was also output from the RRA step as it was required to run the CMC tool. All residual forces and moments were within the "good" range for each data set [80].

Table 3-5. OpenSim-recommended thresholds for the RRA tool to validate the adjustments made to the anatomical model [80].

Quantity	**Threshold**		
	Good	**Okay**	**Bad**
MAX Residual Force (N)	0–10 N	10–25 N	> 25 N
RMS Residual Force (N)	0–5 N	5–10 N	> 10 N
MAX Residual Moment (N·m)	0–50 N·m	50–75 N·m	> 75 N·m
RMS Residual Moment (N·m)	0–30 N·m	30–50 N·m	> 50 N·m

3.3.5 Computed Muscle Control

The static pose muscle excitations were necessary to provide the model with the initial position parameters during the forward dynamics simulations. Computed muscle control calculates muscle excitations that produce a set of kinematic motions [70], [71] and was used in this study to compute the muscle excitations necessary to produce a quiet standing pose. The muscle excitations are also known as model controls. CMC uses a combination of proportional–derivative control and static optimization to calculate model controls, resolving the muscle redundancy problem by minimizing the sum of squared muscle activations that produce the desired kinematics [70], [71]. A set of desired accelerations are computed as the first step of the CMC algorithm, which then drives the coordinates toward the experimental values. The second part of the CMC algorithm uses static optimization to compute the actuator controls (i.e. muscle excitations) necessary to track the accelerations computed in the first step.

As input, the CMC algorithm was provided with the adjusted primary elderly model and the adjusted kinematics from RRA, the experimental GRFs, the actuators file and the tracking tasks file. The controls.xml file output from the CMC tool contained the muscle excitations during quiet standing needed for the forward dynamics simulations.

3.3.6 Forward Dynamics

The forward dynamics tool integrates a set of differential equations defined by an anatomical model, which generates motion based on a set of model controls [70], [71]. These controls represent the excitatory signals sent from the CNS to the muscles. Forces and torques that are applied to the model change its coordinates and velocities as the dynamic equations are integrated forward in time. The derivatives of the model's states (i.e. the muscle activation rates, muscle fiber velocities, and coordinate angular velocities and angular accelerations) are computed

and integrated forward in time to find the trajectory of the musculoskeletal model for the time interval in question [70], [71]. Forward dynamics is an open-loop tool; therefore, no feedback or correction is used to ensure the model tracks a desired trajectory. In theory, if the control inputs to the forward dynamics tool are identical to those computed in CMC, the model should produce the same motion as was input to the CMC tool. However, errors due to round-off or truncation cause the forward dynamics tool to produce different results and, therefore, the forward dynamics simulation is only valid for a short time interval. The forward dynamics simulations generated in this thesis are considered to be valid only until the muscle controls would be affected by the action of reflexes [70], [71].

3.3.6.1 Overview

For the current investigation, four forward dynamics (FWD) simulation sets were generated using the secondary elderly models created for each subject. These FWD simulations will be referred to as simulation sets A, B, C.1 and C.2. Simulation set A of the FWD simulations allowed each model to settle on the ground platform and provided the initial conditions for simulations sets B, C.1 and C.2 (Section 3.3.6.3). Simulation set B was designed to investigate the unassisted simulations (Section 3.3.6.4). Simulation set C.1 performed HAA-assisted simulations to investigate the relationship between actuator placement and magnitude on the MoS (Section 3.3.6.5). Simulation set C.2 performed HAA-assisted simulations to determine the relationship between actuator timing and the assistive torque magnitude required to improve the stability of the elderly subjects (Section 3.3.6.6).

3.3.6.2 Simulation Duration

The FWD simulation duration was defined by the earliest change in joint moment due to active muscle contractions. After this amount of time, a controller would need to be added to the model to estimate the active reflex control that would be generated in response to a perceived loss of balance. Rietdyk et al. determined the earliest estimate of active muscle contractions after a perturbation to be between 125 ms and 150 ms, after considering onset latencies of EMG and neuromechanical delays [81].

Similarly, a study conducted by De Groote et al. found that larger balance-correcting effects measured by EMG were generated by the leg and trunk muscles approximately 100 ms after a perturbation was experienced [82]. However, De Groote et al. did not consider the additional electromechanical delay that is experienced between a measured EMG signal and an active muscle force, which was found to be between 0 and 50 ms in young healthy adults [83]. The electromechanical delay varies depending on the muscle groups that are being evaluated, a person's age, their muscle composition and many other factors [19], [83]. In the elderly specifically, the electromechanical delay between a measured EMG signal and an active muscle force is expected to increase by an average of 10% [79]. Therefore, the total electromechanical delay that was determined for the current simulations was 100 ms to 165 ms after the perturbation was initiated. Therefore, 100 ms and 165 ms after the perturbation is applied to the models represents the lower and upper time bounds on the estimated duration the simulations are valid prior to muscle reflexes playing a significant role in the system's dynamics. The estimated electromechanical delay used for the simulations is also consistent with Sivakumaran et al.'s findings that online corrections during walking were initiated at approximately 100–120 ms to adjust for low stability during the single-limb support phase of gait [84].

The muscle excitations determined from CMC were applied to the model for the duration of the forward simulations. Thus, it was assumed that, prior to the generation of joint moments due to muscle reflexes, the muscle excitations were equal to the constant excitations calculated during quiet standing, similar to the assumption made by DeMers et al. [28].

3.3.6.3 Settling Time

Simulation set A of the forward dynamics simulations began by calculating the settling time of the model once it was released onto the ground. The model was set in the initial static pose defined by the IK step in Section 3.3.3. To analyze the model's settling time, each joint was "locked" except for the translation of the pelvis in the vertical direction (pelvis_ty). A "locked" joint in OpenSim represents a joint that is fixed and therefore does not allow motion between the two bodies the joint connects. The model was then released from a height of 1 cm above the ground plate, which allowed the contact spheres on both feet to interact with the ground. As the contact spheres on the calcaneus, first metatarsal and fifth metatarsal met the ground, an initial vertical oscillation of the model was observed due to the contact elements on the feet and the ground interacting with each other. Before the lateral perturbation was applied, the model settled for 3 seconds to ensure there were no remaining vertical velocity oscillations experienced at the CoM of the model.

3.3.6.4 Unassisted Condition

Throughout simulation set B of the FWD simulations, the unassisted simulations were conducted. Once the model had settled, the coordinates that were unlocked were the pelvis lateral translation, pelvis vertical translation, pelvis list, and hip abduction/adduction. The remaining joints in the model remained locked, thus isolating the current study to the effect on frontal-plane

stability alone. Although ankle inversion and eversion motion controls ML stability, a preliminary investigation showed that the simulation results were insensitive to whether this joint was locked or unlocked throughout the duration of the simulation. Therefore, for each of the FWD simulations, ankle inversion and eversion remained locked to reduce computation time. Lateral forces of magnitude 5, 10 and 15% BW were applied, which is consistent with the methodology used by Matjačić et al. to evaluate the effect of outward-directed pelvis perturbations while walking [55]. The perturbation took the form of a constant force that was applied for 100 ms [55]. Once the impulse force was applied to the model, the remaining simulation was assumed to be valid until muscle forces would be affected by the reflexes of the individual as discussed in Section 3.3.6.2. For each simulation condition, it was assumed that equivalent results would occur due to symmetry if the perturbation was applied in the negative Z-direction. Therefore, each perturbation was applied in the positive Z-direction only.

The perturbation force was applied at zero seconds of simulation set B, assuming the individual would be standing still when the perturbation occurred. To calculate the ML MoS, the position and velocity of the CoM and the position of the BoS were required. The definition of the BoS is inconsistent in the literature. Some studies have defined the ML BoS as the ML position of either the CoP, a lateral toe marker, a point 2 cm lateral from a 2^{nd} or 5^{th} metatarsal marker, or a lateral malleolar marker [43]. However, the most common definition of the BoS is the position of the CoP or an approximation of the CoP using either the toe and heel markers or the midpoint between the markers defined by the heel and the 2^{nd} metatarsal [43]. In the current study, the BoS was defined by the center of mass of the foot body of the Gait2392 model, representing a close estimate of the midpoint between markers defined by the heel and the 2^{nd} metatarsal of the models. For the purposes of the current study, we note that the MoS is used primarily to compare the

effectiveness of various assistance and perturbation conditions rather than comparing absolute MoS values with the existing literature. Table 3-6 describes the subject-specific perturbation forces that were applied to the pelvis for each magnitude of perturbation that was applied to the models.

Table 3-6. Subject-specific parameters for the unassisted simulations.

Subject	Lateral Perturbation Magnitude (%BW)	Lateral Perturbation Magnitude (N)	Lateral Perturbation Time of Application (s)	Total Valid Simulation Time (s)
PDS13	5	32.05	0.0 – 0.1	0.165
	10	64.11		
	15	96.16		
PDS18	5	34.58	0.0 – 0.1	0.165
	10	69.21		
	15	103.74		
PDS19	5	35.44	0.0 – 0.1	0.165
	10	70.88		
	15	106.32		
PDS22	5	34.58	0.0 – 0.1	0.165
	10	69.16		
	15	103.74		

The forward dynamics simulations were then completed for 165 ms after the initiation of the perturbation force. The MoS was calculated and documented using custom-written MATLAB scripts for each perturbation magnitude applied to the model. The unassisted condition provided the baseline MoS for each subject, which was then used to calculate the change in MoS during the assisted conditions.

3.3.6.5 Actuator Position and Torque Magnitude

Simulation set C.1 denotes the first part of the assisted FWD simulations. This set of simulations compared the effect of contralateral hip abduction, ipsilateral hip adduction and

bilateral HAA assistance on the MoS of the elderly subjects. The same lateral perturbation forces were applied to the secondary elderly model for each subject as were applied in the unassisted conditions. The torque actuators that provided assistive HAA moments were ideal, meaning they were massless and were able to generate torques instantaneously. The controller signal was modelled as a step function whose step occurred at 0.124 seconds after the perturbation force was applied to the model. The 0.124 second delay that is modelled with the step function control represents the estimated electromechanical delay between the actuation of an exoskeleton device and the generation of force and is consistent with the findings of Ding et al. [85]. Although dependent on the actuators, control algorithms and actuation methods, the time delay of assistive torque generation was equal for all trials to facilitate comparisons among subjects and exoskeleton designs. Figure 3-4 depicts the direction of assistive torque applied to the model for the "C.1" simulations for the contralateral, ipsilateral and bilateral assistance conditions.

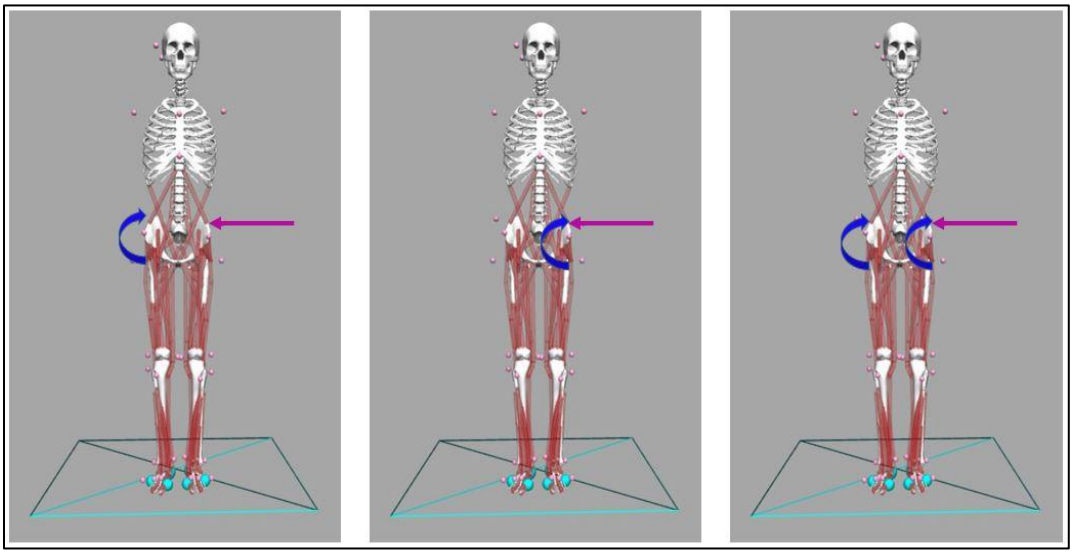

Figure 3-4. Assistive torque for the contralateral hip abduction assistance strategy (left), ipsilateral hip adduction assistance strategy (middle) and bilateral HAA assistance strategy (right). The straight purple arrow represents the perturbation force applied to the pelvis at the beginning of the forward dynamics simulations. The curved blue arrows represent the assistive torques delivered by the HAA exoskeleton in each assistance condition.

Five assistive torque magnitudes were applied to the model for each perturbation magnitude. For this study, HAA torques of 0.15, 0.30, 0.45, 0.60 and 0.75 N·m/kg (normalized by subject mass) were applied to the models for the contralateral and ipsilateral conditions. Therefore, approximately 10 to 50 N·m of torque was applied by the actuators, which is consistent with hip exoskeleton designs that are currently on the market such as the APO, GEMS, SMA and NREL-Exo (see Section 2.6). The applied torques in the current study were also consistent with targeting 50% of the biological joint torque during overground level walking [86]. Subsequently, half the torque applied in the unilateral assistance situations above was applied bilaterally (i.e. to both the contralateral and ipsilateral hip joints). All assistive torques were applied 0.124 seconds after the perturbation was applied to the model. To clarify, the following tables describe example loading conditions for the PDS13 subject. Table 3-7 lists the conditions for the contralateral hip abduction assistance simulations. In Table 3-8, the conditions for the ipsilateral hip adduction assistance simulations are listed, while Table 3-9 lists the conditions for the bilateral HAA assistance simulations. For each loading condition, the MoS was calculated and compared to the unassisted condition. The applied forces and assistance magnitudes for the remaining subjects are presented in Appendix A.

Table 3-7. Conditions for the contralateral hip abduction assistance simulations for subject PDS13 (C.1).

Subject	Lateral Perturbation Magnitude (% BW)	Lateral Perturbation Magnitude (N)	Contralateral Hip Abduction Assistance Magnitude (N·m/kg)	Contralateral Hip Abduction Assistance Magnitude (N·m)	Assistance Activation Time (s)
PDS13	5	32.05	0.15	9.80	0.124
			0.30	19.61	
			0.45	29.41	
			0.60	39.21	
			0.75	49.01	
	10	64.11	0.15	9.80	0.124
			0.30	19.61	
			0.45	29.41	
			0.60	39.21	
			0.75	49.01	
	15	96.16	0.15	9.80	0.124
			0.30	19.61	
			0.45	29.41	
			0.60	39.21	
			0.75	49.01	

Table 3-8. Conditions for the ipsilateral hip adduction assistance simulations for subject PDS13 (C.1).

Subject	Lateral Perturbation Magnitude (%BW)	Lateral Perturbation Magnitude (N)	Ipsilateral Hip Adduction Assistance Magnitude (N·m/kg)	Ipsilateral Hip Adduction Assistance Magnitude (N·m)	Assistance Activation Time (s)
PDS13	5	32.05	0.15	9.80	0.124
			0.30	19.61	
			0.45	29.41	
			0.60	39.21	
			0.75	49.01	
	10	64.11	0.15	9.80	0.124
			0.30	19.61	
			0.45	29.41	
			0.60	39.21	
			0.75	49.01	
	15	96.16	0.15	9.80	0.124
			0.30	19.61	
			0.45	29.41	
			0.60	39.21	
			0.75	49.01	

Table 3-9. Conditions for the bilateral HAA assistance simulations for subject PDS13 (C.1).

Subject	Lateral Perturbation Magnitude (%BW)	Lateral Perturbation Magnitude (N)	HAA Assistance Magnitude (Nm/kg)	C - Hip Abd Assistance Magnitude (Nm)	I - Hip Add Assistance Magnitude (Nm)	Assistance Activation Time (s)
PDS13	5	32.05	0.075	4.90	4.90	0.124
			0.15	9.80	9.80	
			0.225	14.70	14.70	
			0.3	19.61	19.61	
			0.375	24.51	24.51	
	10	64.11	0.075	4.90	4.90	0.124
			0.15	9.80	9.80	
			0.225	14.70	14.70	
			0.3	19.61	19.61	
			0.375	24.51	24.51	
	15	96.16	0.075	4.90	4.90	0.124
			0.15	9.80	9.80	
			0.225	14.70	14.70	
			0.3	19.61	19.61	
			0.375	24.51	24.51	

3.3.6.6 Actuator Torque Timing and Magnitude

To investigate the effect of actuator timing on the MoS of the elderly subjects, the electromechanical delay experienced by the actuator was modified in simulation set C.2. It is well documented that stability depends on the speed of muscle activations, neural commands and reactions to situations causing imbalance [3], [39]. In simulation set C.2, the actuator timing was modified to be 5, 10 and 15% faster than the neutral actuator timing simulated in part C.1. The 15% BW perturbation condition was used to evaluate the effect of actuator timing on the MoS of the elderly subjects. Table 3-10 describes the assistance conditions applied to each subject during the set C.2 simulations for the contralateral hip abduction case for each assistive torque magnitude from simulation set C.1.

Table 3-10. Conditions for the hip abduction assistance simulations C.2. The assistance conditions are applied to each magnitude of contralateral hip abduction assistance that were explored in simulations C.1.

HAA Assistance Time of Application (% decrease relative to timing in simulations C.1)	HAA Assistance Time of Application (s)
15	0.105
10	0.112
5	0.118
0	0.124

3.3.7 Statistical Analysis

An analysis of variance (repeated measures ANOVA) and a post-hoc paired sample t-test were performed to determine the statistical significance of the changes in MoS among simulation conditions. Paired sample t-tests were first used to determine whether significant differences were observed between each of the following: the contralateral and ipsilateral assistance strategies, the contralateral and bilateral assistance strategies, and the ipsilateral and bilateral assistance strategies. The paired sample t-tests were calculated for each set of actuator locations and magnitudes. Paired sample t-tests were also conducted to determine whether the torque magnitude of each assistive strategy affected the most favourable location for hip exoskeleton assistance. Repeated measures ANOVA and paired t-tests were conducted with a significance value of $\alpha = 0.01$ to decrease the potential of a Type I error. A p-value less than 0.01 was interpreted as being statistically significant for the t-tests and is often used to provide evidence against the null hypothesis [87]. However, due to the small sample size, the p-value was reported for each statistical analysis. All statistical analyses were performed in MATLAB.

Chapter 4: Results and Discussion

In this chapter, the MoS of the unassisted and assisted simulations will be presented. The data will be analyzed and discussed in relation to existing literature. The simulations were performed using OpenSim 4.3 and the data were evaluated using custom-written MATLAB scripts.

4.1 Simulation Set A – Model Settling Time

To begin each forward dynamics simulation, the model was released from a height of 1 cm, as described in Section 3.3.6.3, and then settled onto the ground platform before the perturbation was applied. To ensure the model had fully settled onto the ground platform, the vertical velocity of the CoM was displayed. As an example, Figure 4-1 illustrates the vertical velocity of the PDS13 subject's CoM after the model was released from a height of 1 cm. An initial vertical oscillation of the model can be visualized, as the model oscillates around zero from approximately time = 0 s to time = 0.8 s, once the contact elements on the feet of the models contacted the ground platform. The model settling time simulation was completed for a duration of 3 seconds for each subject. The vertical oscillation of the CoM was plotted to ensure each model had sufficient time to fully settle onto the ground platform. Once a model had fully settled onto the ground platform, its position was stored for use as the initial position for the simulations in simulation sets B and C.

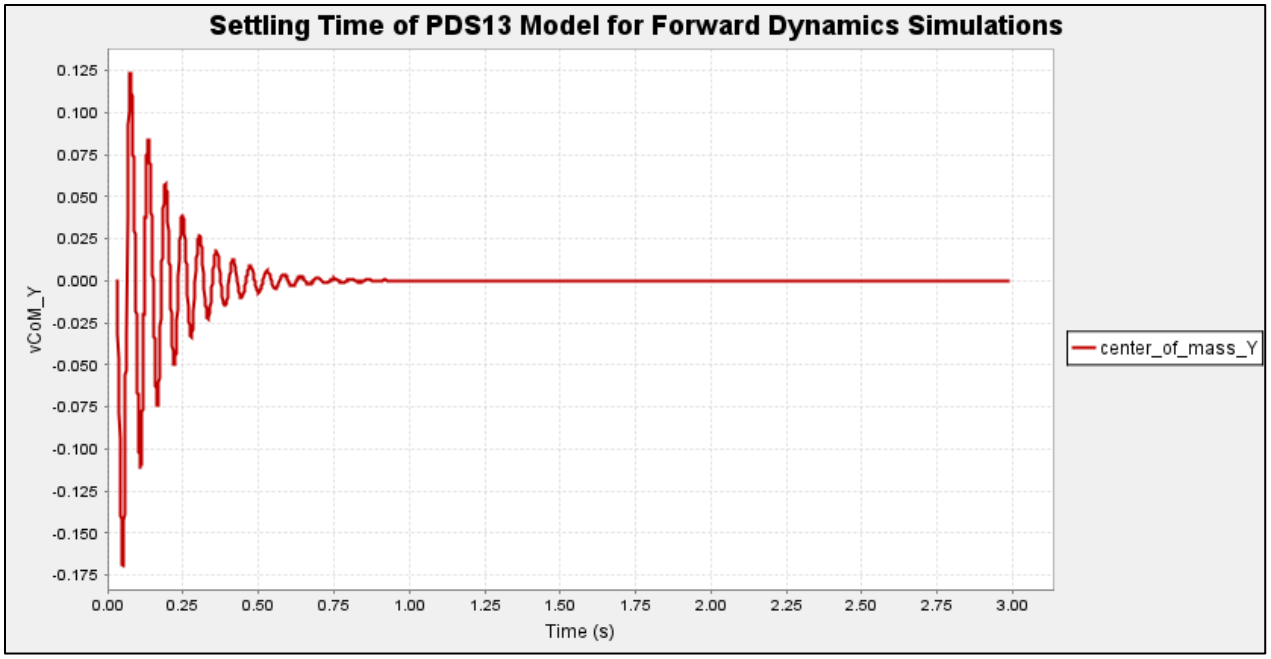

Figure 4-1. Determination of the settling time for the forward dynamics simulations of the PDS13 subject.

4.2 Unperturbed and Unassisted Simulation

A preliminary forward dynamics simulation was conducted to test the assumption that the model would remain upright prior to the initiation of a perturbation or an assistive torque from the exoskeleton. The MoS for each subject during the preliminary forward dynamics simulations can be observed in Figure 4-2. These unperturbed simulations were conducted once, after the model had fully settled onto the ground platform. The model coordinates as described in Section 3.3.6.4 were unlocked and the forward dynamics simulation was performed for 0.2 seconds. The MoS of these test show that each of the model shows insignificant changes in the MoS when no external forces are applied, confirming the assumption that prior to external forces being applied to the models, the body is in a static standing position.

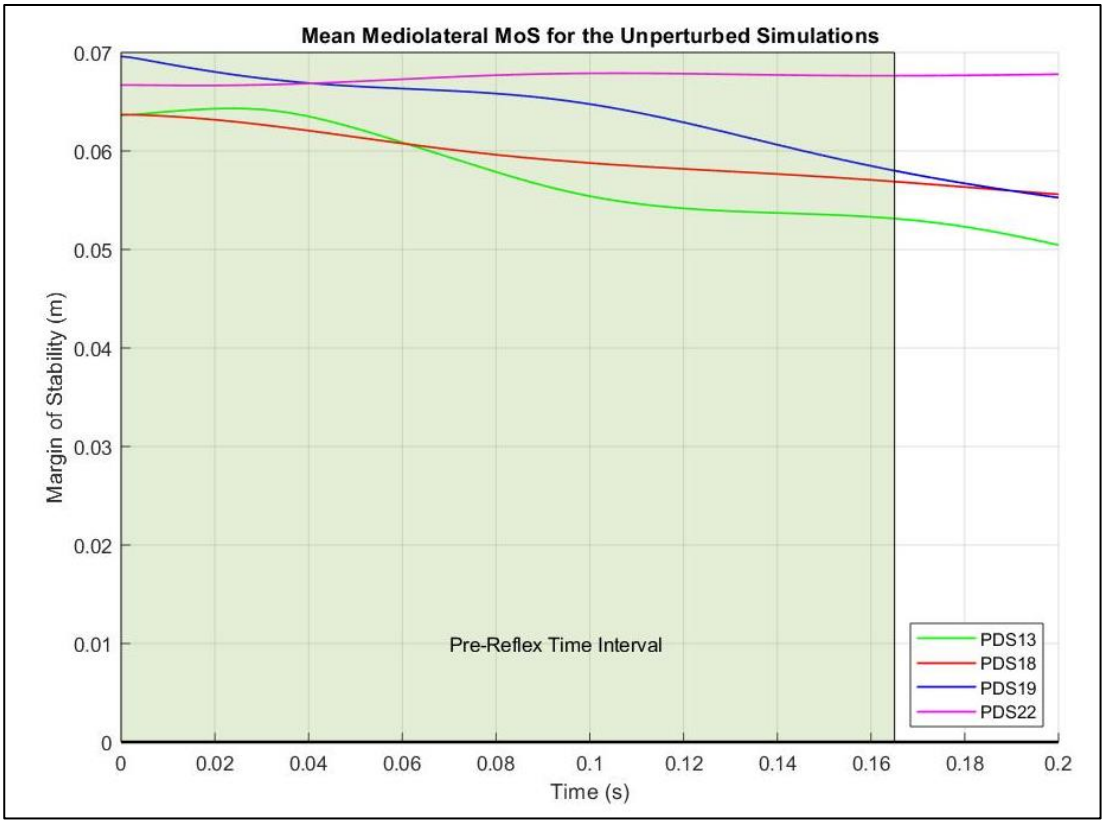

Figure 4-2. Mediolateral MoS for the four subjects with no perturbation or assistive torques applied to the model. The green shaded area represents the time interval before reflexes affect muscle forces.

4.3 Simulation Set B – Margin of Stability Without Assistance

The mean MoS during the unassisted simulations is shown in Figure 4-3. The grey area represents the time the lateral perturbation is being applied to the model and the green area represents the time before muscle reflexes begin to have substantial effects on the model's motion. A positive MoS indicates that the system is stable; a negative MoS indicates an unstable system that would result in a fall to the right-hand side of the subject if an alternative stabilizing strategy were not used (e.g., stepping). The 15% BW perturbation was the only unassisted condition that resulted in the mean MoS becoming negative. The 5% and 10% BW perturbations moved the models toward the unstable region; however, these perturbations did not cause the model to

become unstable within the time period before the muscle reflexes could contribute to avoiding a fall.

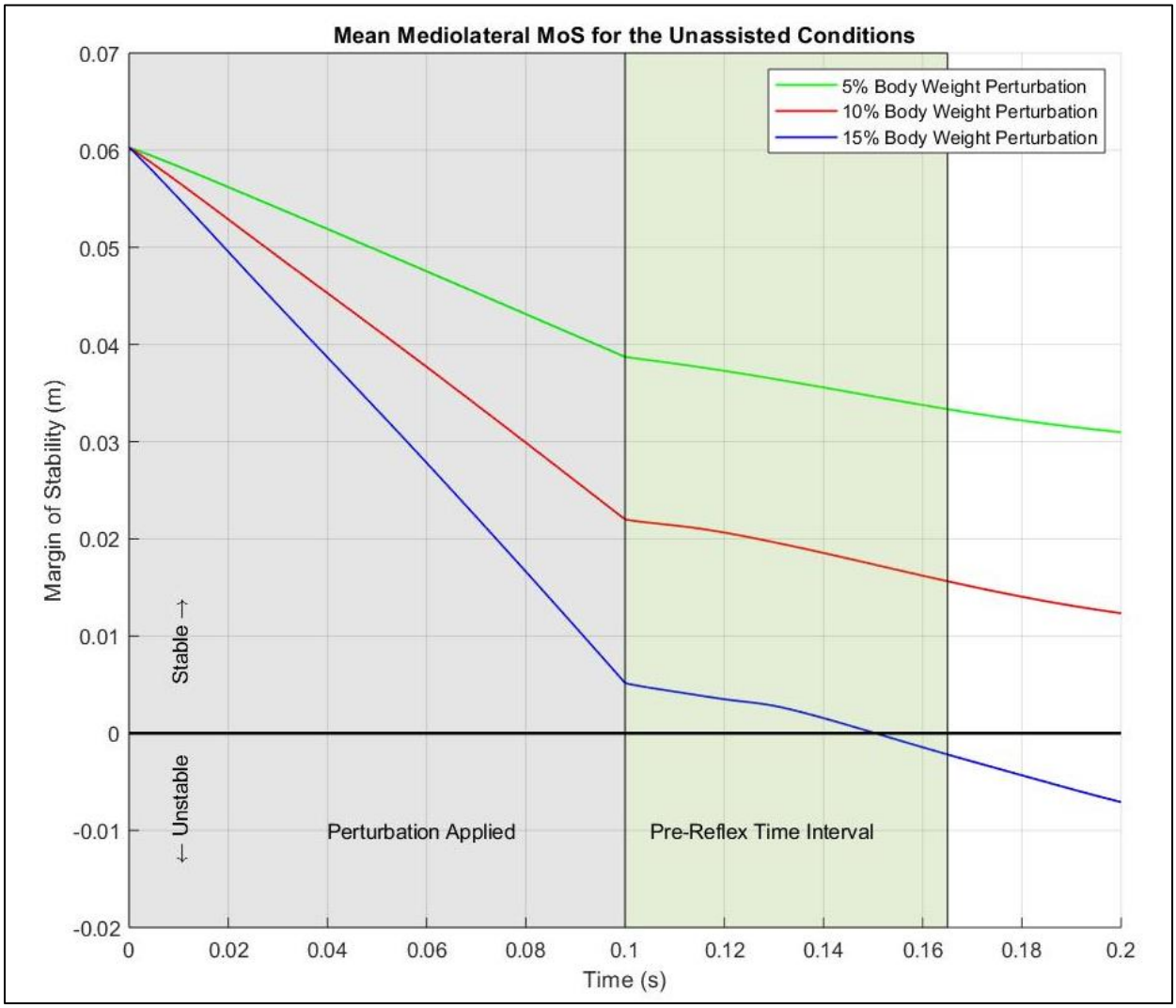

Figure 4-3. The mean MoS for the unassisted simulations with 5% (green), 10% (red) and 15% (blue) BW lateral pelvis perturbations. The grey shaded area indicates the time during which the perturbation was being applied to the model. The green shaded area represents the time interval before reflexes affect muscle forces.

To compare the MoS across each trial and loading condition, the MoS at the upper time bound (i.e. 0.165 seconds) was used. The mean MoS at the upper time bound for the 5%, 10% and 15% BW perturbations were 3.33 ± 1.75, 1.56 ± 1.75 and 0.23 ± 1.70 cm, respectively. Table 4-1 shows the MoS at the upper time bound for each subject when unassisted.

Table 4-1. The baseline mediolateral MoS for each subject at the upper time bound of the simulations when the models are unassisted. Mean and standard deviation (SD) are computed across the population.

Subject	Unassisted MoS (m)		
	5% BW Perturbation	**10% BW Perturbation**	**15% BW Perturbation**
PDS13	0.0328	0.0134	-0.0060
PDS18	0.0411	0.0248	0.0081
PDS19	0.0093	-0.0080	-0.0246
PDS22	0.0500	0.0321	0.0133
Mean ± SD	0.0333 ± 0.0175	0.0156 ± 0.0175	-0.0023 ± 0.0170

4.3.1 Center of Mass Displacement after the Perturbation

To verify that the location of the whole-body CoM was within a typical range after a perturbation was applied at the pelvis, comparisons were made to the observations of published studies. Rietdyk et al. investigated biomechanical responses to ML perturbations at the hip and shoulder. Their findings suggested that with a perturbation applied to the pelvis of magnitude 1.42 N/kg on average and duration 100 ms, the CoM experienced an approximately 1.25 cm lateral translation 0.165 s after the perturbation was applied [81]. (Recall that 0.165 s is the amount of time that is expected to elapse before muscle reflexes play a substantial role in determining the model's motion.) To investigate the CoM motion during the unassisted simulations, an additional unassisted FWD simulation was conducted for each subject where a lateral perturbation was applied at the pelvis in the positive Z-direction. The perturbation force was modelled as a constant force of magnitude 1.42 N/kg and duration 100 ms, replicating the conditions of the experiments performed by Rietdyk et al. and consistent with the experiments performed by Matjačić et al. [81], [88]. In these simulations, a mean ML CoM displacement of 1.35 cm was observed 0.165 s after the perturbation was applied. Therefore, the displacement of the CoM in our simulations was within a similar range as that observed by Rietdyk et al., with an average error of approximately 7.4%. The subjects from whom data were collected in the study performed by Rietdyk et al. were

ten male participants aged 26 ± 4.2 years, with no known disabilities. These subjects would likely be very effective at controlling stability; thus, an error would be expected between the simulation results on elderly subjects and the experimental observations of Rietdyk et al.

4.4 Simulation Set C.1 – Actuator Position and Torque Magnitude

The assisted simulations in part C.1 were generated to compare the effectiveness of contralateral hip abduction, ipsilateral hip adduction and bilateral HAA assistance on the MoS. The simulation framework was applied to the four elderly subjects for the 5%, 10% and 15% BW perturbations; the results for these three conditions are presented in Sections 4.4.1, 4.4.2, 4.4.3, respectively.

4.4.1 Mean ML MoS for the 5% Body Weight Perturbation

The MoS was averaged over all subjects at each point in time during the simulation (referred to as "mean MoS") and was used to quantify the effect of each assistance strategy on the MoS. Figure 4-4 shows the mean MoS with five magnitudes of contralateral hip abduction assistance vs. the unassisted condition for the 5% BW perturbations. The vertical dotted black line at 0.124 s indicates the time at which the actuators began applying assistive torques to the model's hip joints. A mean MoS greater than zero indicates a stable condition, while a negative mean MoS indicates an unstable condition.

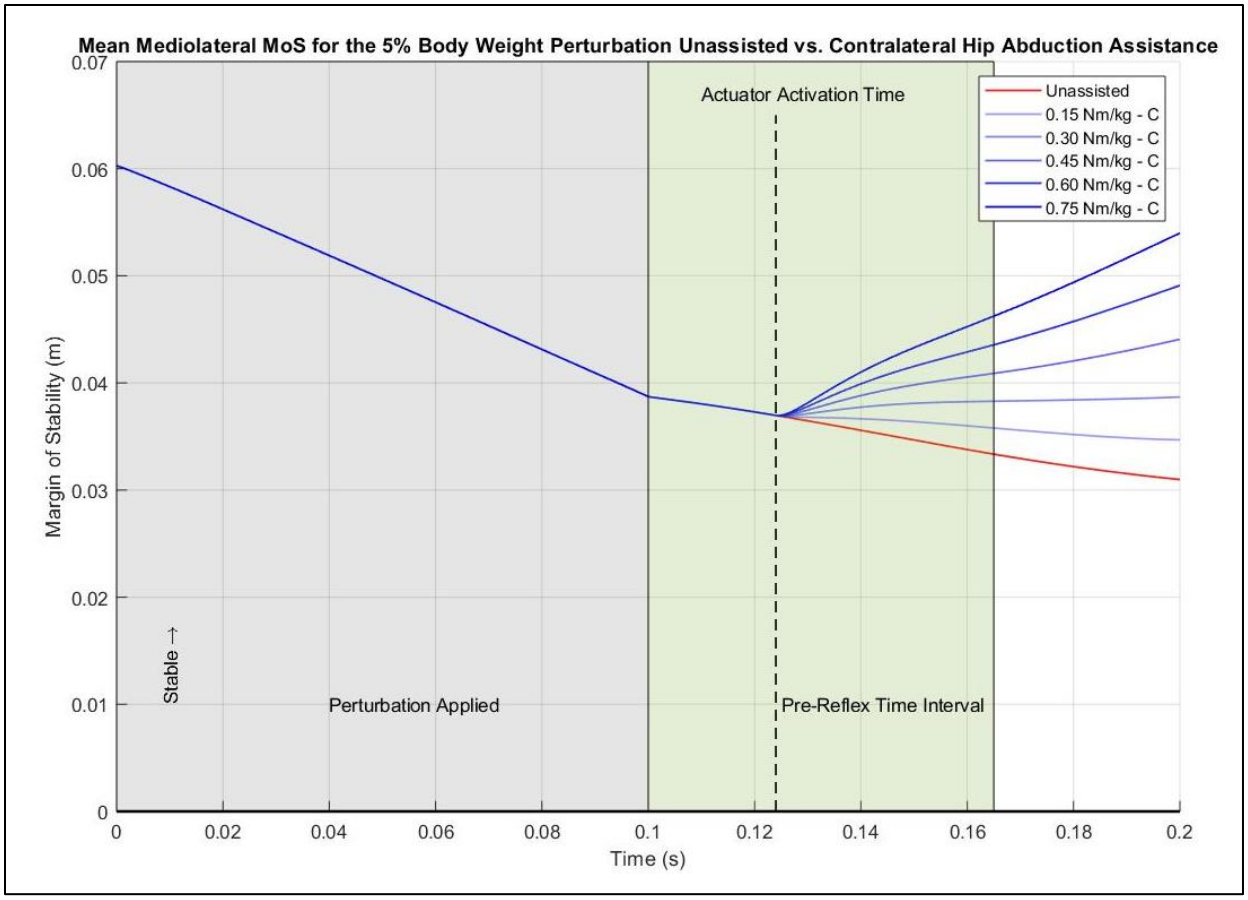

Figure 4-4. Mean ML MoS for the 5% BW perturbation. Unassisted (red line); contralateral hip abduction assistance (blue lines). The grey area indicates the time during which the lateral perturbation was applied to the model. The green area indicates the time during which muscle reflexes would not have a substantial effect on the model's motion. The vertical dashed line represents the time at which the exoskeleton begins applying assistive torques.

The mean MoS for contralateral hip abduction assistance improves as the assistive torque magnitude increases, as expected. The improvement in mean MoS is approximately linear with increases in the assistive magnitude. These results suggest that each increase in the magnitude of assistance results in an incremental increase in the MoS. A contralateral hip abduction torque of 0.75 N·m/kg provided the greatest improvement in the MoS, resulting in mean improvement of 1.31 ± 0.0987 cm at $t = 0.165$ s.

The mean MoS for the ipsilateral hip adduction assistance strategy is displayed in Figure 4-5. For clarity, assistive magnitudes of 0.15, 0.45 and 0.75 N·m/kg are shown (magnitudes of

0.30 and 0.60 N·m/kg were excluded). A complete visualization of the mean MoS with each magnitude of assistance is shown in Appendix B.

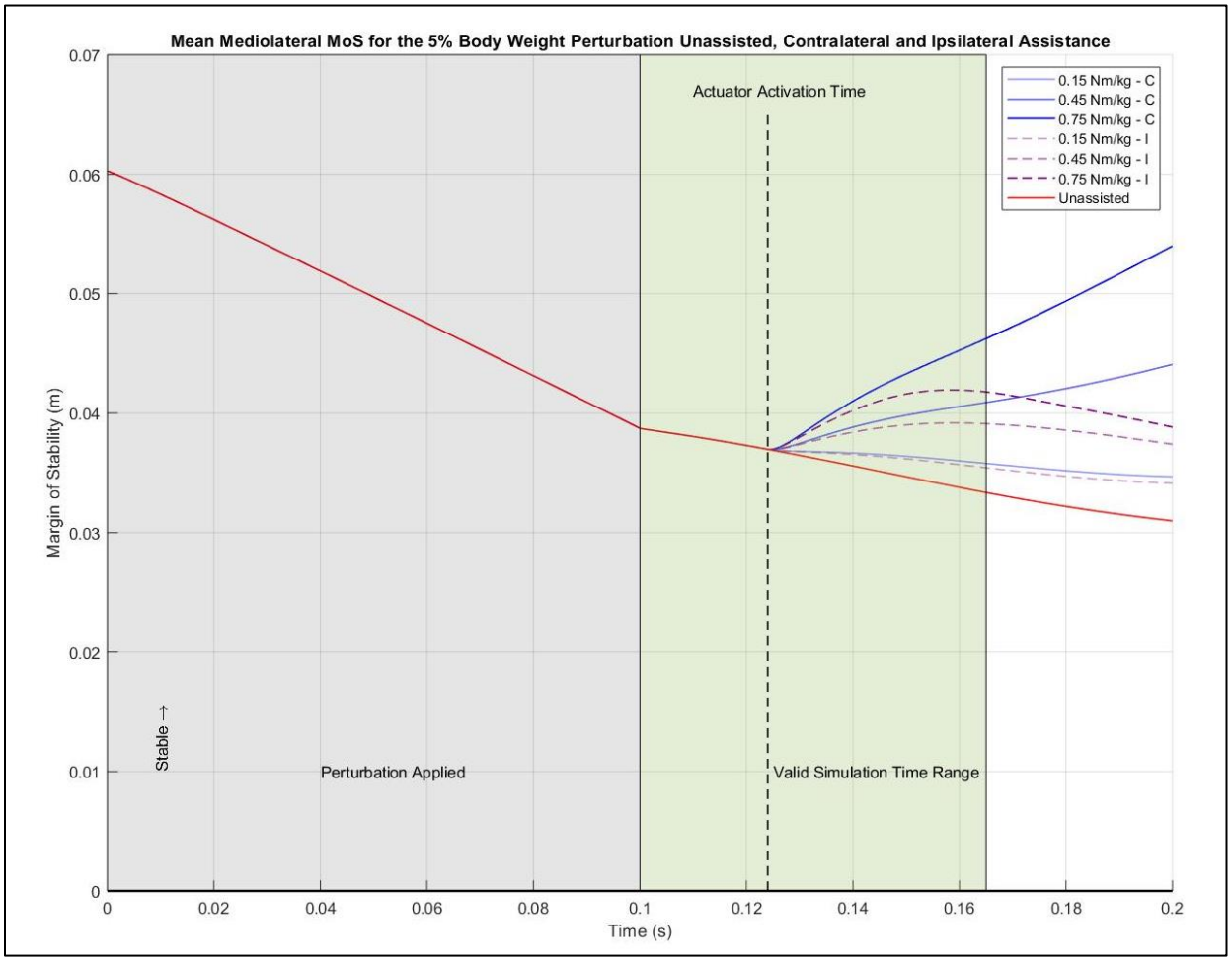

Figure 4-5. Mean ML MoS for the 5% BW perturbation condition showing the unassisted condition and the contralateral and ipsilateral assistance strategies. Unassisted (red line); contralateral hip abduction assistance (blue solid lines, "C"); ipsilateral hip adduction assistance (purple dashed lines, "I"). The grey area indicates the time during which the lateral perturbation was applied to the model. The green area indicates the time during which muscle reflexes would not have a substantial effect on the model's motion. The vertical dashed line represents the time at which the exoskeleton begins applying assistive torques.

Overall, the ipsilateral hip adduction assistance strategy was less effective at improving the MoS for each assistive magnitude tested. The greatest improvement with the ipsilateral assistance strategy occurred when the greatest assistive torque of 0.75 N·m/kg was applied to the subjects, yielding a mean improvement of 0.84 ± 0.14 cm at t = 0.165 s. It is possible that the ipsilateral hip adduction strategy is less effective is due to the kinematics of the body as it is subjected to the

lateral perturbation. When the perturbation is applied to the pelvis in the positive Z-direction, the vertical ground reaction force on the ipsilateral limb decreases while the weight of the body is transferred to the contralateral limb. Thus, when the ipsilateral hip exoskeleton assistance is activated, the ground reaction force beneath the ipsilateral foot is reduced, causing the foot to slip as increasing assistive torques are being applied to the subject. This decrease in ipsilateral hip adduction assistance effectiveness can be seen as the assistive magnitude increases by analyzing the rate of change of the MoS before reflexes begin to affect muscle forces, as shown in Figure 4-6.

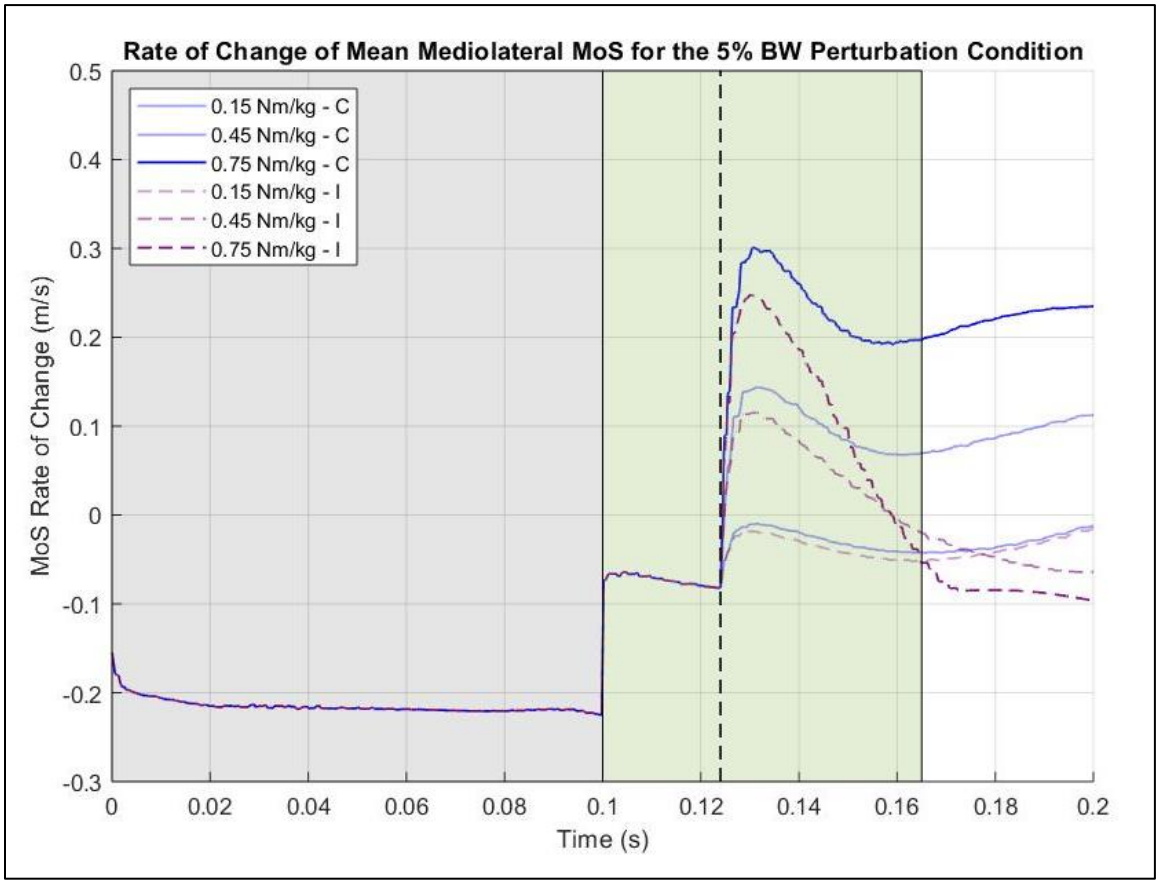

Figure 4-6. Rate of change for the mean ML MoS for the 5% BW perturbation condition showing the contralateral and ipsilateral assistance strategies. Contralateral hip abduction assistance (blue solid lines, "C"); ipsilateral hip adduction assistance (purple dashed lines, "I"). The grey area indicates the time during which the lateral perturbation was applied to the model. The green area indicates the time during which muscle reflexes would not have a substantial effect on the model's motion. The vertical dashed line represents the time at which the exoskeleton begins applying assistive torques.

In addition, as the ipsilateral torque magnitude increases, a sharper decrease in the MoS can be seen at approximately 0.13 seconds. Figure 4-6 also shows that the ipsilateral assistance strategy provides a brief amount of immediate assistance after the activation of the actuator; however, it is unable to continue improving the MoS of the models. Comparing the contralateral and ipsilateral assistance strategies in Figure 4-6 highlights the ability of the contralateral assistance strategy to continue improving the MoS for the duration of the simulation. For the 0.75 N·m/kg assistance condition, the contralateral hip abduction assistance resulted in an improvement in the MoS of 1.31 ± 0.0987 cm at t = 0.165 s, whereas the ipsilateral assistance strategy resulted in an improvement of only 0.84 ± 0.14 cm. The comparison of ipsilateral and contralateral HAA assistance at 0.75 N·m/kg provided an approximate difference in the improvement of the MoS of 0.46 cm. However, the 0.15 N·m/kg magnitude resulted in an improvement in the MoS of 0.24 ± 0.0117 cm for the contralateral strategy, whereas the ipsilateral strategy increased the MoS by 0.21 ± 0.00935 cm. The comparison of ipsilateral and contralateral HAA assistance at 0.15 N·m/kg provided an approximate difference in the improvement of the MoS of 0.0343 cm. Therefore, as the ipsilateral assistance magnitude increased, its capacity to improve the MoS decreased, suggesting there is an optimal magnitude of assistance when it is applied to the ipsilateral limb. It is hypothesized that this optimal magnitude is proportional to the vertical ground reaction force beneath the foot of the ipsilateral leg. A more detailed model that allows for hip, knee and ankle flexion/extension would be needed to investigate this aspect of ML balance control, as a combination of these movements have also been implemented as strategies to counteract ML perturbations biomechanically and through exoskeleton assistance [66], [88], [89]. Mechanically, for the assistive torque to be translated from the contralateral to ipsilateral hip joint, an additional

vertical force would need to be applied due to the translation of this force from the midplane of the body.

In Figure 4-7, the mean MoS with the bilateral assistance strategy is compared to the MoS for the contralateral assistance, ipsilateral assistance and the unassisted conditions for the 5% BW perturbation. For clarity, the simulations with assistive magnitudes of only 0.15, 0.45 and 0.75 N·m/kg are shown (the results for magnitudes of 0.30 and 0.60 N·m/kg were excluded). A complete visualization of the results using each magnitude of assistance is shown in Appendix B.

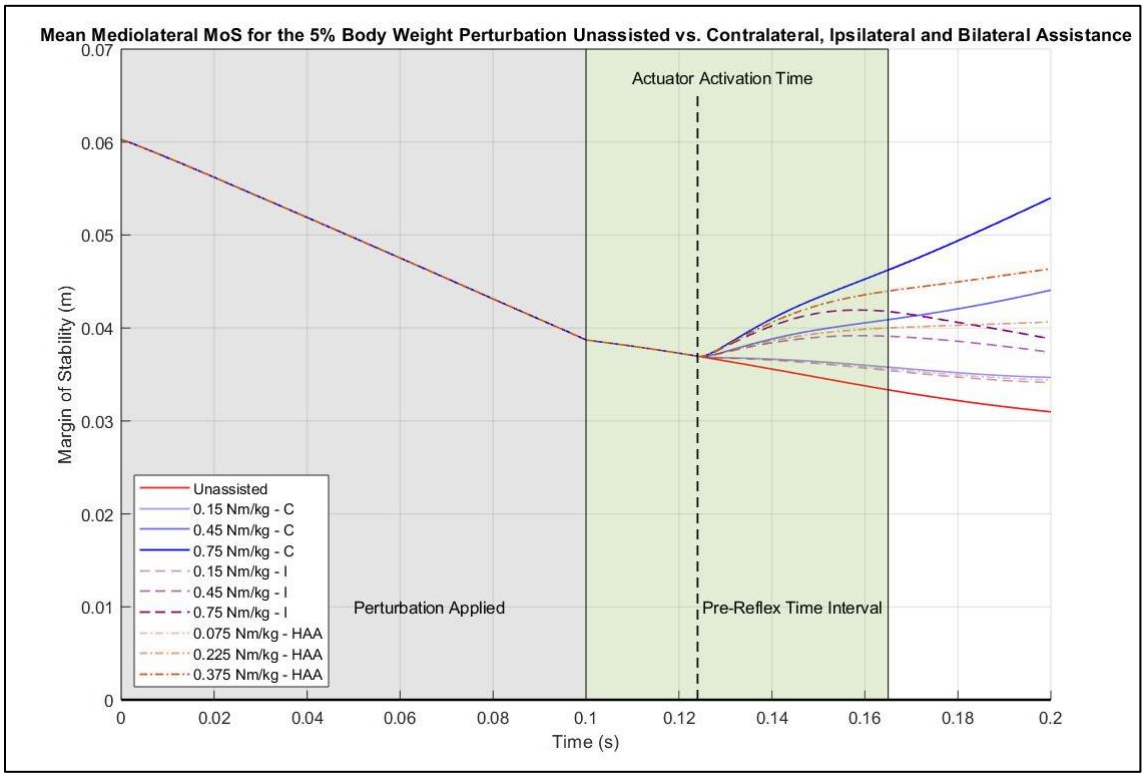

Figure 4-7. Mean ML MoS for the 5% BW perturbation condition showing the unassisted condition and the contralateral, ipsilateral and bilateral assistance strategies. Unassisted (red line); contralateral hip abduction assistance (blue solid lines, "C"); ipsilateral hip adduction assistance strategy (purple dashed lines, "I"); bilateral HAA assistance strategy (orange dash-dotted lines, "HAA"). The grey area indicates the time during which the lateral perturbation was applied to the model. The green area indicates the time during which muscle reflexes would not have a substantial effect on the model's motion. The vertical dashed line represents the time at which the exoskeleton begins applying assistive torques.

In general, the MoS when using the bilateral assistance strategy lies between the MoS when using the contralateral and ipsilateral strategies for each magnitude, which was expected since the

total assistive torque was divided equally between the two legs in the bilateral strategy. As was observed with the contralateral assistance strategy, the mean MoS for the bilateral strategy experiences a constant increase as the magnitude of assistive torque increases. In contrast, the mean MoS for the ipsilateral assistance strategy does not experience a constant improvement as the magnitude increases and the assistance strategy becomes less effective as the torque magnitude increases relative to the contralateral and bilateral strategies.

Table 4-2 shows the mean improvement in the MoS for each subject during the 5% BW perturbations for each assistance condition and torque magnitude at t = 0.165 s.

Table 4-2. Improvement in ML MoS at t = 0.165 s for the 5% BW perturbation. (SD = standard deviation.)

Subject	Unassisted MoS (m)	Assistance Magnitude (N·m/kg)	Contralateral		Ipsilateral		Bilateral (half assistance magnitude)	
			MoS (m)	Improvement (m)	MoS (m)	Improvement (m)	MoS (m)	Improvement (m)
PDS13	0.0328	0.15	0.0352	0.0024	0.0349	0.0021	0.0350	0.0022
		0.30	0.0376	0.0047	0.0370	0.0042	0.0373	0.0044
		0.45	0.0400	0.0072	0.0390	0.0062	0.0395	0.0067
		0.60	0.0425	0.0096	0.0409	0.0081	0.0417	0.0089
		0.75	0.0452	0.0123	0.0426	0.0098	0.0439	0.0110
PDS18	0.0411	0.15	0.0437	0.0026	0.0434	0.0022	0.0435	0.0024
		0.30	0.0464	0.0053	0.0455	0.0044	0.0459	0.0048
		0.45	0.0493	0.0082	0.0475	0.0064	0.0484	0.0072
		0.60	0.0522	0.0110	0.0491	0.0079	0.0506	0.0095
		0.75	0.0554	0.0143	0.0503	0.0091	0.0527	0.0116
PDS19	0.0093	0.15	0.0118	0.0025	0.0114	0.0021	0.0115	0.0022
		0.30	0.0145	0.0052	0.0131	0.0038	0.0138	0.0045
		0.45	0.0173	0.0079	0.0143	0.0050	0.0158	0.0065
		0.60	0.200	0.0107	0.0151	0.0058	0.0175	0.0082
		0.75	0.0228	0.0135	0.0160	0.0066	0.0194	0.0100
PDS22	0.0500	0.15	0.0524	0.0024	0.0520	0.0020	0.0522	0.0022
		0.30	0.0548	0.0048	0.0539	0.0039	0.0543	0.0043
		0.45	0.0572	0.0072	0.0556	0.0056	0.0564	0.0064
		0.60	0.0597	0.0097	0.0571	0.0071	0.0584	0.0084
		0.75	0.0622	0.0122	0.0581	0.0081	0.0602	0.0102
			Improvement (m)		Improvement (m)		Improvement (m)	
Mean ± SD	0.0333 ± 0.0175	0.15	$0.0024 \pm 1.17 \times 10^{-4}$		$0.0021 \pm 9.36 \times 10^{-5}$		$0.0022 \pm 1.10 \times 10^{-4}$	
		0.30	$0.005 \pm 2.89 \times 10^{-4}$		$0.0041 \pm 2.72 \times 10^{-4}$		$0.0045 \pm 2.04 \times 10^{-4}$	
		0.45	$0.0076 \pm 5.07 \times 10^{-4}$		$0.0058 \pm 6.17 \times 10^{-4}$		$0.0067 \pm 3.76 \times 10^{-4}$	
		0.60	$0.0103 \pm 7.06 \times 10^{-4}$		0.0072 ± 0.001		$0.0087 \pm 5.74 \times 10^{-4}$	
		0.75	$0.0131 \pm 9.87 \times 10^{-4}$		0.0084 ± 0.001		$0.0107 \pm 7.28 \times 10^{-4}$	

To clearly visualize the mean improvements in the ML MoS before the reflexes affect muscle forces, a box plot is presented in Figure 4-8 presenting the ML MoS at t = 0.165 s.

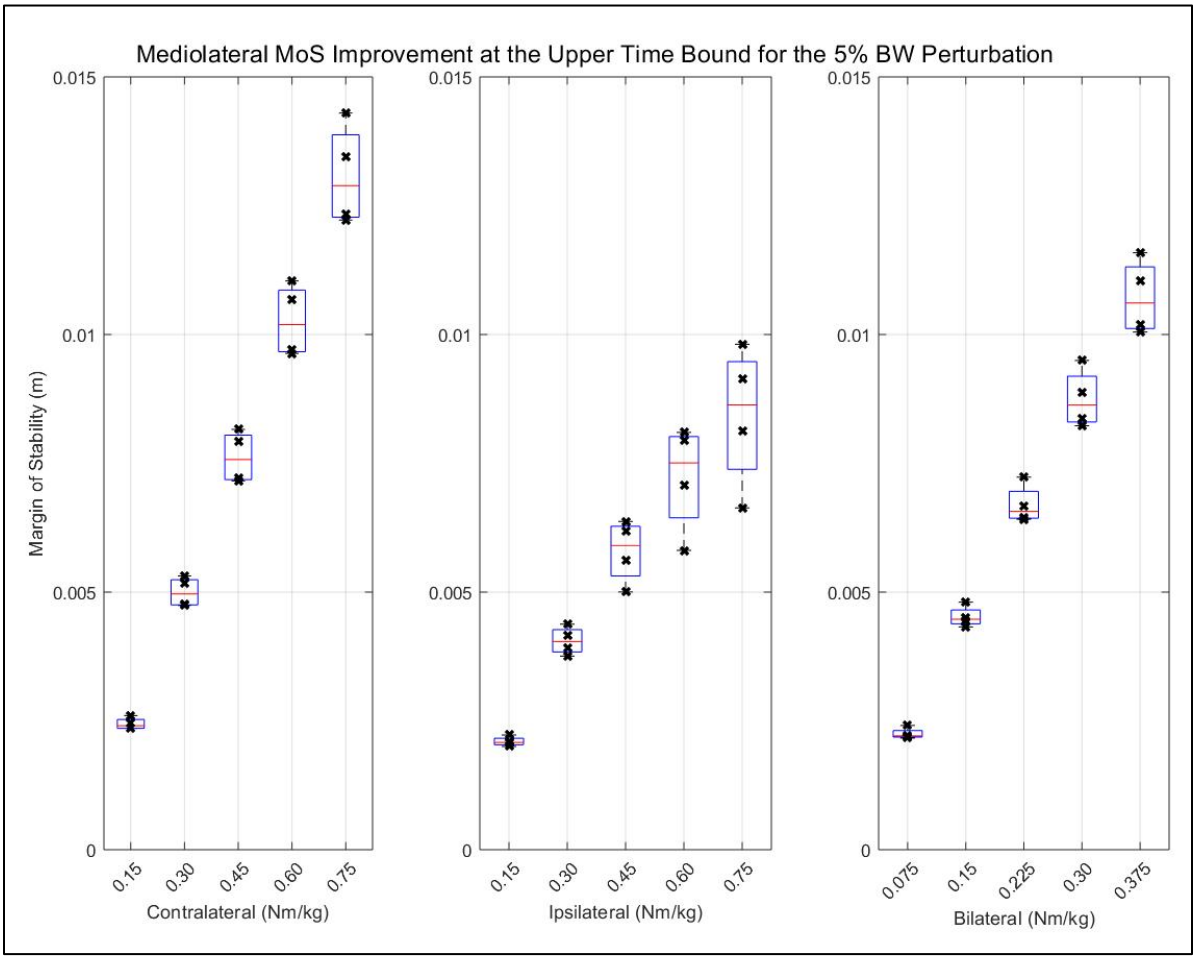

Figure 4-8. Box plot comparing the effectiveness of each assistance condition for the 5% BW perturbation condition. The red horizontal line indicates the mean value, while the lower and upper edges of the box indicate the 25th and 75th percentiles, respectively. The whiskers extend to the most extreme data points. Data are shown as black crosses.

The maximum standard deviations for the contralateral, ipsilateral, and bilateral strategies were 0.0987 cm, 0.1 cm and 0.0728 cm, respectively. When large standard deviations are observed within the simulated results, this could translate to greater difficulties designing assistive devices that accommodate different subjects and perturbation conditions [75]. Accommodating a wide range of individuals is especially difficult when designing exoskeletons that regulate stability,

since there is a vast variety of imbalances that elderly individuals may experience. Therefore, the relatively smaller standard deviation in MoS that was observed while providing the subjects with bilateral assistance compared to the contralateral and ipsilateral assistance strategies may be preferable for exoskeleton designers who wish to develop assistance strategies that apply to a range of activities requiring stabilization assistance.

4.4.1.1 Statistical Analysis

In this section, the statistical significance of the data obtained for the 5% BW perturbations is discussed. Repeated measures ANOVA and post-hoc paired t-tests were used to determine whether the mean improvements among actuator magnitudes and locations were significant. The null hypothesis states that there is no significant difference between contralateral vs. ipsilateral, contralateral vs. bilateral or ipsilateral vs. bilateral assistance strategies for any actuator magnitude. The results of the one-way repeated measures ANOVA are presented in Table 4-3. A Shapiro-Wilk Test determined that the normality assumption could not be rejected. Table 4-4 shows the results of the paired-sample t-tests, where a p-value less than 0.01 is interpreted as statistically significant evidence against the null hypothesis. A Bonferroni correction was not applied to the paired-sample t-tests due to the small sample size of the collected data.

Table 4-3. Results of the repeated measures ANOVA between MoS improvements for each assistance condition, actuator magnitude and actuator position evaluated for the 5% BW perturbations. P-values are reported; statistically significant differences are denoted by an asterisk (*).

Groups	**Repeated Measures ANOVA (p-value)**				
	0.15 N·m/kg	**0.30 N·m/kg**	**0.45 N·m/kg**	**0.60 N·m/kg**	**0.75 N·m/kg**
Contralateral vs. Ipsilateral vs Bilateral	0.00003226*	0.001217*	0.001953*	0.002838*	0.0149

Table 4-4. Results of the paired-sample t-tests between MoS improvements for each assistance condition, actuator magnitude and actuator position evaluated for the 5% BW perturbations. P-values are reported; statistically significant differences are denoted by an asterisk (*).

Groups	Paired-Sample t-Test (p-value)				
	0.15 N·m/kg	**0.30 N·m/kg**	**0.45 N·m/kg**	**0.60 N·m/kg**	**0.75 N·m/kg**
Contralateral vs. Ipsilateral	0.0006*	0.01523	0.01929	0.0236	0.01498
Contralateral vs. Bilateral	0.002896*	0.008754*	0.01626	0.02785	0.01508
Ipsilateral vs. Bilateral	0.01385	0.02586	0.02398	0.01988	0.01507

The results of the post-hoc paired-sample t-tests yielded statistically significant differences between the four subjects for 0.15 N·m/kg of contralateral vs. ipsilateral and contralateral vs. bilateral strategies. At assistance magnitudes greater than 0.15 N·m/kg, however, only the contralateral vs. bilateral strategies at 0.3 N·m/kg yielded a statistically significant difference.

The simulations using a bilateral HAA strategy suggest that half the assistive torque of the unilateral strategies applied bilaterally had very similar effects on the MoS for each individual torque magnitude simulated. For example, bilateral HAA assistance of 0.375 N·m/kg resulted in a mean improvement to the MoS of 1.07 ± 0.0728 cm compared to the unassisted condition, whereas 0.75 N·m/kg applied to the contralateral limb resulted in a 1.31 ± 0.0987 cm improvement to the mean MoS, as shown in Table 4-2. Although 0.75 N·m/kg applied to the contralateral limb resulted in a greater mean improvement in MoS than 0.375 N·m/kg applied bilaterally, it was desired to determine whether the mean improvement experienced between these two assistive strategies was statistically significant. Paired-sample t-tests were conducted between the mean improvement in MoS for each assistance location and magnitude; the results are summarized in Table 4-5 and Table 4-6. Assistance on the contralateral limb of 0.30 N·m/kg yielded no significant difference in MoS improvement compared to assisting the ipsilateral limb with 0.75 N·m/kg. In other words, the actuator acting on the contralateral limb hip joint was able to provide an equivalent amount of stability assistance to the subjects with 0.45 N·m/kg less torque applied to the body. However,

0.30 N·m/kg of contralateral assistance did not show a significant difference compared to 0.30 N·m/kg on the ipsilateral limb, suggesting that the position of the actuator does not have a large impact on the effectiveness of the exoskeleton when relatively small perturbation forces are applied to the pelvis.

Table 4-5. Results of the paired-sample t-tests between MoS improvements for the contralateral vs. ipsilateral assistance for the 5% BW perturbations. P-values are reported; statistically non-significant differences are denoted by the highlighted cells.

Ipsilateral (N·m/kg)	**Contralateral (N·m/kg)**				
	0.15	0.30	0.45	0.60	0.75
0.15	0.0015	1.42×10^{-4}	1.47×10^{-4}	1.34×10^{-4}	1.57×10^{-4}
0.30	8.09×10^{-4}	0.0123	8.60×10^{-4}	3.84×10^{-4}	2.85×10^{-4}
0.45	0.0015	0.1028	0.0212	0.0026	8.98×10^{-4}
0.60	0.0027	0.0302	0.5890	0.0224	0.0042
0.75	0.0033	0.0194	0.3899	0.1245	0.0142

Table 4-6. Results of the paired-sample t-tests between MoS improvements for the contralateral vs. bilateral HAA assistance for the 5% BW perturbations. P-values are reported; statistically non-significant differences are denoted by the highlighted cells.

Bilateral (N·m/kg)	**Contralateral (N·m/kg)**				
	0.15	0.30	0.45	0.60	0.75
0.075	0.0031	1.37×10^{-4}	1.43×10^{-4}	1.32×10^{-4}	1.54×10^{-4}
0.15	2.98×10^{-5}	0.0087	4.03×10^{-4}	2.30×10^{-4}	2.24×10^{-4}
0.225	8.44×10^{-5}	0.0015	0.0217	0.0011	4.52×10^{-4}
0.30	1.39×10^{-4}	7.56×10^{-4}	0.0334	0.0235	0.0018
0.375	1.44×10^{-4}	4.82×10^{-4}	0.0380	0.3628	0.0137

4.4.2 Mean ML MoS for the 10% Body Weight Perturbation

The mean MoS for the 10% BW perturbation conditions are shown in Figure 4-9. For this perturbation magnitude, similar overall trends in the results were observed compared to the 5% BW perturbation condition. Figure 4-9 displays the results for the contralateral, ipsilateral, and bilateral HAA assistance strategies. For clarity, results obtained using assistance magnitudes of only 0.15, 0.45 and 0.75 N·m/kg were included in the figure (results for 0.30 and 0.60 N·m/kg were excluded).

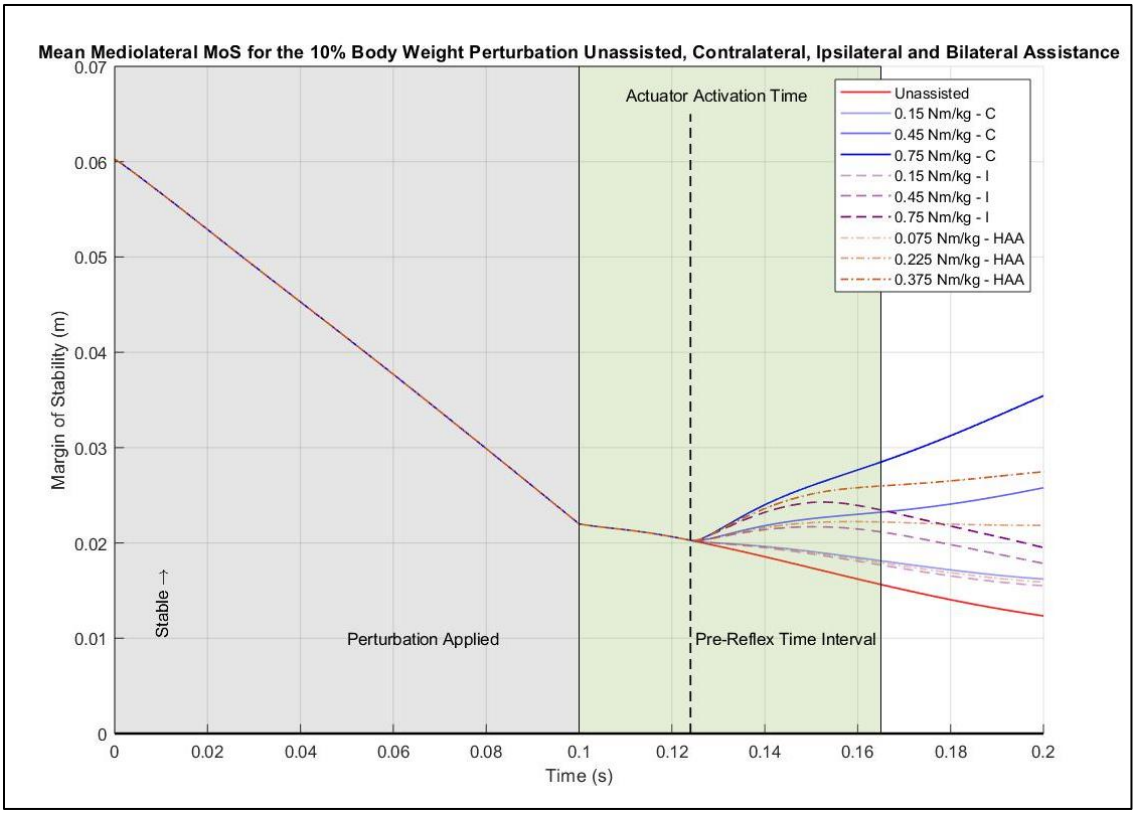

Figure 4-9. Mean ML MoS for the 10% BW perturbation condition showing the unassisted condition and the contralateral, ipsilateral and bilateral assistance strategies. Unassisted (red line); contralateral hip abduction assistance (blue solid lines, "C"); ipsilateral hip adduction assistance strategy (purple dashed lines, "I"); bilateral HAA assistance strategy (orange dash-dotted lines, "HAA"). The grey area indicates the time during which the lateral perturbation was applied to the model. The green area indicates the time during which muscle reflexes would not have a substantial effect on the model's motion. The vertical dashed line represents the time at which the exoskeleton begins applying assistive torques.

The results are consistent with those found for the 5% BW perturbation, where the contralateral assistance strategy provided the greatest mean MoS for each assistive torque magnitude. The ipsilateral assistance strategy was less effective at each magnitude, while also becoming less effective as the magnitude of assistance increased compared to the trend observed using the contralateral assistance strategy. The ipsilateral assistance strategy does not experience a linear improvement to MoS as the magnitude increases linearly. Similarly to the 5% BW perturbation condition, the ipsilateral strategy at 0.75 N·m/kg results in a sharp decline in MoS at approximately 0.15 s.

Table 4-7 outlines the mean improvement in the MoS for each subject during the 10% BW perturbations. The improvements (m) were evaluated at t = 0.165 s (i.e. 0.165 s after the perturbation was applied to the subject). The greatest improvement in MoS was observed when the 0.75 N·m/kg contralateral assistance strategy was used, yielding a mean improvement of 1.30 ± 0.0946 cm. A paired t-test determined that there was no significant difference in the improvement in MoS for the 5% BW perturbation condition vs. the 10% BW perturbation condition when 0.75 N·m/kg of contralateral hip abduction assistance was applied to the models (p=0.5452). Therefore, the contralateral hip abduction assistance strategy was able to maintain its effectiveness on the improvement in MoS when the perturbation magnitude increased from 5% to 10% BW.

Table 4-7. Improvement in ML MoS at t = 0.165 s for the 10% BW perturbation. (SD = standard deviation.)

Subject	Unassisted MoS (m)	Assistance Magnitude (N·m/kg)	Contralateral		Ipsilateral		Bilateral (half assistance magnitude)	
			MoS (m)	Improvement (m)	MoS (m)	Improvement (m)	MoS (m)	Improvement (m)
PDS13	0.0134	0.15	0.0158	0.0023	0.0153	0.0020	0.0157	0.0023
		0.30	0.0181	0.0048	0.0175	0.0041	0.0178	0.0044
		0.45	0.0205	0.0072	0.0195	0.0059	0.0200	0.0066
		0.60	0.0230	0.0097	0.0213	0.0076	0.0221	0.0086
		0.75	0.0254	0.0123	0.0228	0.0088	0.0242	0.0105
PDS18	0.0248	0.15	0.0274	0.0026	0.0270	0.0022	0.0272	0.0024
		0.30	0.0301	0.0053	0.0289	0.0040	0.0295	0.0046
		0.45	0.0328	0.0080	0.0305	0.0052	0.0317	0.0067
		0.60	0.0359	0.0111	0.0316	0.0061	0.0338	0.0086
		0.75	0.0388	0.0139	0.0324	0.0069	0.0357	0.0105
PDS19	-0.0080	0.15	-0.0054	0.0029	-0.0059	0.0024	-0.0056	0.0027
		0.30	-0.0026	0.0057	-0.0042	0.0042	-0.0034	0.0050
		0.45	0.0002	0.0084	-0.0029	0.0058	-0.0013	0.0071
		0.60	0.0029	0.0111	-0.0018	0.0074	0.0006	0.0092
		0.75	0.0056	0.0138	-0.0007	0.0086	0.0024	0.0112
PDS22	0.0321	0.15	0.0346	0.0025	0.0342	0.0020	0.0344	0.0023
		0.30	0.0370	0.0051	0.0360	0.0040	0.0365	0.0045
		0.45	0.0396	0.0076	0.0374	0.0056	0.0384	0.0066
		0.60	0.0419	0.0102	0.0384	0.0067	0.0402	0.0084
		0.75	0.0445	0.0125	0.0392	0.0074	0.0418	0.0100
			Improvement (m)		Improvement (m)		Improvement (m)	
Mean ± SD	0.0156 ± 0.0175	0.15	$0.0025 \pm 1.49 \times 10^{-4}$		$0.0021 \pm 1.20 \times 10^{-4}$		$0.0023 \pm 1.03 \times 10^{-4}$	
		0.30	$0.0051 \pm 3.67 \times 10^{-4}$		$0.0040 \pm 1.48 \times 10^{-4}$		$0.0045 \pm 1.59 \times 10^{-4}$	
		0.45	$0.0077 \pm 5.09 \times 10^{-4}$		$0.0056 \pm 4.06 \times 10^{-4}$		$0.0066 \pm 2.43 \times 10^{-4}$	
		0.60	$0.0104 \pm 7.75 \times 10^{-4}$		$0.0068 \pm 7.55 \times 10^{-4}$		$0.0086 \pm 3.81 \times 10^{-4}$	
		0.75	$0.0130 \pm 9.46 \times 10^{-4}$		0.0079 ± 0.0011		$0.0104 \pm 5.13 \times 10^{-4}$	

To clearly visualize the mean improvements on the ML MoS before the reflexes affect muscle forces, a box plot is presented in Figure 4-10 presenting the ML MoS at t = 0.165 s.

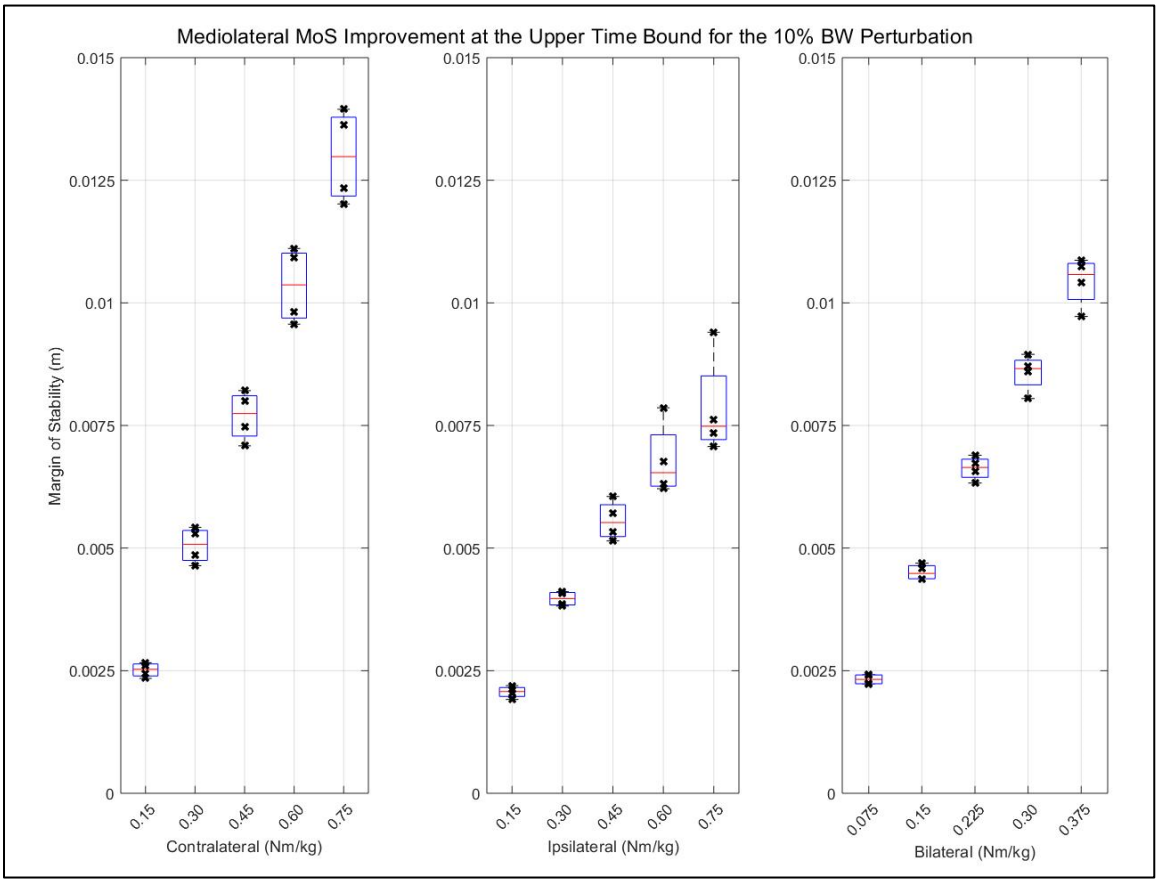

Figure 4-10. Box plot comparing the effectiveness of each assistance condition for the 10% BW perturbation condition. The red horizontal line indicates the mean value, while the lower and upper edges of the box indicate the 25th and 75th percentiles, respectively. The whiskers extend to the most extreme data points. Data are shown as black crosses.

The maximum standard deviations were 0.0946 cm, 0.11 cm, and 0.0513 cm for the contralateral, ipsilateral, and bilateral HAA assistance strategies, respectively. Compared to the 5% BW perturbation condition, the standard deviations for contralateral and ipsilateral assistance strategies were greater during the 10% BW perturbation condition, while the bilateral HAA strategy experienced smaller standard deviations for each torque magnitude.

4.4.2.1 Statistical Analysis

In this section, the statistical significance of the data obtained for the 10% BW perturbations is discussed. Repeated measures ANOVA and post-hoc paired t-tests were used to determine whether the mean improvement in MoS between actuator magnitude and location were significant. Table 4-8 shows the results of the repeated measures ANOVA, while

Table 4-9 shows the results of the paired-sample t-tests.

Table 4-8. Results of the repeated measures ANOVA between MoS improvements for each assistance condition, actuator magnitude and actuator position evaluated for the 10% BW perturbations. P-values are reported; statistically significant differences are denoted by an asterisk (*).

Groups	**Repeated Measures ANOVA (p-value)**				
	0.15 N·m/kg	**0.30 N·m/kg**	**0.45 N·m/kg**	**0.60 N·m/kg**	**0.75 N·m/kg**
Contralateral vs. Ipsilateral vs Bilateral	0.000103*	0.0182	0.01522	0.0008697*	0.0005107*

Table 4-9. Results of the paired-sample t-tests between MoS improvements for each assistance condition, actuator magnitude and actuator position evaluated for the 10% BW perturbations. P-values are reported; statistically significant differences are denoted by an asterisk (*).

Groups	**Paired-Sample t-Test (p-value)**				
	0.15 N·m/kg	**0.30 N·m/kg**	**0.45 N·m/kg**	**0.60 N·m/kg**	**0.75 N·m/kg**
Contralateral vs. Ipsilateral	0.002896*	0.01821	0.01569	0.01286	0.009766*
Contralateral vs. Bilateral	0.01628	0.02463	0.01437	0.01096	0.009657*
Ipsilateral vs. Bilateral	0.003239*	0.01322	0.01821	0.01492	0.01026

The results of the paired-sample t-tests show statistically significant differences for contralateral vs. ipsilateral and ipsilateral vs. bilateral assistance at 0.15 N·m/kg, as well as contralateral vs. ipsilateral and contralateral vs. bilateral assistance for the 0.75 N·m/kg conditions. At 0.30, 0.45 and 0.60 N·m/kg, no statistically significant differences were observed.

Table 4-10 and Table 4-11 show the results of the paired-sample t-tests comparing adjustments in actuator magnitude for the contralateral vs. ipsilateral and the contralateral vs.

bilateral assistance locations. No significant difference was found between providing exoskeleton assistance on the contralateral limb with 0.30 N·m/kg of torque vs. applying 0.75 N·m/kg of torque on the ipsilateral limb. Similarly, the results suggest that there is no significant difference between applying 0.45 N·m/kg on the contralateral hip joint vs. applying 0.225 N·m/kg (i.e. half the unilateral magnitude) bilaterally. This result is important to note, as low exoskeleton torques are desirable, specifically in the elderly population [51], [58], [59].

Table 4-10. Results of the paired-sample t-tests between MoS improvements for the contralateral vs. ipsilateral assistance for the 10% BW perturbations. P-values are reported; statistically non-significant differences are denoted by the highlighted cells.

Ipsilateral (N·m/kg)	**Contralateral (N·m/kg)**				
	0.15	0.30	0.45	0.60	0.75
0.15	7.47×10^{-4}	1.89×10^{-4}	1.02×10^{-4}	1.41×10^{-4}	1.22×10^{-4}
0.30	0.0012	0.0152	0.0010	5.20×10^{-4}	3.27×10^{-4}
0.45	0.0013	0.2415	0.0146	0.0025	0.0010
0.60	0.0022	0.0450	0.2224	0.0130	0.0036
0.75	0.0027	0.0236	0.8345	0.0523	0.0098

Table 4-11. Results of the paired-sample t-tests between MoS improvements for the contralateral vs. bilateral HAA assistance for the 10% BW perturbations. P-values are reported; statistically non-significant differences are denoted by the highlighted cells.

Bilateral (N·m/kg)	**Contralateral (N·m/kg)**				
	0.15	0.30	0.45	0.60	0.75
0.075	0.0058	2.57×10^{-4}	1.24×10^{-4}	1.62×10^{-4}	1.37×10^{-4}
0.15	1.36×10^{-5}	0.0190	4.64×10^{-4}	3.26×10^{-4}	2.22×10^{-4}
0.225	2.19×10^{-5}	0.0012	0.0127	0.0011	4.53×10^{-4}
0.30	5.75×10^{-5}	4.79×10^{-4}	0.0476	0.0123	0.0016
0.375	7.28×10^{-5}	3.24×10^{-4}	0.0040	0.8343	0.0104

4.4.3 Mean ML MoS for the 15% Body Weight Perturbation

The 15% BW perturbation is the maximum disturbance force that each subject was exposed to in this study. The mean MoS for the 15% BW perturbation conditions are shown in Figure 4-11. For this perturbation magnitude, the mean MoS when unassisted moves into the unstable region

approximately 0.15 s after the perturbation is applied. Again, the 0.15, 0.45 and 0.75 N·m/kg of contralateral and ipsilateral assistance are displayed, as well as 0.075, 0.225 and 0.375 N·m/kg of bilateral HAA assistance. Graphs displaying each assistive magnitude and actuator position have been provided in Appendix B.

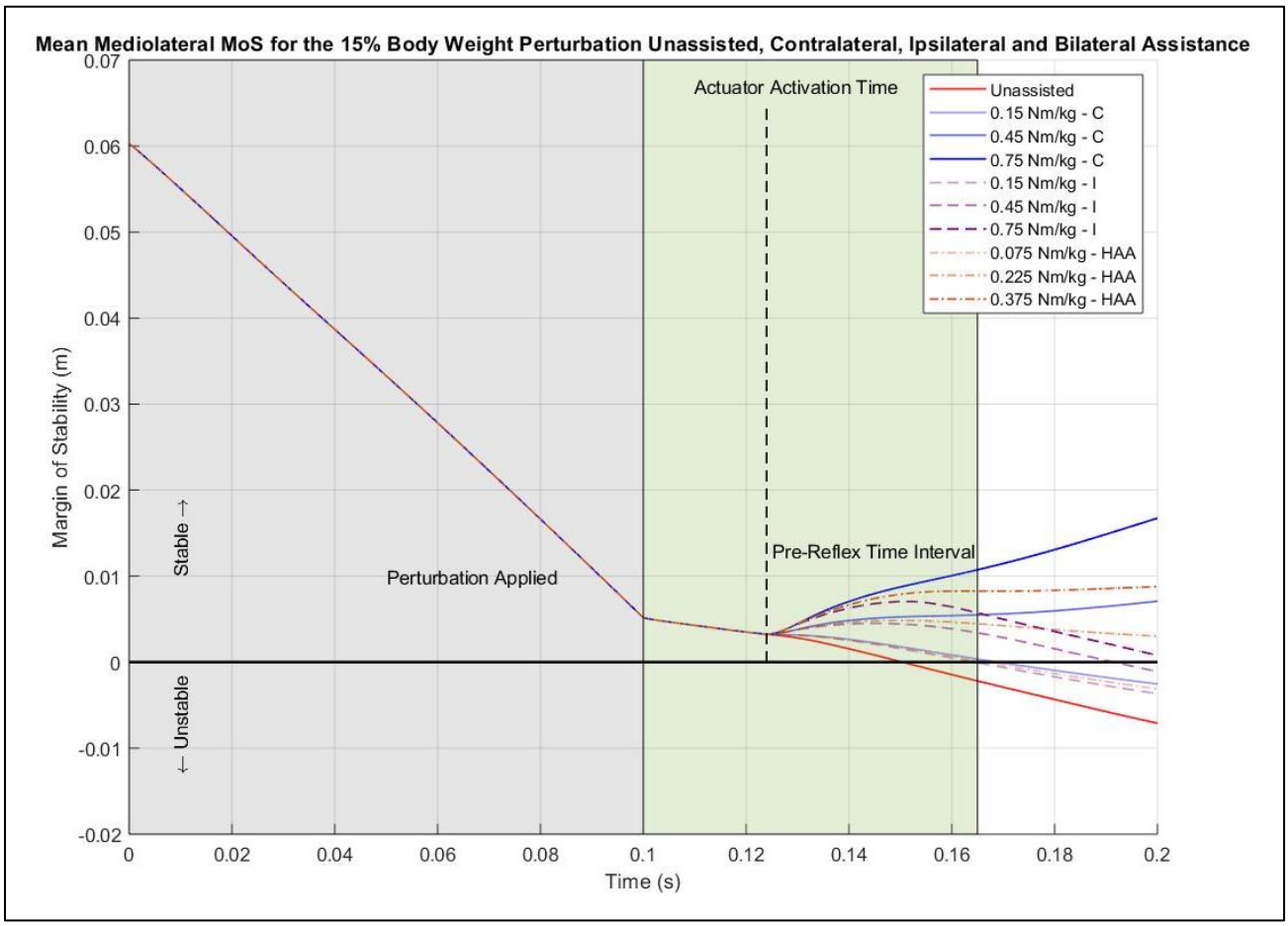

Figure 4-11. Mean ML MoS for the 15% BW perturbation condition showing the unassisted condition and the contralateral, ipsilateral and bilateral assistance strategies. Unassisted (red line); contralateral hip abduction assistance (blue solid lines, "C"); ipsilateral hip adduction assistance strategy (purple dashed lines, "I"); bilateral HAA assistance strategy (orange dash-dotted lines, "HAA"). The grey area indicates the time during which the lateral perturbation was applied to the model. The green area indicates the time during which muscle reflexes would not have a substantial effect on the model's motion. The vertical dashed line represents the time at which the exoskeleton begins applying assistive torques.

Mean MoS improvements were observed for the 0.15 and 0.3 N·m/kg contralateral, 0.15 and 0.3 N·m/kg ipsilateral, and 0.075 and 0.15 N·m/kg bilateral HAA assistance strategies; however, none of these assistance scenarios provided the subjects with enough assistance to return

to the stable region. However, it should be noted that each of these assistance strategies would increase the amount of time the elderly subjects would have to initiate an alternative strategy to prevent a fall, such as a stepping or braking strategy. The effect of each assistance strategy on the additional time an elderly person would have to react to bouts of imbalance is a secondary outcome of the current study and must be evaluated further. Similarly to the 5% BW perturbation condition, the rate of change of the MoS before reflexes begin to affect muscle forces can be observed in Figure 4-12. Figure 4-12 also shows a distinct transition from a positive rate of change to a negative rate of change at 0.13 s. The ipsilateral assistance strategy also shows an immediate improvement in the MoS for approximately 0.01 s after the assistive torque is applied to the body, however this level of assistance was not maintained as the simulation continued. In contrast, the contralateral assistance strategy was able to continue improving the MoS for the duration of the simulations.

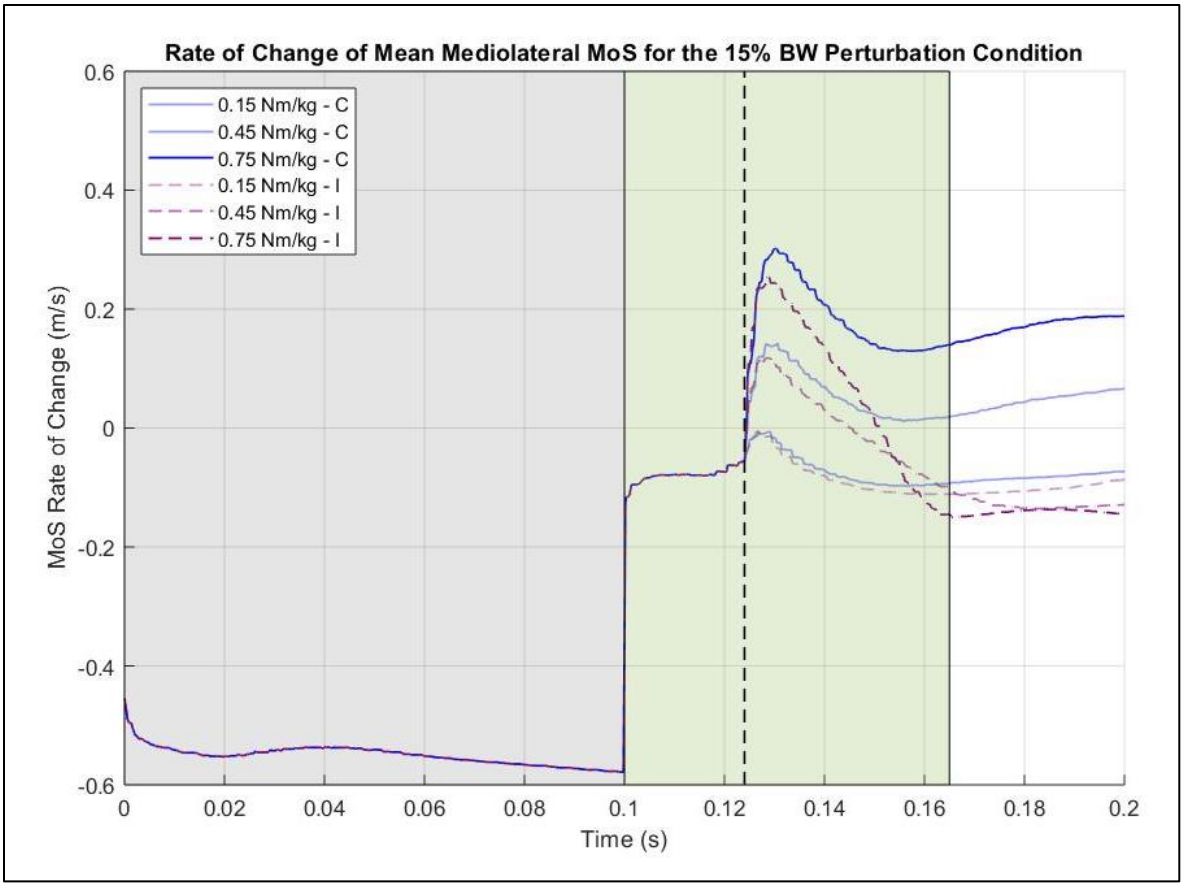

Figure 4-12. Rate of Change for the Mean ML MoS for the 15% BW perturbation condition showing the contralateral and ipsilateral assistance strategies. Contralateral hip abduction assistance (blue solid lines, "C"); ipsilateral hip adduction assistance (purple dashed lines, "I"). The grey area indicates the time during which the lateral perturbation was applied to the model. The green area indicates the time during which muscle reflexes would not have a substantial effect on the model's motion. The vertical dashed line represents the time at which the exoskeleton begins applying assistive torques.

The 0.45, 0.60 and 0.75 N·m/kg of contralateral hip abduction assistance provided the torque necessary to return the model to the stable region. Similarly, the 0.75 N·m/kg of ipsilateral hip adduction assistance was able to return the model to the stable region, however a sharp decline in the effectiveness of the assistive device was observed at approximately 0.15 seconds.

Table 4-12 outlines the mean improvement in the MoS for each subject during the 15% BW perturbations. The improvement (m) in MoS was evaluated at t = 0.165 s (recall that this is the time after the perturbation is applied before reflexes affect the muscle forces) after the perturbation was applied to the subject. The greatest improvement in the MoS was observed when

using the 0.75 N·m/kg contralateral assistance strategy, yielding a mean improvement of 1.31 ± 0.0816 cm. A paired t-test determined that no significant difference was experienced when the MoS improvement during the 10% and 15% BW perturbations were compared for 0.75 N·m/kg of contralateral hip abduction assistance (p=0.8634, p=0.2053). Therefore, it was determined that the contralateral hip abduction actuator was able to maintain its effectiveness at improving the MoS of the models when the perturbation magnitude increased from 10% to 15% BW.

Table 4-12. Improvement in ML MoS at t = 0.165 s for the 15% BW perturbation. (SD = standard deviation.)

Subject	Unassisted MoS (m)	Assistance Magnitude (N·m/kg)	Contralateral		Ipsilateral		Bilateral (half assistance magnitude)	
			MoS (m)	Improvement (m)	MoS (m)	Improvement (m)	MoS (m)	Improvement (m)
PDS13	-0.0060	0.15	-0.0037	0.0023	-0.0040	0.0020	-0.0037	0.0023
		0.30	-0.0012	0.0048	-0.0019	0.0041	-0.0016	0.0044
		0.45	0.0012	0.0072	-0.0001	0.0059	0.0005	0.0066
		0.60	0.0037	0.0097	0.0016	0.0076	0.0026	0.0086
		0.75	0.0063	0.0123	0.0028	0.0088	0.0045	0.0105
PDS18	0.0081	0.15	0.0108	0.0026	0.0103	0.0022	0.0105	0.0024
		0.30	0.0134	0.0053	0.0121	0.0040	0.0128	0.0046
		0.45	0.0162	0.0080	0.0134	0.0052	0.0148	0.0067
		0.60	0.0192	0.0111	0.0143	0.0061	0.0167	0.0086
		0.75	0.0220	0.0139	0.0150	0.0069	0.0186	0.0105
PDS19	-0.0246	0.15	-0.0217	0.0029	-0.0223	0.0024	-0.0220	0.0027
		0.30	-0.0190	0.0057	-0.0204	0.0042	-0.0197	0.0050
		0.45	-0.0163	0.0084	-0.0188	0.0058	-0.0175	0.0071
		0.60	-0.0136	0.0111	-0.0172	0.0074	-0.0154	0.0092
		0.75	-0.0109	0.0138	-0.0160	0.0086	-0.0134	0.0112
PDS22	0.0133	0.15	0.0159	0.0025	0.0154	0.0020	0.0157	0.0023
		0.30	0.0184	0.0051	0.0173	0.0040	0.0179	0.0045
		0.45	0.0210	0.0076	0.0189	0.0056	0.0200	0.0066
		0.60	0.0235	0.0102	0.0200	0.0067	0.0218	0.0084
		0.75	0.0259	0.0125	0.0208	0.0074	0.0234	0.0100
			Improvement (m)		Improvement (m)		Improvement (m)	
Mean ± SD	-0.0023 ± 0.0170	0.15	$0.0026 \pm 2.50 \times 10^{-4}$		$0.0021 \pm 1.87 \times 10^{-4}$		$0.0024 \pm 1.66 \times 10^{-4}$	
		0.30	$0.0052 \pm 3.83 \times 10^{-4}$		$0.0041 \pm 1.17 \times 10^{-4}$		$0.0046 \pm 2.47 \times 10^{-4}$	
		0.45	$0.0078 \pm 5.08 \times 10^{-4}$		$0.0056 \pm 2.92 \times 10^{-4}$		$0.0067 \pm 2.41 \times 10^{-4}$	
		0.60	$0.0105 \pm 6.74 \times 10^{-4}$		$0.0070 \pm 6.78 \times 10^{-4}$		$0.0087 \pm 3.32 \times 10^{-4}$	
		0.75	$0.0131 \pm 8.16 \times 10^{-4}$		$0.0079 \pm 9.31 \times 10^{-4}$		$0.0106 \pm 4.98 \times 10^{-4}$	

A box plot is presented in Figure 4-13 illustrating the improvements in the MoS at t = 0.165 s. Again, t = 0.165 s is the time prior to when muscle reflexes are estimated to affect the simulation results.

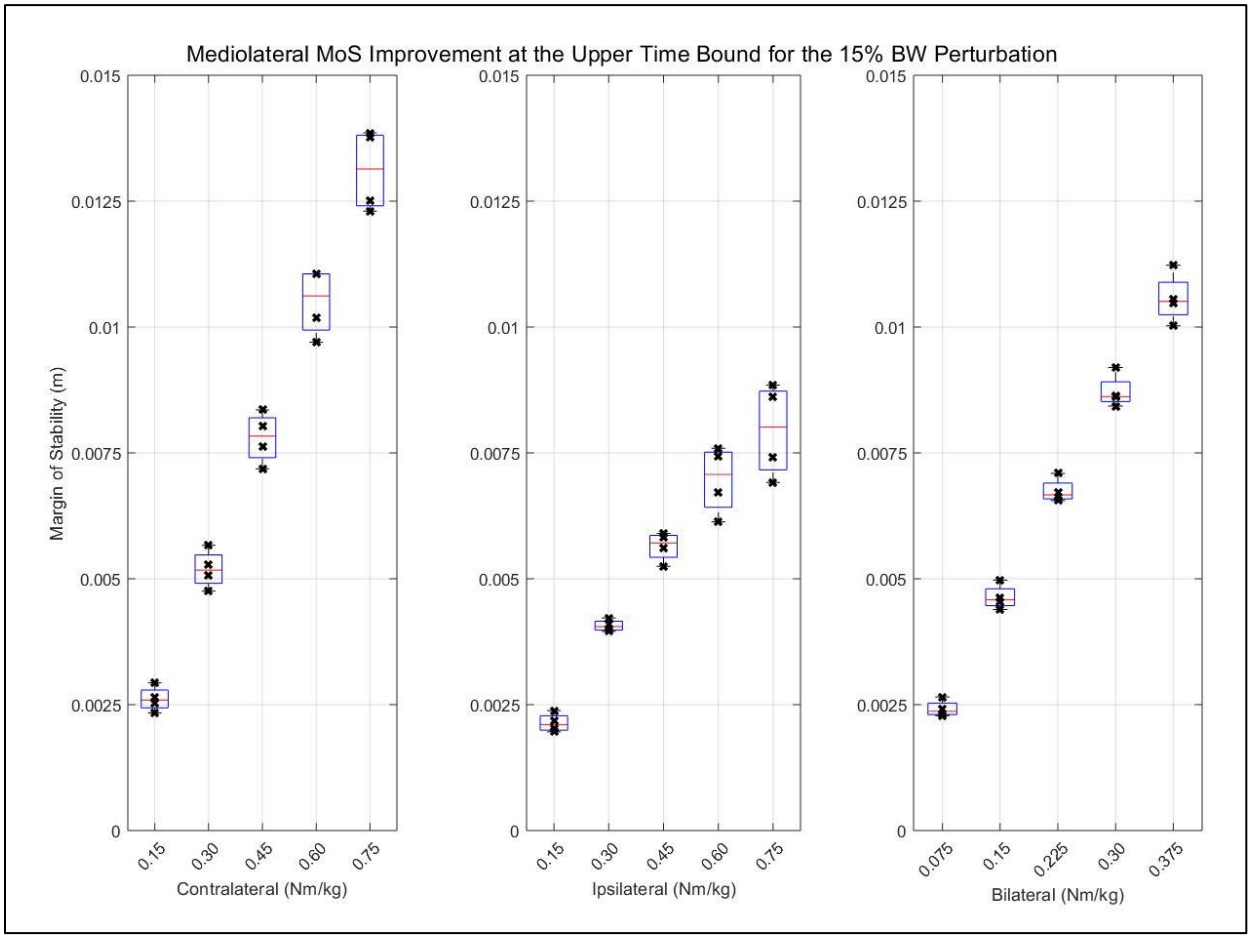

Figure 4-13. Box plot comparing the effectiveness of each assistance condition for the 15% BW perturbation condition. The red horizontal line indicates the mean value, while the lower and upper edges of the box indicate the 25th and 75th percentiles, respectively. The whiskers extend to the most extreme data points. Data are shown as black crosses.

The greatest standard deviations were 0.0816 cm, 0.0931 cm and 0.0498 cm for the contralateral, ipsilateral, and bilateral HAA actuators, respectively. Compared to the 5% and 10% BW perturbation conditions, the standard deviations were lower, suggesting that the observed results were more consistent across subjects during the 15% BW perturbation.

Overall, for each perturbation applied to the subjects, the mean MoS was most improved as the actuator torque magnitude increased. However, this is not the most user-friendly strategy as higher forces are potentially dangerous for the elderly as their bones are more fragile and fracture more easily [90]. There is also generally less muscle and fatty tissue to distribute the pressure at the body–device interface, potentially making the exoskeleton less comfortable [91]. In this way, the bilateral HAA assistance strategy has potential benefits in terms of both exoskeleton design and user satisfaction. Mechanically, higher actuator torque applied by an exoskeleton generally correlates with larger and heavier batteries and actuators to support the increased power requirements [92]. This is undesirable as elderly individuals are more affected by additional weight added to the body than younger adults, and heavier devices are more cumbersome to use (e.g., donning and doffing), also leading to higher device rejection [51], [58], [59].

4.4.3.1 Statistical Analysis

ANOVA and post-hoc paired t-tests were used to determine whether the mean improvement in MoS between actuator magnitudes and locations were significant. Table 4-14 shows the results of the paired-sample t-tests. The one-way ANOVA test calculated a p-value of 1.57×10^{-34}, indicating that the MoS improvements for each test were not equivalent.

Table 4-13. Results of the repeated measures ANOVA between MoS improvements for each assistance condition, actuator magnitude and actuator position evaluated for the 15% BW perturbations. P-values are reported; statistically significant differences are denoted by an asterisk (*).

Groups	**Repeated Measures ANOVA (p-value)**				
	0.15 N·m/kg	**0.30 N·m/kg**	**0.45 N·m/kg**	**0.60 N·m/kg**	**0.75 N·m/kg**
Contralateral vs. Ipsilateral vs Bilateral	0.0001671*	0.0002582*	0.0003116*	0.009166*	0.0001562*

Table 4-14. Results of the paired-sample t-tests between MoS improvements for each assistance condition, actuator magnitude and actuator position evaluated for the 15% BW perturbations. P-values are reported; statistically significant differences are denoted by an asterisk (*).

Groups	Paired-Sample t-Test (p-value)				
	0.15 N·m/kg	**0.30 N·m/kg**	**0.45 N·m/kg**	**0.60 N·m/kg**	**0.75 N·m/kg**
Contralateral vs. Ipsilateral	0.003013*	0.006687*	0.007582*	0.009173*	0.005372*
Contralateral vs. Bilateral	0.05767	0.003437*	0.007966*	0.007859*	0.004288*
Ipsilateral vs. Bilateral	0.001609*	0.01322	0.00763*	0.01069	0.006603*

Table 4-15. Results of the paired-sample t-tests between MoS improvements for the contralateral vs. ipsilateral assistance for the 15% BW perturbations. P-values are reported; statistically non-significant differences are denoted by the highlighted cells.

Ipsilateral (N·m/kg)	**Contralateral (N·m/kg)**				
	0.15	0.30	0.45	0.60	0.75
0.15	0.0010	7.90×10^{-5}	5.57×10^{-5}	6.43×10^{-5}	5.96×10^{-5}
0.30	8.85×10^{-4}	0.0074	5.98×10^{-4}	3.13×10^{-4}	1.97×10^{-4}
0.45	6.47×10^{-4}	0.1806	0.0074	0.0015	6.45×10^{-2}
0.60	0.0013	0.0224	0.1775	0.0087	0.0022
0.75	0.0016	0.0131	0.8211	0.0325	0.0054

Table 4-16. Results of the paired-sample t-tests between MoS improvements for contralateral vs bilateral assistance for the 15% BW perturbations. The P-value is reported, while statistically non-significant differences are denoted by the highlighted cells.

Bilateral (N·m/kg)	**Contralateral (N·m/kg)**				
	0.15	0.30	0.45	0.60	0.75
0.075	0.0283	1.54×10^{-4}	8.57×10^{-5}	8.74×10^{-5}	7.54×10^{-5}
0.15	1.07×10^{-6}	0.0047	2.08×10^{-4}	1.60×10^{-4}	1.19×10^{-4}
0.225	1.34×10^{-6}	3.79×10^{-4}	0.0068	7.08×10^{-4}	3.05×10^{-4}
0.30	1.04×10^{-5}	9.66×10^{-5}	0.0164	0.0081	9.90×10^{-4}
0.375	2.85×10^{-5}	9.17×10^{-5}	0.0012	0.8340	0.0047

The results in Table 4-14 suggest that by assisting the contralateral limb, greater improvements in the ML MoS can be obtained while providing less torque to the body compared to the ipsilateral and bilateral assistance strategies. This observation is less conclusive during the 5% and 10% BW perturbation conditions as there are greater standard deviations in these results (see Figure 4-8, Figure 4-10 and Figure 4-13). It can also be observed that as the perturbation

magnitude increases, the standard deviation of the MoS improvement increases for the contralateral and ipsilateral assistance strategies, while the standard deviation decreases for the bilateral assistance strategy for each magnitude tested.

Furthermore, as was the case with the 5% and 10% BW perturbation simulations, the results for a 15% BW perturbation suggest that exoskeleton designers should prioritize assisting the contralateral limb when developing assistance strategies to improve ML stability. The results also suggest that contralateral-limb assistance is increasingly important as perturbation magnitude increases, or as the MoS moves further into the unstable region; this is also due to the weight of the body being transferred to the contralateral limb as discussed in Section 4.4.1. Similarly to the 5% and 10% BW perturbations, the ipsilateral assistance strategy became less effective with the larger 15% BW perturbation magnitude and with larger assistive torque magnitudes.

4.4.4 Summary

Contralateral hip abduction assistance was the most effective strategy to improve the MoS of the elderly subjects. Bilateral HAA assistance was more effective than ipsilateral hip adduction assistance, but not as effective as contralateral hip abduction assistance. It was also found that as perturbation magnitude increased, the contralateral limb's role in stabilizing the body became more important. These trends are consistent with biological coordination of joint torques to improve the ML MoS investigated by Rietdyk et al. In their study, it was found that the greatest joint torques of the balance recovery response following a perturbation applied to the pelvis (listed from greatest to least amount of compensatory torque) was provided at the contralateral hip, the ipsilateral hip, the contralateral ankle and the ipsilateral ankle [81].

As perturbation magnitude increased, the standard deviation of the improvement in MoS increased for the contralateral and ipsilateral assistance strategies; however, smaller standard deviations were observed for the bilateral assistance strategy at each torque magnitude. The smaller standard deviations observed for the improvement in MoS with the bilateral assistance strategy suggest that the bilateral HAA exoskeleton could be more adaptable to loading conditions and bouts of imbalance, as well as different subject-specific parameters such as body mass index (BMI), muscle strength and reflex speed, among many others [75].

Regardless of the perturbation magnitude, each actuator position and torque magnitude improved the ML MoS of each subject. This finding is important as it suggests that a HAA assistive exoskeleton can be adaptable to many perturbation conditions that elderly subjects would frequently encounter. The exoskeleton's adaptability to other external forces applied to the body should be explored in detail, such as perturbations applied at the shoulder and other locations on the body. Future work will be discussed in Section 5.3. The results of this study suggest that the perturbation magnitude does not influence the improvement to the MoS when wearing the HAA assistive exoskeleton compared to the unassisted MoS, regardless of actuator position. However, due to the small sample size used in this study, further investigation is necessary.

4.5 Simulation Set C.2 – Actuator Torque Magnitude and Timing

The simulations in set C.2 were conducted to investigate the effect of actuator timing on the MoS of the elderly subjects. The simulation framework was applied to the four elderly subjects for the 15% BW perturbation as outlined in Section 3.3.6.6.

4.5.1 Mean ML MoS for Contralateral Hip Abduction Assistance with Faster Actuators

The assistance torque from the actuators that were simulated in Section 4.4 were activated by a controller at t = 0.124 s, as described in Section 3.3.6.5. The activation time of 0.124 s is referred to as the nominal activation time for the remainder of the results. In this section, the results of the simulation when the time delay of the controller signal that is activating the contralateral torque actuator is modified to be 5%, 10% and 15% faster than the nominal activation time investigated in Section 4.4. Figure 4-14 displays the results for the contralateral assistance strategy when the actuator was activated at the nominal activation time as described in Section 4.4.3 for assistive torques of 0.15 N·m/kg, 0.45 N·m/kg and 0.75 N·m/kg (results for 0.30 and 0.60 N·m/kg were excluded).

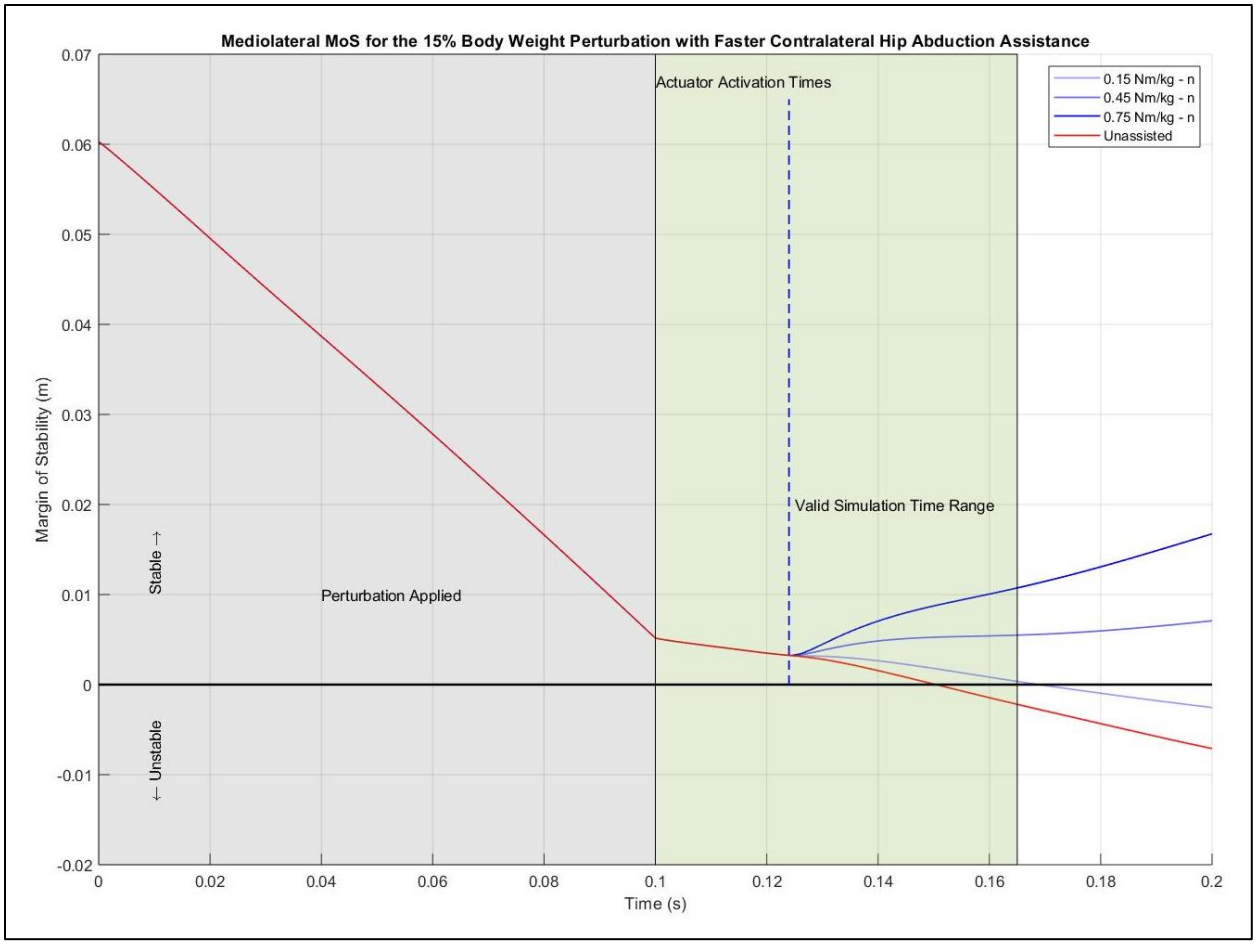

Figure 4-14. Mean ML MoS for the 15% BW perturbation. Unassisted (red lines); contralateral hip abduction assistance (blue lines). The grey area indicates the time during which the lateral perturbation was applied to the model. The green area indicates the time during which muscle reflexes would not have a substantial effect on the model's motion. The vertical dashed line represents the time at which the exoskeleton begins applying assistive torques.

A discussion of the results observed in Figure 4-14 can be found in Section 4.4.3. Next, Figure 4-15 displays the mean MoS of the subjects when the activation time of the contralateral hip actuator was 5% faster than the nominal activation time.

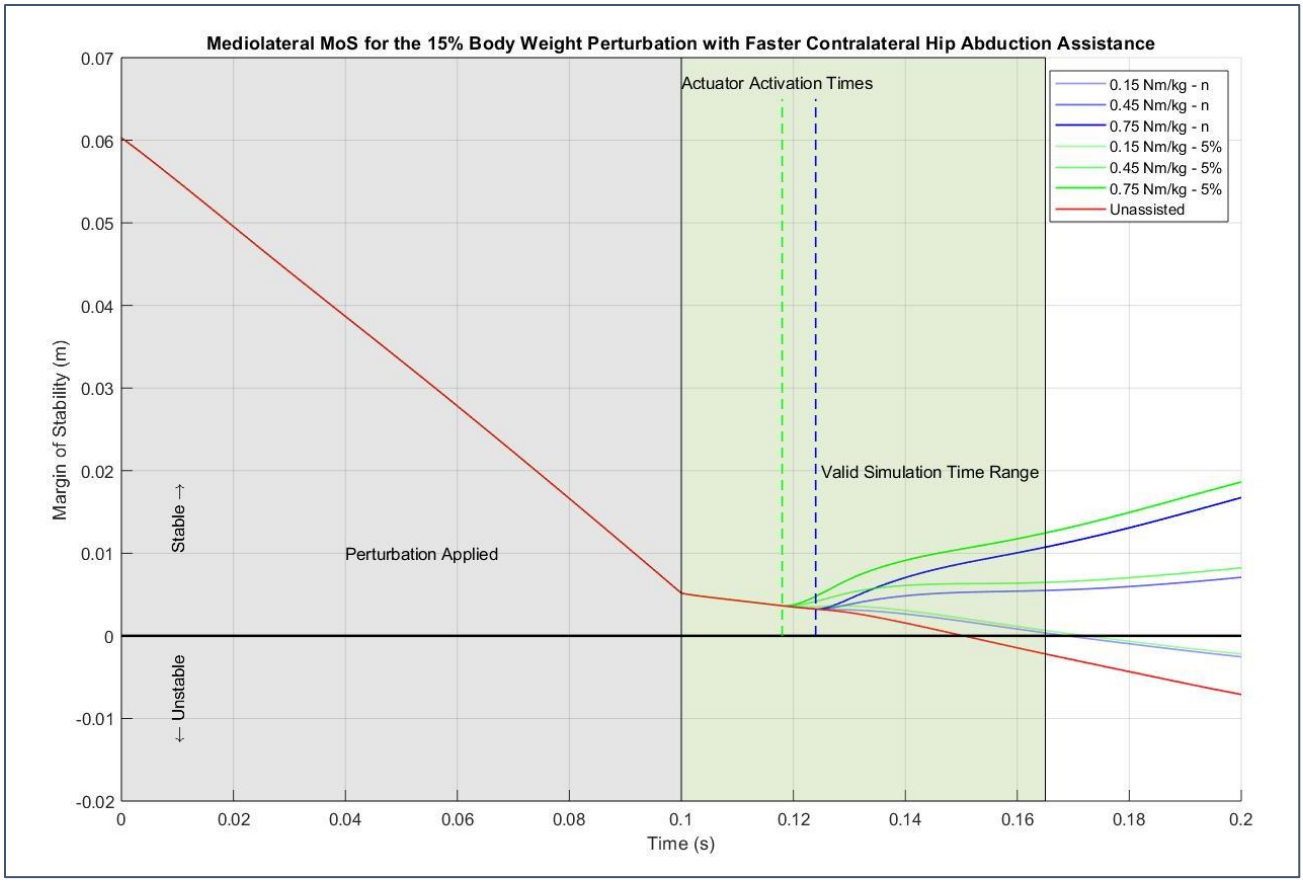

Figure 4-15. Mean ML MoS for the 15% BW perturbation. Unassisted (red lines); contralateral hip abduction assistance nominal activation time (blue lines, "n"); contralateral hip abduction assistance 5% faster activation time (green lines, "5%"). The grey area indicates the time during which the lateral perturbation was applied to the model. The green area indicates the time during which muscle reflexes would not have a substantial effect on the model's motion. The vertical dashed line represents the time at which the exoskeleton begins applying assistive torques.

It can be seen from Figure 4-15 that an approximately constant improvement is experienced between the nominal activation time and the 5% faster actuator for each assistive torque magnitude. The 0.15 N·m/kg actuator that was 5% faster was able to improve the mean MoS beyond the improvement achieved by the neutrally timed 0.15 N·m/kg actuator; however, neither was able to avoid instability. Both of these assistance strategies resulted in an unstable MoS just after the region where the subjects' reflexes would begin to affect the muscle forces. For each of the 0.45 N·m/kg and 0.75 N·m/kg actuators, the MoS improved when the actuator torque was applied to the body, and the mean MoS continued increasing as the simulation progressed. Figure

4-16 and Figure 4-17, also include the results from the 10% and 15% faster actuator activation times, corresponding to the contralateral hip abduction torque being initiated at t = 0.112 s and 0.105 s, respectively.

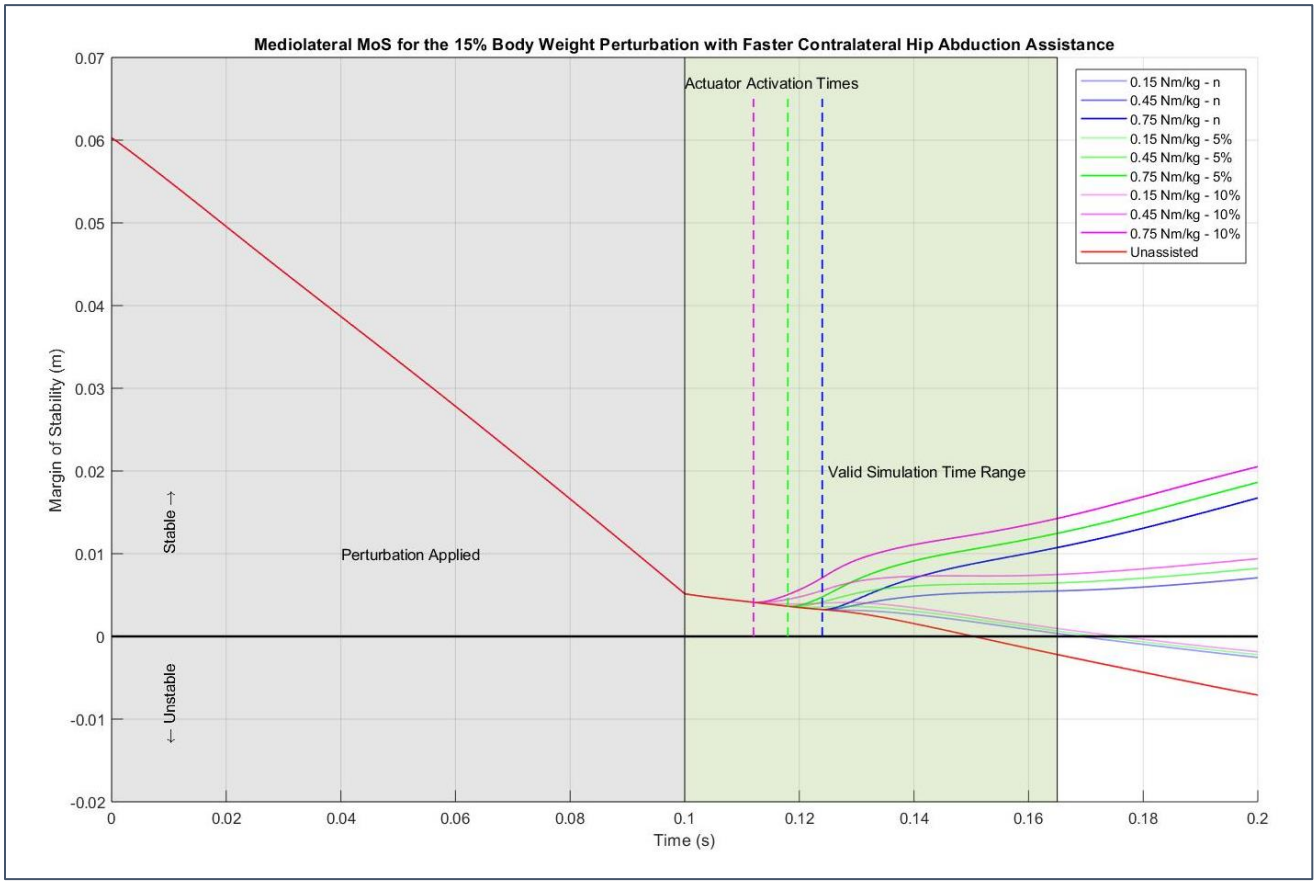

Figure 4-16. Mean ML MoS for the 15% BW perturbation. Unassisted (red lines); contralateral hip abduction assistance nominal activation time (blue lines, "n"); contralateral hip abduction assistance 5% faster activation time (green lines, "5%"); contralateral hip abduction assistance 10% faster activation time (magenta lines, "10%"). The grey area indicates the time during which the lateral perturbation was applied to the model. The green area indicates the time during which muscle reflexes would not have a substantial effect on the model's motion. The vertical dashed line represents the time at which the exoskeleton begins applying assistive torques.

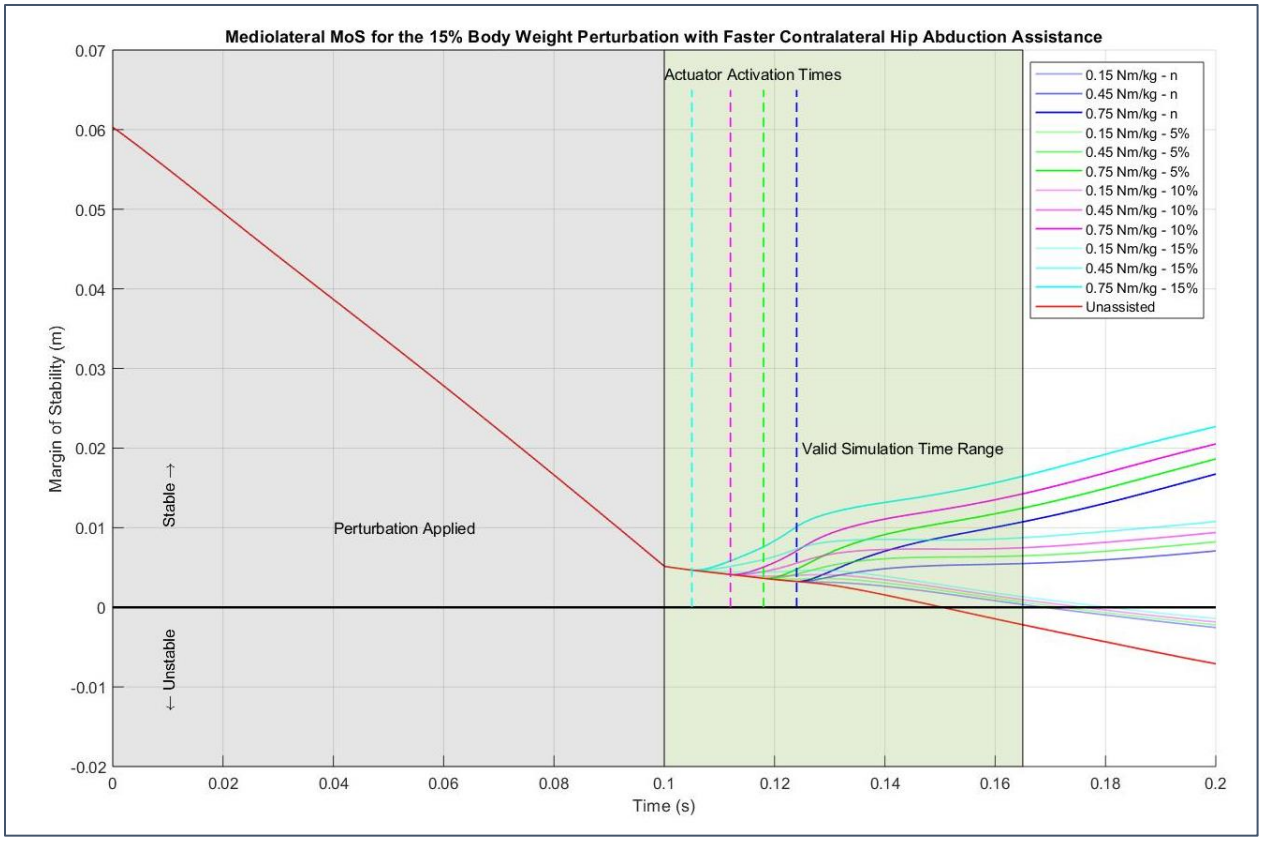

Figure 4-17. Mean ML MoS for the 15% BW perturbation. Unassisted (red lines); contralateral hip abduction assistance nominal activation time (blue lines, "n"); contralateral hip abduction assistance 5% faster activation time (green lines, "5%"); contralateral hip abduction assistance 10% faster activation time (magenta lines, "10%"); contralateral hip abduction assistance 15% faster activation time (cyan lines, "15%"). The grey area indicates the time during which the lateral perturbation was applied to the model. The green area indicates the time during which muscle reflexes would not have a substantial effect on the model's motion. The vertical dashed line represents the time at which the exoskeleton begins applying assistive torques.

The results displayed in Figure 4-17 show that the greatest improvement in the mean MoS occurred when the actuator was the fastest (activated at t = 0.105 s) and with the greatest torque (0.75 N·m/kg). This result was expected because after the perturbation was applied at the pelvis, the CoM of the body began to move towards the lateral BoS and increased in velocity as the time after the perturbation increased. Greater perturbation magnitudes and greater delays between the perturbation and the generation of assistive torque both result in greater lateral velocity of the body as the MoS moves toward the unstable region. Therefore, greater assistive torque is needed to have similar effects on the MoS of the subjects when longer time delay is observed between the

perturbation being applied to the body and the activation of assistive torque. By decreasing the delay between the perturbation and the generation of assistive torque, the negative effects the perturbation has on the body decrease, therefore the MoS prior to activating the assistive torque is not as close to the unstable region, as seen by the intersection of the dotted lines for each actuator activation time in Figure 4-17. The improvement to the MoS before reflexes affect the muscle forces at t = 0.165 s was calculated and is displayed in Table 4-17. This table shows each subject's MoS improvement for each actuator speed, as well as the mean and standard deviation for each condition.

Table 4-17. Improvement in ML MoS at nominal activation time and 5%, 10% and 15% faster activation time of the assistive contralateral hip abduction torques for the 15% BW perturbation. (SD = standard deviation.)

Subject	**Assistance Magnitude (N·m/kg)**	**Nominal Activation Time (0.124 s)**	**5% Faster (0.118 s)**	**10% Faster (0.112 s)**	**15% Faster (0.105 s)**
		Improvement (m)	**Improvement (m)**	**Improvement (m)**	**Improvement (m)**
PDS13	0.15	0.0023	0.0026	0.0028	0.0029
	0.30	0.0048	0.0052	0.0056	0.0061
	0.45	0.0072	0.0079	0.0087	0.0096
	0.60	0.0097	0.0108	0.0120	0.0133
	0.75	0.0123	0.0138	0.0152	0.0170
PDS18	0.15	0.0026	0.0029	0.0032	0.0035
	0.30	0.0053	0.0059	0.0065	0.0073
	0.45	0.0080	0.0091	0.0102	0.0115
	0.60	0.0111	0.0125	0.0139	0.0156
	0.75	0.0139	0.0157	0.0175	0.0197
PDS19	0.15	0.0029	0.0034	0.0037	0.0043
	0.30	0.0057	0.0065	0.0074	0.0084
	0.45	0.0084	0.0096	0.0109	0.0125
	0.60	0.0111	0.0127	0.0145	0.0167
	0.75	0.0138	0.0158	0.0181	0.0209
PDS22	0.15	0.0025	0.0029	0.0032	0.0035
	0.30	0.0051	0.0057	0.0063	0.0070
	0.45	0.0076	0.0085	0.0094	0.0105
	0.60	0.0102	0.0112	0.0125	0.0141
	0.75	0.0125	0.0140	0.0156	0.0174
		Improvement (m)	**Improvement (m)**	**Improvement (m)**	**Improvement (m)**
Mean ± SD	0.15	$0.0026 \pm 2.50\times10^{-4}$	$0.0029 \pm 3.05\times10^{-4}$	$0.0032 \pm 3.87\times10^{-4}$	$0.0036 \pm 5.74\times10^{-4}$
	0.30	$0.0052 \pm 3.83\times10^{-4}$	$0.0058 \pm 5.26\times10^{-4}$	$0.0064 \pm 7.32\times10^{-4}$	$0.0072 \pm 9.43\times10^{-4}$
	0.45	$0.0078 \pm 5.08\times10^{-4}$	$0.0088 \pm 7.27\times10^{-4}$	$0.0098 \pm 9.47\times10^{-4}$	0.0110 ± 0.0013
	0.60	$0.0105 \pm 6.74\times10^{-4}$	$0.0118 \pm 9.53\times10^{-4}$	0.0132 ± 0.0012	0.0149 ± 0.0015
	0.75	$0.0131 \pm 8.16\times10^{-4}$	0.0148 ± 0.0011	0.0166 ± 0.0014	0.0188 ± 0.0019

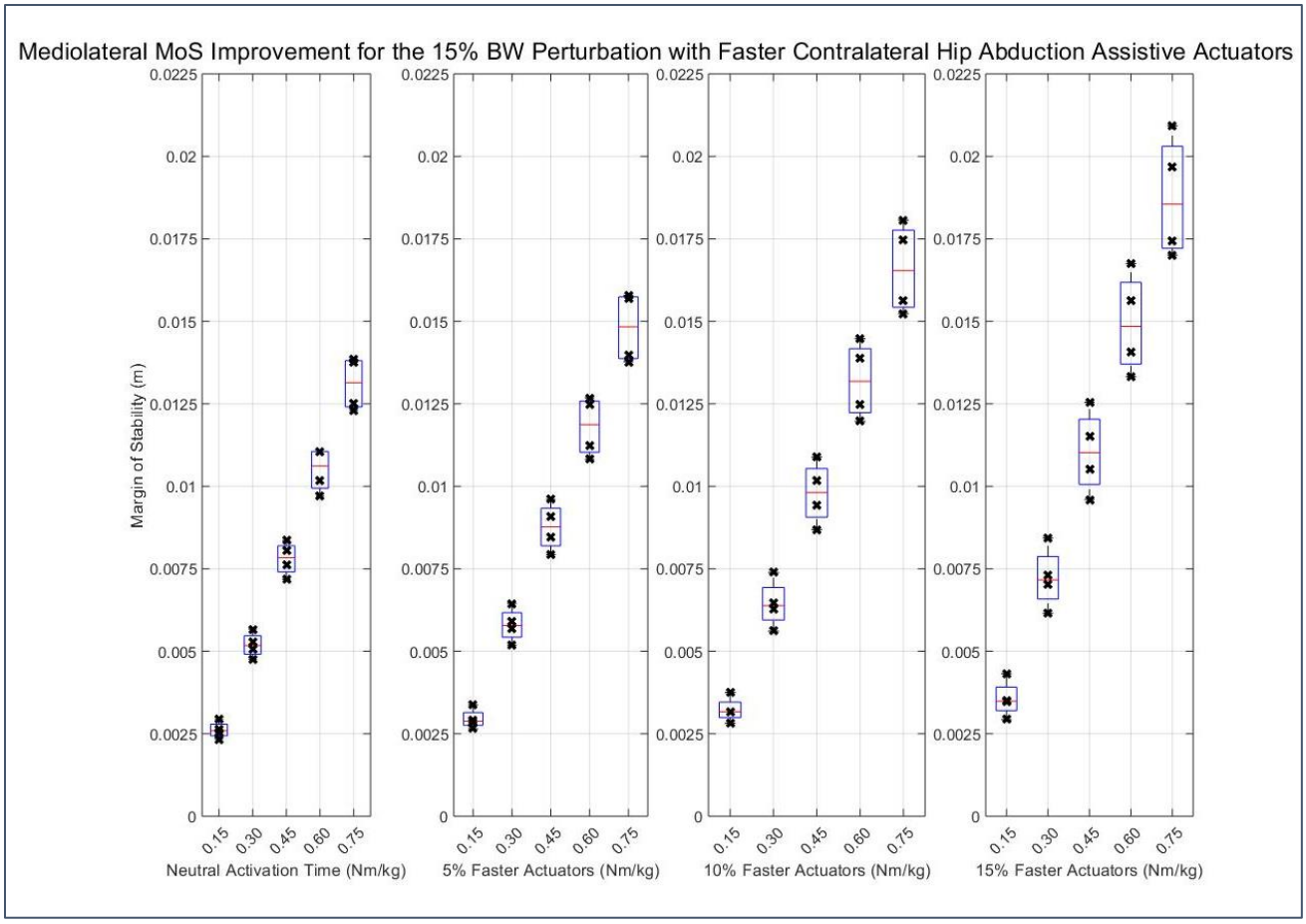

Figure 4-18. Box plot comparing the effectiveness of each assistance condition for the 15% BW perturbation condition. The red horizontal line indicates the mean value, while the lower and upper edges of the box indicate the 25th and 75th percentiles, respectively. The whiskers extend to the most extreme data points. Data are shown as black crosses.

Figure 4-18 displays a box chart of the results from Table 4-17 showing the change in mean MoS for the faster contralateral hip abduction actuators. As actuator speed increased, the standard deviation in MoS also increased, suggesting that the 15% faster actuator would be the most difficult to implement on a physical exoskeleton design [75].

The greater standard deviation observed as the actuator becomes faster could be a result of each subject's unique muscle activations and pose at the beginning of the simulations. Increased muscle activation of the hip abductor or adductor muscles would increase stiffness of the corresponding hip joint, making the subject less prone to falling due to the perturbation.

Alternatively, a smaller initial base of support would make the subject less resilient against perturbations, resulting in the subject being more likely to fall. As actuator delay increases, the model's MoS becomes closer to the unstable region, requiring greater assistive torque magnitudes to have similar improvements on the MoS.

4.5.2 Statistical Analysis

In this section, a statistical analysis on the results from Figure 4-18 is conducted. Paired-sample t-tests are used to compare the statistical significance of the MoS improvement experienced during the 5%, 10% and 15% faster actuator conditions, compared to the results obtained for the neutral activation time.

Table 4-18. Results of the paired-sample t-tests between MoS improvements for contralateral hip abduction assistance nominal activation time vs 5% faster actuator response time for the 15% BW perturbations. The P-value is reported, while statistically non-significant differences are denoted by the highlighted cells.

Nominal Activation Time (N·m/kg)	**5% Faster Actuators (N·m/kg)**				
	0.15	0.30	0.45	0.60	0.75
0.15	0.0028	1.81×10^{-4}	1.35×10^{-4}	1.20×10^{-4}	1.03×10^{-4}
0.30	3.38×10^{-5}	0.0037	2.61×10^{-4}	1.82×10^{-4}	1.39×10^{-4}
0.45	4.13×10^{-5}	4.18×10^{-5}	0.0033	3.63×10^{-4}	2.07×10^{-4}
0.60	6.72×10^{-5}	8.19×10^{-5}	5.15×10^{-4}	0.0022	3.17×10^{-4}
0.75	6.41×10^{-5}	7.68×10^{-5}	1.09×10^{-4}	5.69×10^{-4}	0.0012

Table 4-19. Results of the paired-sample t-tests between MoS improvements for contralateral hip abduction assistance nominal activation time vs 10% faster actuator response time for the 15% BW perturbations. The P-value is reported, while statistically non-significant differences are denoted by the highlighted cells.

Nominal Activation Time (N·m/kg)	**10% Faster Actuators (N·m/kg)**				
	0.15	0.30	0.45	0.60	0.75
0.15	0.0039	5.49×10^{-4}	2.57×10^{-4}	1.88×10^{-4}	1.54×10^{-4}
0.30	3.65×10^{-5}	0.0060	5.12×10^{-4}	2.78×10^{-4}	2.00×10^{-4}
0.45	3.16×10^{-4}	0.0024	0.0028	5.31×10^{-4}	2.92×10^{-4}
0.60	6.44×10^{-5}	2.37×10^{-4}	0.0321	0.0021	5.01×10^{-4}
0.75	6.46×10^{-5}	1.23×10^{-4}	4.49×10^{-4}	0.7011	0.0015

Table 4-20. Results of the paired-sample t-tests between MoS improvements for contralateral hip abduction assistance nominal activation time vs 15% faster actuator response time for the 15% BW perturbations. The P-value is reported, while statistically non-significant differences are denoted by the highlighted cells.

Nominal Activation Time (N·m/kg)	**15% Faster Actuators (N·m/kg)**				
	0.15	0.30	0.45	0.60	0.75
0.15	0.0109	9.22×10^{-4}	4.91×10^{-4}	3.16×10^{-4}	2.81×10^{-4}
0.30	7.41×10^{-4}	0.0055	9.56×10^{-4}	4.60×10^{-4}	3.70×10^{-4}
0.45	4.73×10^{-5}	0.0925	0.0035	8.29×10^{-4}	5.45×10^{-4}
0.60	6.60×10^{-5}	9.32×10^{-4}	0.2019	0.0023	9.34×10^{-4}
0.75	6.38×10^{-5}	2.43×10^{-4}	0.0073	0.0212	0.0021

The results from Table 4-20 show that there are no statistically significant differences between the mean MoS improvement when using the 0.30 N·m/kg – 15% faster actuator vs. the 0.45 N·m/kg – nominal actuator, the 0.45 N·m/kg – 15% faster actuator vs. the 0.60 N·m/kg nominal actuator, or the 0.60 N·m/kg – 15% faster actuator vs. the 0.75 N·m/kg nominal actuator.

The results presented in Chapter 4 also provide valuable information for exoskeleton designers who wish to select specific hardware for their applications. In contrast to exoskeletons that are being designed to reduce the metabolic cost of walking, the required torque for ML-stabilizing exoskeletons is directly related to the actuation response time. Similarly, exoskeletons that are designed to reduce metabolic cost rely on the timing of actuators for increased precision to apply assistive torques at the desired moment throughout locomotion. For the HAA assistive exoskeleton explored in this study, there is a clear trade-off between actuator response time and the torque required to provide a significant improvement in the MoS.

Due to the improvement in the MoS when using the 15% faster actuator, the results of this study suggest that predictive postural stabilization exoskeletons may be significantly more beneficial to prevent falls in the elderly as opposed to reactive stabilizing mechanisms. A study

conducted by Kanekar et al. found that impairments to anticipatory postural adjustments in the elderly led to an increased risk of falling [35]. The researchers suggested that the subject's reliance on weaker and slower muscles to implement compensatory postural adjustments were less effective at reducing falls than the corresponding muscles in younger individuals. In this way, adding predictive postural control strategies to a HAA exoskeleton could assist in positioning the CoM of the body in a more stable position prior to the onset of an imbalance. Future investigations should apply corrective postural adjustments prior to the onset of a perturbation and compare the resulting MoS with the results obtained using purely reactionary assistive torques as were investigated in the present study.

Chapter 5: Conclusions

In this chapter, the main contributions and the limitations of the study are discussed. The chapter will conclude by proposing potential future work that could be conducted from this research and future applications of this technology.

5.1 Study Contributions

Historically, WAEs have targeted sagittal-plane assistance strategies to reduce the metabolic cost of walking for a wide variety of patient populations, including the elderly [23], [61], [62], [66]. Hip exoskeletons specifically have offered a promising solution for assisting older adults. The current research first highlighted the potential benefits of a frontal-plane assistance strategy to improve stability and reduce the risk of falling in the elderly. An in-depth analysis of why elderly individuals experience an increased risk of falling and the changes to physiological parameters affecting stability was presented. The changes due to ageing that could be addressed through exoskeleton technology were also discussed in detail.

In this study, the OpenSim biomechanics software was used to investigate the relationship between assistive torque magnitude, assistive torque timing, and actuator placement of an assistive hip exoskeleton to improve stability. This thesis presents the predicted improvements to the MoS for each assistance strategy and concludes that HAA assistance can indeed improve the stability of elderly individuals when perturbed from a static standing position. The simulations also provide insight into the exoskeleton parameters that have the greatest impact on improving stability, such as actuator position, torque magnitude and torque timing. The results of this study suggest that, as the MoS of elderly subjects moves closer to the unstable region due to a perturbation magnitude

increasing, or as the CoM moves closer to the boundaries of the BoS, the more imperative it is to assist the contralateral limb to maintain stability. The advantages of providing bilateral assistive torque to the user's hip joints was discussed, while maintaining an emphasis on more assistance being applied to the contralateral limb (the weight-bearing limb) as balance is being challenged. The results suggest that as perturbation magnitude increases, larger standard deviations in the improvement in MoS are experienced for the contralateral and ipsilateral assistance strategies. As perturbation magnitude increases, the standard deviations associated with the bilateral HAA assistance strategy remain smaller than for the contralateral and ipsilateral strategies, suggesting that the bilateral strategy may be preferable for exoskeleton designers who wish to develop assistance strategies that apply to a range of activities that require stability assistance. The research also shows the potential benefits of a bilateral HAA assistance strategy for assisting elderly stability due to the lower actuator torque magnitudes that are needed to improve the MoS compared to the contralateral and ipsilateral assistance strategies, as lower exoskeleton torque is specifically desirable in the elderly population [51], [58], [59]. The conclusions arising from this study could impact designers' decisions in selecting hardware, software, and control strategies for this class of exoskeletons. Most existing research on assistive exoskeletons focuses on improvements to metabolic cost; more research on stability assistance is needed. This research has highlighted the advantages of frontal-plane stability assistance and should guide future investigations and exoskeleton designs.

This study highlights the importance of actuator timing and provides insight into the applied magnitude of assistance that would be needed to improve the MoS of elderly individuals when actuator response time is adjusted. The results also present the possibility of providing predictive postural adjustments to arrange the body's CoM in more stable positions before a falling

incident may occur. This may be an effective strategy to improve the stability of elderly individuals while providing modest assistive forces to the body; however, these strategies have not been explored in depth. Overall, the conclusions made throughout this thesis appear to be consistent, but further investigation is necessary. The results of this research suggest a large area of improvement and exploration into these types of exoskeletons that could provide many benefits to a growing elderly population.

5.2 Study Limitations

To investigate the effectiveness of the HAA assistive exoskeleton, several limitations arose due to the assumptions that were made in order to perform the simulations. The following section describes the study limitations in four categories: the musculoskeletal model, the HAA exoskeleton model, experimental data and the loading conditions.

5.2.1 The Musculoskeletal Model

To simulate human movement, the Gait2392 musculoskeletal model adopts simplified models of the bones and muscles in the lower extremities. The assumptions made to produce the Gait2392 model are widely accepted in the biomechanics community and have been validated in many studies [28], [71], [93].

The Gait2392 model was adjusted to reflect a generic "elderly" model that was used for all experimental subjects, regardless of each subject's particular physiology. Chapter 3 described the adjustments made to the musculoskeletal model, which are described by Thelen [79]. These adjustments were applied to the model regardless of the subject's age, BMI, sex, muscle strength and other properties. Each of these subject-specific parameters would ideally be used to calibrate the generic model for each individual, but the detailed calibration data that would be required were

not provided in the data set [78]. For this study, the adjustments made by Thelen were also validated for the muscles surrounding the ankle joint and were applied to each muscle in the lower limb [79]. To improve the calibration of the subject-specific models and accuracy of the simulations, these parameters should be validated further.

Biologically, humans control balance through a highly complex interaction between the CNS and the muscles in the body [32]. Depending on the loading conditions and the state of the body when a perturbation is applied, the CNS will implement different stabilizing strategies in addition to a HAA strategy. Flexion and extension of the knee and hip joints provides additional control over the CoM by creating a counter-moment to applied perturbations [81], [94], [95]. Moving the CoM closer to the ground has been shown to be an effective strategy for increasing stability, and muscles in the trunk can also be used to provide corrections to the CoM [32], [81]. To isolate the motion of the models to the frontal plane, the simulations performed in this study ignore the effects that sagittal-plane motion has on the CoM of the individual, and consequently, the whole-body movements implemented by the CNS to control ML stability. Furthermore, the center of pressure moves mediolaterally and anteroposteriorly when recovering from and responding to a perturbation [55]. Throughout the simulations generated in this study, the model for the BoS that was adopted does not account for ML or AP movement of the CoP. Therefore, modifying the current methodology and calculating the BoS at the position of the CoP could enhance the results of the study.

Furthermore, the models do not account for anticipatory muscle activations which humans can implement prior to a perturbation or in situations that could challenge one's balance [35]. It was assumed throughout the study that the muscle activations due to active contraction dynamics

remained unchanged from a static standing position; however it is known that anticipatory muscle activation could increase joint stiffness [35].

The foot–floor contact model used in the forward dynamics simulations represented a rubber-on-rubber model with a shoe sole thickness of 2 cm. The three contact spheres on the bottom of the foot detailed the parameters for the rubber-on-rubber model of the shoe sole thickness; however, modelling the geometry of typical footwear may provide a more accurate representation of the foot–floor interaction during day-to-day activities. More realistic foot–floor contact modelling may also provide results that are more comparable to what is commonly found in the literature, as most balance studies are performed while shod [28], [55], [81], [88], [96], [97]. However, introducing a model of a shoe may also introduce additional modelling uncertainties that could further degrade the results that were obtained throughout the study. The simulations are also dependent on the geometry, friction, dissipation, and stiffness parameters of the foot–floor contact model, as these define the amount of slip that would occur when assistance is applied by an assistive device. In addition, the interaction between the foot and the floor provides the model with the initial base of support, which has been shown to change a person's stability depending on the footwear being worn [98]. Providing and calibrating the model further with a more accurate foot–floor contact model may improve the accuracy of the obtained results. However, we note that the aim of this study was primarily to compare the effectiveness of various assistance and perturbation conditions rather than to predict MoS in an absolute sense. Comparisons among assistance strategies (e.g., which strategy leads to a greater increase in MoS) may be less affected by the modelling assumptions than the absolute MoS predictions.

5.2.2 The HAA Exoskeleton Model

The actuators that provide torque assistance to the hip joint of the model in the frontal plane were massless and able to produce torque instantaneously based on the input control signal that was applied. This represented an ideal scenario for comparing the effect of torques from each assistance strategy, as investigated in Chapter 4. For these actuators, the activation dynamics could also be investigated, rather than providing the actuators with a step function input; however, more accurate models of the electromechanical components of the actuator should be implemented to provide more realistic behaviour of the modelled exoskeleton.

The mass of a specific exoskeleton design would also affect the baseline MoS that was calculated in Chapter 4 for each subject. The inertia of the exoskeleton would change the position and velocity of the CoM after a perturbation, which would result in different calculations of the subject-specific MoS. Again, the trends in the results between each assistance strategy, magnitude and activation time were evaluated throughout the study, therefore design parameters such as exoskeleton mass would not add additional value to this study. However, researchers may wish to investigate how an exoskeleton prototype is predicted to affect the MoS of a subject and would likely include the mass specifications of their prototype. The practical difficulty of performing perturbation studies on elderly individuals and the lack of stabilizing hip exoskeletons on the market provide limited literature to compare the results generated in this study; thus, there remains uncertainty in the accuracy of the results obtained in this study.

5.2.3 Experimental Data

The data used to generate the static position kinematics and ground reaction forces were obtained from a public data set [78]. Some irregularities could have arisen during data collection or post-processing that were not reported by Dos Santos et al. and were therefore not accounted

for in the present study. Errors could arise due to marker placement and calibration of the measurement equipment, for example. Many other potential sources of error exist in typical data acquisition studies.

The data presented in the public database do not include muscle parameters such as maximum volumetric isometric contraction (MVIC), which could be used to calibrate the musculoskeletal model parameters for each subject [78]. Therefore, this study does not recognize the variability between individual muscle strength and relies on the adjustments previously described by Thelen [79]. The data do not include upper-extremity motion, which is known to greatly affect the stability of individuals when balance is being coordinated. The upper extremities should be included in future work involving longer-duration simulations or experiments for more complete analyses.

5.2.4 Loading Conditions

The loading conditions considered in this study were limited to perturbations applied at the pelvis in the positive Z-direction. Elderly subjects are constantly at risk of losing stability due to various disturbances. Surface translations, shoulder perturbations, eye tracking and uneven terrain are some of the most common factors causing instability that are noted in the literature [35], [55], [81], [88]. These perturbations should also be evaluated to provide more clarity on the effectiveness of HAA assistance on elderly stability due to perturbations at several locations on the body. Furthermore, applying the perturbation above or below the CoM changes how the body responds and may affect the ability of an exoskeleton assistance strategy to maintain balance.

5.3 Future Work

This research provides several suggestions to increase researchers' attention to exoskeleton designs that focus on frontal-plane assistance strategies for balance improvement. This is a relatively underexplored area of research and has many potential applications in addition to stability in elderly individuals. Individuals with amyotrophic lateral sclerosis (ALS) or those suffering from knee osteoarthritis (OA), among many other medical conditions, could benefit from this class of frontal-plane assistive exoskeleton. Assistive HAA torque from a hip exoskeleton should be further investigated to study their effectiveness for these specific patient populations.

The current study presents predictive simulations of assistance strategies that should be validated experimentally. Prototype devices should be validated through mechanical testing before assisting the human body. However, it is challenging to test balance-coordination strategies without exoskeleton assistance due to the risk of injuries occurring during fall tests. It is also challenging to experimentally investigate exoskeletons due to the complex interactions between the device and the human body particularly due to the variety of situations that could cause a loss of balance in the elderly and the variability of balance-correcting strategies that are implemented between subjects.

Future work should also be carried out to simulate the effect of different perturbation types and assistance strategies. As previously discussed, applying the perturbations at different locations on the model would be useful to explore how the effectiveness of exoskeleton assistance changes in different real-world scenarios. Biologically, ankle invertor/evertor, trunk and hip flexion/extension strategies are all used in coordination to control the state of the CoM and, effectively, the MoS of each individual. As a result, each of these joints provides a feasible location

for exoskeleton assistance to address the decline in balance control observed in the elderly population. These strategies should be investigated further to provide insight into which exoskeleton assistance strategy offers the most significant improvement to the MoS. For example, certain assistance strategies may be more or less effective depending on the joint to which assistance is applied and the location and magnitude of the perturbation. Larger subject sample sizes would also be beneficial to strengthen the statistical conclusions that can be drawn. In this study, four subjects were used due to the time constraints of the study; longer-term research projects could allow for the investigation of a larger number of subjects covering large ranges of heights, weights, strengths, and other pertinent parameters.

The current simulations investigate the effectiveness of electromechanical actuators with force-generating profiles modelled as step functions. To provide a more detailed investigation into different actuation methods, accurate models of specific actuators should be used. This could include defining actuator controllers that include specific electromechanical delays used for prototype designs. This approach would provide more precise representations of how physical actuators provide assistive forces to the body and allow for the evaluation of their effect on the subjects' MoS. In addition, different actuator types, such as passive, pneumatic, and hydraulic could be investigated by providing the simulations with detailed models of their control strategies and force-generating properties. Actuator mass should also be considered, as it is known to affect device performance for exoskeletons targeting metabolic cost and, similarly, will affect the MoS [58], [88]. Defining physical exoskeleton parameters would enable researchers to simulate prototype designs and calibrate parameters that would have the most significant effect on the MoS for different subjects.

A key limitation of the study was the assumption that active muscle contractions remained constant throughout the simulation. This assumption limited the duration of analysis that could be performed after the perturbation was applied to the body, presenting a short duration of how the elderly might respond to perturbations and assistive torques applied to the body. To conduct more in-depth analyses through simulations, reflex controllers should be designed to characterize how humans generate muscle forces in response to perturbations. The simulation framework could then be implemented using subject-specific responses to perturbations while providing exoskeleton assistance. The addition of a reflex controller could include the development of optimization algorithms to produce muscle excitations in response to perturbations. Modelling the CNS and the strategies humans use to coordinate balance recovery strategies is highly nontrivial; however, such models would enable researchers to perform longer analyses and evaluate more complex balance recovery and assistance strategies.

References

[1] Government of Canada, "Seniors and aging statistics," Feb. 08, 2019. https://www.statcan.gc.ca/eng/subjects-start/seniors_and_aging (accessed Nov. 18, 2020).

[2] P. Mahlknecht *et al.*, "Prevalence and burden of gait disorders in elderly men and women aged 60–97 years: A population-based study," *PLoS ONE*, vol. 8, no. 7, Jul. 2013, doi: 10.1371/journal.pone.0069627.

[3] M. Y. Osoba, A. K. Rao, S. K. Agrawal, and A. K. Lalwani, "Balance and gait in the elderly: A contemporary review," *Laryngoscope Investig. Otolaryngol.*, vol. 4, no. 1, pp. 143–153, 2019, doi: https://doi.org/10.1002/lio2.252.

[4] S. Gafner *et al.*, "Evaluation of hip abductor and adductor strength in the elderly: a reliability study," *Eur. Rev. Aging Phys. Act.*, vol. 14, Apr. 2017, doi: 10.1186/s11556-017-0174-6.

[5] F. Daun and A. Kibele, "Different strength declines in leg primary movers versus stabilizers across age—Implications for the risk of falls in older adults?," *PLoS ONE*, vol. 14, no. 3, Mar. 2019, doi: 10.1371/journal.pone.0213361.

[6] "Important Facts about Falls | Home and Recreational Safety | CDC Injury Center," Feb. 01, 2019. https://www.cdc.gov/homeandrecreationalsafety/falls/adultfalls.html (accessed Aug. 22, 2021).

[7] M. J. Hilliard *et al.*, "Lateral balance factors predict future falls in community-living older adults," *Arch. Phys. Med. Rehabil.*, vol. 89, no. 9, pp. 1708–1713, Sep. 2008, doi: 10.1016/j.apmr.2008.01.023.

[8] T. Ikeda *et al.*, "Effects of perioperative factors and hip geometry on hip abductor muscle strength during the first 6 months after anterolateral total hip arthroplasty," *J. Phys. Ther. Sci.*, vol. 29, no. 2, pp. 295–300, Feb. 2017, doi: 10.1589/jpts.29.295.

[9] M. W. Rogers and M.-L. Mille, "Lateral stability and falls in older people," *Exerc. Sport Sci. Rev.*, vol. 31, no. 4, pp. 182–187, Oct. 2003.

[10] N. Deshpande, E. J. Metter, F. Lauretani, S. Bandinelli, and L. Ferrucci, "Interpreting fear of falling in the elderly: What Do We Need to Consider?," *J. Geriatr. Phys. Ther. 2001*, vol. 32, no. 3, pp. 91–96, 2009.

[11] A. W. Smith and D. P. Wong, "Sagittal and frontal plane gait initiation kinetics in healthy, young subjects," *J. Hum. Kinet.*, vol. 67, pp. 85–100, Jul. 2019, doi: 10.2478/hukin-2018-0087.

[12] S. H. Collins, M. B. Wiggin, and G. S. Sawicki, "Reducing the energy cost of human walking using an unpowered exoskeleton," *Nature*, vol. 522, no. 7555, pp. 212–215, Jun. 2015, doi: 10.1038/nature14288.

[13] K. Junius, M. Degelaen, N. Lefeber, E. Swinnen, B. Vanderborght, and D. Lefeber, "Bilateral, misalignment-compensating, full-dof hip exoskeleton: design and kinematic validation," *Applied Bionics and Biomechanics*, 2017. https://www.hindawi.com/journals/abb/2017/5813154/ (accessed Nov. 26, 2019).

[14] S. Sawicki and P. Ferris, "Mechanics and energetics of incline walking with robotic ankle exoskeletons," *Co. Biol. 2009*, vol. 212, pp. 32–41, Oct. 2008, doi: doi:10.1242/jeb.017277.

[15] "Exoskeleton for stroke recovery gait training," *Ekso Bionics*. https://eksobionics.com/eksohealth/eksonr/patients/ (accessed Dec. 01, 2019).

[16] A.-M. De Cock *et al.*, "Gait characteristics under different walking conditions: Association with the presence of cognitive impairment in community-dwelling older people," *PLoS ONE*, vol. 12, no. 6, p. e0178566, Jun. 2017, doi: 10.1371/journal.pone.0178566.
[17] T. Al-Aama, "Falls in the elderly," *Can. Fam. Physician*, vol. 57, no. 7, pp. 771–776, Jul. 2011.
[18] L. Silva and N. Stergiou, "The basics of gait analysis," Chapter 7. https://reader.elsevier.com (accessed Mar. 14, 2021).
[19] T. K. Uchida and S. L. Delp, *Biomechanics of Movement: The Science of Sports, Robotics and Rehabilitation*, 1st ed. MIT Press, 2021.
[20] D. Purves *et al.*, "The regulation of muscle force," *Neurosci. 2nd Ed.*, 2001, Accessed: Feb. 26, 2022. [Online]. Available: http://www.ncbi.nlm.nih.gov/books/NBK11021/
[21] A. K. M. Lai, A. A. Biewener, and J. M. Wakeling, "Metabolic cost underlies task-dependent variations in motor unit recruitment," *J. R. Soc. Interface*, vol. 15, no. 148, p. 20180541, Nov. 2018, doi: 10.1098/rsif.2018.0541.
[22] E. Henneman, G. Somjen, and D. O. Carpenter, "Functional significance of cell size in spinal motoneurons," *J. Neurophysiol.*, vol. 28, no. 3, pp. 560–580, May 1965, doi: 10.1152/jn.1965.28.3.560.
[23] C. L. Dembia, A. Silder, T. K. Uchida, J. L. Hicks, and S. L. Delp, "Simulating ideal assistive devices to reduce the metabolic cost of walking with heavy loads," *PLoS ONE*, vol. 12, no. 7, Jul. 2017, doi: 10.1371/journal.pone.0180320.
[24] C. A. McGibbon, "Toward a better understanding of gait changes with age and disablement: neuromuscular adaptation," *Exerc. Sport Sci. Rev.*, vol. 31, no. 2, pp. 102–108, Apr. 2003.
[25] L. Tesio and V. Rota, "The motion of body center of mass during walking: A review oriented to clinical applications," *Front. Neurol.*, vol. 10, 2019, Accessed: Feb. 28, 2022. [Online]. Available: https://www.frontiersin.org/article/10.3389/fneur.2019.00999
[26] C. F. Ong, T. Geijtenbeek, J. L. Hicks, and S. L. Delp, "Predicting gait adaptations due to ankle plantarflexor muscle weakness and contracture using physics-based musculoskeletal simulations," *PLoS ONE Comput. Biol.*, vol. 15, no. 10, p. e1006993, Oct. 2019, doi: 10.1371/journal.pcbi.1006993.
[27] D. Kim and J.-M. Hwang, "The center of pressure and ankle muscle co-contraction in response to anterior-posterior perturbations," *PLoS ONE*, vol. 13, no. 11, p. e0207667, Nov. 2018, doi: 10.1371/journal.pone.0207667.
[28] M. S. DeMers, J. L. Hicks, and S. L. Delp, "Preparatory co-activation of the ankle muscles may prevent ankle inversion injuries," *J. Biomech.*, vol. 52, pp. 17–23, Feb. 2017, doi: 10.1016/j.jbiomech.2016.11.002.
[29] B. Ugurlu *et al.*, "Variable ankle stiffness improves balance control: experiments on a bipedal exoskeleton," *IEEE ASME Trans. Mechatron.*, vol. 21, no. 1, pp. 79–87, Feb. 2016, doi: 10.1109/TMECH.2015.2448932.
[30] J. F. Abulhasan and M. J. Grey, "Anatomy and physiology of knee stability," *J. Funct. Morphol. Kinesiol.*, vol. 2, no. 4, Art. no. 4, Dec. 2017, doi: 10.3390/jfmk2040034.
[31] L. Zhang *et al.*, "Knee joint biomechanics in physiological conditions and how pathologies can affect it: A systematic review," *Appl. Bionics Biomech.*, vol. 2020, p. e7451683, Apr. 2020, doi: 10.1155/2020/7451683.
[32] C. D. MacKinnon and D. A. Winter, "Control of whole body balance in the frontal plane during human walking," *J. Biomech.*, vol. 26, no. 6, pp. 633–644, Jun. 1993, doi: 10.1016/0021-9290(93)90027-c.

[33] D. A. Neumann, "Kinesiology of the hip: A focus on muscular actions," *J. Orthop. Sports Phys. Ther.*, vol. 40, no. 2, pp. 82–94, Feb. 2010, doi: 10.2519/jospt.2010.3025.
[34] L. E. Cofré Lizama, M. Pijnappels, G. H. Faber, P. N. Reeves, S. M. Verschueren, and J. H. van Dieën, "Age effects on mediolateral balance control," *PLoS ONE*, vol. 9, no. 10, p. e110757, Oct. 2014, doi: 10.1371/journal.pone.0110757.
[35] N. Kanekar and A. S. Aruin, "Aging and balance control in response to external perturbations: role of anticipatory and compensatory postural mechanisms," *Age*, vol. 36, no. 3, p. 9621, Jun. 2014, doi: 10.1007/s11357-014-9621-8.
[36] P. Morfis and M. Gkaraveli, "Effects of aging on biomechanical gait parameters in the healthy elderly and the risk of falling," Journal of Research and Practice on the Musculoskeletal System (2021), p. 6.
[37] S. Papegaaij, W. Taube, S. Baudry, E. Otten, and T. Hortobágyi, "Aging causes a reorganization of cortical and spinal control of posture," *Front. Aging Neurosci.*, vol. 6, 2014, Accessed: Mar. 12, 2022. [Online]. Available: https://www.frontiersin.org/article/10.3389/fnagi.2014.00028
[38] H. Reimann, T. Fettrow, D. Grenet, E. D. Thompson, and J. J. Jeka, "Phase-dependency of medial-lateral balance responses to sensory perturbations during walking," *Front. Sports Act. Living*, vol. 1, 2019, Accessed: Feb. 26, 2022. [Online]. Available: https://www.frontiersin.org/article/10.3389/fspor.2019.00025
[39] B. E. Maki, P. J. Holliday, and A. K. Topper, "A prospective study of postural balance and risk of falling in an ambulatory and independent elderly population," *J. Gerontol.*, vol. 49, no. 2, pp. M72-84, Mar. 1994, doi: 10.1093/geronj/49.2.m72.
[40] J. S. Brach and J. M. VanSwearingen, "Interventions to improve walking in older adults," *Curr. Transl. Geriatr. Exp. Gerontol. Rep.*, vol. 2, no. 4, p. 10.1007/s13670-013-0059–0, Dec. 2013, doi: 10.1007/s13670-013-0059-0.
[41] E. Fernando, M. Fraser, J. Hendriksen, C. H. Kim, and S. W. Muir-Hunter, "Risk factors associated with falls in older adults with dementia: A systematic review," *Physiother. Can.*, vol. 69, no. 2, pp. 161–170, 2017, doi: 10.3138/ptc.2016-14.
[42] R. R. Neptune and C. P. McGowan, "Muscle contributions to frontal plane angular momentum during walking," *J. Biomech.*, vol. 49, no. 13, pp. 2975–2981, Sep. 2016, doi: 10.1016/j.jbiomech.2016.07.016.
[43] F. Watson, P. C. Fino, M. Thornton, C. Heracleous, R. Loureiro, and J. J. H. Leong, "Use of the margin of stability to quantify stability in pathologic gait – a qualitative systematic review," *BMC Musculoskelet. Disord.*, vol. 22, no. 1, p. 597, Jun. 2021, doi: 10.1186/s12891-021-04466-4.
[44] J. H. van Dieën and M. Pijnappels, "Balance control in older adults," in *Locomotion and Posture in Older Adults: The Role of Aging and Movement Disorders*, F. A. Barbieri and R. Vitório, Eds. Cham: Springer International Publishing, 2017, pp. 237–262. doi: 10.1007/978-3-319-48980-3_16.
[45] T. Zhang, M. Tran, and H. Huang, "Design and experimental verification of hip exoskeleton with balance capacities for walking assistance," *IEEE ASME Trans. Mechatron.*, vol. 23, no. 1, pp. 274–285, Feb. 2018, doi: 10.1109/TMECH.2018.2790358.
[46] M. E. Johnson and M.-L. Mille, "Age-related changes in hip abductor and adductor joint torques," *Arch. Phys. Med. Rehabil*, vol. 85, Apr. 2004. 593-7. doi: 10.1016/j.apmr.2003.07.022. PMID: 15083435.

[47] A. A. Biewener, “Tendons and Ligaments: Structure, mechanical behavior and biological function,” in *Collagen: Structure and Mechanics*, P. Fratzl, Ed. Boston, MA: Springer US, 2008, pp. 269–284. doi: 10.1007/978-0-387-73906-9_10.
[48] T. K. Uchida, J. L. Hicks, C. L. Dembia, and S. L. Delp, “Stretching your energetic budget: how tendon compliance affects the metabolic cost of running,” *PLoS ONE*, vol. 11, no. 3, p. e0150378, Mar. 2016, doi: 10.1371/journal.pone.0150378.
[49] D. J. Rutherford and C. Hubley-Kozey, “Explaining the hip adduction moment variability during gait: Implications for hip abductor strengthening,” *Clin. Biomech.*, vol. 24, no. 3, pp. 267–273, Mar. 2009, doi: 10.1016/j.clinbiomech.2008.12.006.
[50] S. Morrison *et al.*, “Walking-induced fatigue leads to increased falls risk in older adults,” *J. Am. Med. Dir. Assoc.*, vol. 17, no. 5, pp. 402–409, May 2016, doi: 10.1016/j.jamda.2015.12.013.
[51] S. W. Renner *et al.*, “Higher fatigue prospectively increases the risk of falls in older men,” *Innov. Aging*, vol. 5, no. 1, Jan. 2021, doi: 10.1093/geroni/igaa061.
[52] S. Song and H. Geyer, “Predictive neuromechanical simulations indicate why walking performance declines with ageing,” *J. Physiol.*, vol. 596, no. 7, pp. 1199–1210, 2018, doi: 10.1113/JP275166.
[53] U. Granacher, I. Wolf, A. Wehrle, S. Bridenbaugh, and R. W. Kressig, “Effects of muscle fatigue on gait characteristics under single and dual-task conditions in young and older adults,” *J. NeuroEngineering Rehabil.*, vol. 7, p. 56, Nov. 2010, doi: 10.1186/1743-0003-7-56.
[54] A. L. Hof, M. G. J. Gazendam, and W. E. Sinke, “The condition for dynamic stability,” *J. Biomech.*, vol. 38, no. 1, pp. 1–8, Jan. 2005, doi: 10.1016/j.jbiomech.2004.03.025.
[55] Z. Matjačić, M. Zadravec, and A. Olenšek, “Biomechanics of in-stance balancing responses following outward-directed perturbation to the pelvis during very slow treadmill walking show complex and well-orchestrated reaction of central nervous system,” *Front. Bioeng. Biotechnol.*, vol. 8, 2020, Accessed: Jan. 25, 2022. [Online]. Available: https://www.frontiersin.org/article/10.3389/fbioe.2020.00884
[56] “The health benefits of walking for seniors,” *Companions For Seniors*, Apr. 03, 2019. https://companionsforseniors.com/2019/04/health-benefits-walking-seniors/ (accessed Mar. 18, 2021).
[57] L. I. E. Oddsson, P. Boissy, and I. Melzer, “How to improve gait and balance function in elderly individuals—compliance with principles of training,” *Eur. Rev. Aging Phys. Act.*, vol. 4, no. 1, Apr. 2007, doi: 10.1007/s11556-007-0019-9.
[58] R. C. Browning, J. R. Modica, R. Kram, and A. Goswami, “The effects of adding mass to the legs on the energetics and biomechanics of walking,” *Med. Sci. Sports Exerc.*, vol. 39, no. 3, p. 515, Mar. 2007, doi: 10.1249/mss.0b013e31802b3562.
[59] A. Kyvelidou, M. J. Kurz, J. L. Ehlers, and N. Stergiou, “Aging and partial body weight support affects gait variability,” *J. NeuroEngineering Rehabil.*, vol. 5, no. 1, p. 22, Sep. 2008, doi: 10.1186/1743-0003-5-22.
[60] C. Buesing *et al.*, “Effects of a wearable exoskeleton stride management assist system (SMA®) on spatiotemporal gait characteristics in individuals after stroke: a randomized controlled trial,” *J. NeuroEngineering Rehabil.*, vol. 12, no. 1, p. 69, Aug. 2015, doi: 10.1186/s12984-015-0062-0.
[61] K. Seo, J. Lee, and Y. J. Park, “Autonomous hip exoskeleton saves metabolic cost of walking uphill,” in *2017 International Conference on Rehabilitation Robotics (ICORR)*, Jul. 2017, pp. 246–251. doi: 10.1109/ICORR.2017.8009254.

[62] F. Giovacchini *et al.*, “A light-weight active orthosis for hip movement assistance,” *Robot. Auton. Syst.*, vol. 73, pp. 123–134, Nov. 2015, doi: 10.1016/j.robot.2014.08.015.
[63] R. Kitatani, K. Ohata, H. Takahashi, S. Shibuta, Y. Hashiguchi, and N. Yamakami, “Reduction in energy expenditure during walking using an automated stride assistance device in healthy young adults,” *Arch. Phys. Med. Rehabil.*, vol. 95, no. 11, pp. 2128–2133, Nov. 2014, doi: 10.1016/j.apmr.2014.07.008.
[64] H. Lee *et al.*, “A wearable hip assist robot can improve gait function and cardiopulmonary metabolic efficiency in elderly adults,” *IEEE Trans. Neural Syst. Rehabil. Eng.*, vol. 25, no. 9, pp. 1549–1557, Sep. 2017, doi: 10.1109/TNSRE.2017.2664801.
[65] E. Martini *et al.*, “Gait training using a robotic hip exoskeleton improves metabolic gait efficiency in the elderly,” *Sci. Rep.*, vol. 9, no. 1, May 2019, doi: 10.1038/s41598-019-43628-2.
[66] V. Monaco *et al.*, “An ecologically-controlled exoskeleton can improve balance recovery after slippage,” *Sci. Rep.*, vol. 7, no. 1, p. 46721, May 2017, doi: 10.1038/srep46721.
[67] Y. Zhang, M. Wang, J. Awrejcewicz, G. Fekete, F. Ren, and Y. Gu, “Using gold-standard gait analysis methods to assess experience effects on lower-limb mechanics during moderate high-heeled jogging and running,” *J. Vis. Exp. JoVE*, no. 127, Sep. 2017, doi: 10.3791/55714.
[68] E. P. Grabke, K. Masani, and J. Andrysek, “Lower limb assistive device design optimization using musculoskeletal modeling: a review,” *J. Med. Devices*, vol. 13, no. 040801, Oct. 2019, doi: 10.1115/1.4044739.
[69] L. Zhang, Y. Liu, R. Wang, C. Smith, and E. M. Gutierrez-Farewik, “Modeling and simulation of a human knee exoskeleton’s assistive strategies and interaction,” *Front. Neurorobotics*, vol. 15, 2021, doi: 10.3389/fnbot.2021.620928.
[70] S. L. Delp *et al.*, “OpenSim: open-source software to create and analyze dynamic simulations of movement,” *IEEE Trans. Biomed. Eng.*, vol. 54, no. 11, pp. 1940–1950, Nov. 2007, doi: 10.1109/TBME.2007.901024.
[71] A. Seth *et al.*, “OpenSim: Simulating musculoskeletal dynamics and neuromuscular control to study human and animal movement,” *PLOS Comput. Biol.*, vol. 14, no. 7, p. e1006223, Jul. 2018, doi: 10.1371/journal.pcbi.1006223.
[72] “C-Motion Inc.” https://www.c-motion.com/#visual3d (accessed Mar. 22, 2021).
[73] “AssistiveDevices.” https://www.anybodytech.com/industries/assistive-devices/ (accessed Mar. 22, 2021).
[74] T. Khanna, M. Doumit, and T. K. Uchida, “Modelling and simulation of ideal and torque-limited devices to assist elderly walking,” MASc. Thesis, Department of Mechanical Engineering, University of Ottawa, 2021. [Online]. Available: http://dx.doi.org/10.20381/ruor-26261
[75] T. K. Uchida, A. Seth, S. Pouya, C. L. Dembia, J. L. Hicks, and S. L. Delp, “Simulating ideal assistive devices to reduce the metabolic cost of running,” *PLoS ONE*, vol. 11, no. 9, p. e0163417, Sep. 2016, doi: 10.1371/journal.pone.0163417.
[76] S. L. Delp, J. P. Loan, M. G. Hoy, F. E. Zajac, E. L. Topp, and J. M. Rosen, “An interactive graphics-based model of the lower extremity to study orthopaedic surgical procedures,” *IEEE Trans. Biomed. Eng.*, vol. 37, no. 8, pp. 757–767, Aug. 1990, doi: 10.1109/10.102791.
[77] F. C. Anderson and M. G. Pandy, “Dynamic optimization of human walking,” *J. Biomech. Eng.*, vol. 123, no. 5, pp. 381–390, May 2001, doi: 10.1115/1.1392310.

[78] D. A. dos Santos, C. A. Fukuchi, R. K. Fukuchi, and M. Duarte, “A data set with kinematic and ground reaction forces of human balance,” *PeerJ*, Jul. 2017, doi: https://doi.org/10.7717/peerj.3626.
[79] D. G. Thelen, “Adjustment of muscle mechanics model parameters to simulate dynamic contractions in older adults,” *J. Biomech. Eng.*, vol. 125, no. 1, pp. 70–77, Feb. 2003, doi: 10.1115/1.1531112.
[80] J. L. Hicks, T. K. Uchida, A. Seth, A. Rajagopal, and S. L. Delp, “Is my model good enough? best practices for verification and validation of musculoskeletal models and simulations of movement,” *J. Biomech. Eng.*, vol. 137, no. 2, pp. 0209051–02090524, Feb. 2015, doi: 10.1115/1.4029304.
[81] S. Rietdyk, A. E. Patla, D. A. Winter, M. G. Ishac, and C. E. Little, “Balance recovery from medio-lateral perturbations of the upper body during standing,” *J. Biomech.*, vol. 32, no. 11, pp. 1149–1158, Nov. 1999, doi: 10.1016/S0021-9290(99)00116-5.
[82] F. De Groote, J. L. Allen, and L. H. Ting, “Contribution of muscle short-range stiffness to initial changes in joint kinetics and kinematics during perturbations to standing balance: A simulation study,” *J. Biomech.*, vol. 55, pp. 71–77, Apr. 2017, doi: 10.1016/j.jbiomech.2017.02.008.
[83] H. Begovic, G.-Q. Zhou, and T. Li, “Detection of the electromechanical delay and its components during voluntary isometric contraction of the quadriceps femoris muscle,” Dec. 2014, [Online]. Available: https://www-frontiersin-org.proxy.bib.uottawa.ca/articles/10.3389/fphys.2014.00494/full
[84] S. Sivakumaran, A. Schinkel-Ivy, K. Masani, and A. Mansfield, “Relationship between margin of stability and deviations in spatiotemporal gait features in healthy young adults,” *Hum. Mov. Sci.*, vol. 57, pp. 366–373, Feb. 2018, doi: 10.1016/j.humov.2017.09.014.
[85] M. Ding, M. Nagashima, S.-G. Cho, J. Takamatsu, and T. Ogasawara, “Control of walking assist exoskeleton with time-delay based on the prediction of plantar force,” *IEEE Access*, Jul. 2020, doi: 10.1109/ACCESS.2020.3010644.
[86] O. Addison, M. Inacio, W.-N. Bair, B. A. Beamer, A. S. Ryan, and M. W. Rogers, “Role of hip abductor muscle composition and torque in protective stepping for lateral balance recovery in older adults,” *Arch. Phys. Med. Rehabil.*, vol. 98, no. 6, pp. 1223–1228, Jun. 2017, doi: 10.1016/j.apmr.2016.10.009.
[87] T. Dahiru, “P – value, a true test of statistical significance? A cautionary Note” *Ann. Ib. Postgrad. Med.*, vol. 6, no. 1, pp. 21–26, Jun. 2008.
[88] Z. Matjačić, M. Zadravec, and A. Olenšek, “An effective balancing response to lateral perturbations at pelvis level during slow walking requires control in all three planes of motion,” *J. Biomech.*, vol. 60, pp. 79–90, Jul. 2017, doi: 10.1016/j.jbiomech.2017.06.020.
[89] “NREL-Exo: A 4-DoFs wearable hip exoskeleton for walking and balance assistance in locomotion.” http://ieeexplore.ieee.org/document/8202201 (accessed Feb. 04, 2021).
[90] A. D. Woolf and K. Åkesson, “Preventing fractures in elderly people,” *BMJ*, vol. 327, no. 7406, pp. 89–95, Jul. 2003.
[91] E. Volpi, R. Nazemi, and S. Fujita, “Muscle tissue changes with aging,” *Curr. Opin. Clin. Nutr. Metab. Care*, vol. 7, no. 4, pp. 405–410, Jul. 2004.
[92] A. F. Pérez Vidal *et al.*, “Soft exoskeletons: development, requirements, and challenges of the last decade,” *Actuators*, vol. 10, no. 7, Art. no. 7, Jul. 2021, doi: 10.3390/act10070166.

[93] C. L. Dembia, N. A. Bianco, A. Falisse, J. L. Hicks, and S. L. Delp, “OpenSim Moco: musculoskeletal optimal control,” *PLoS ONE Comput. Biol.*, vol. 16, no. 12, p. e1008493, Dec. 2020, doi: 10.1371/journal.pcbi.1008493.
[94] R. T.-L. Zhu, P.-Z. Lyu, S. Li, C. Y. Tong, Y. T. Ling, and C. Z.-H. Ma, “How does lower limb respond to unexpected balance perturbations? New insights from synchronized human kinetics, kinematics, muscle electromyography (EMG) and mechanomyography (MMG) data,” *Biosensors*, vol. 12, no. 6, p. 430, Jun. 2022, doi: 10.3390/bios12060430.
[95] S. Batcir, G. Shani, A. Shapiro, and I. Melzer, “Characteristics of step responses following varying magnitudes of unexpected lateral perturbations during standing among older people – a cross-sectional laboratory-based study,” *BMC Geriatr.*, vol. 22, no. 1, Dec. 2022, doi: 10.1186/s12877-022-03080-w.
[96] Z. Matjačić, M. Voigt, D. Popović, and T. Sinkjær, “Functional postural responses after perturbations in multiple directions in a standing man: a principle of decoupled control,” *J. Biomech.*, vol. 34, no. 2, pp. 187–196, Feb. 2001, doi: 10.1016/S0021-9290(00)00182-2.
[97] M. Y. Osoba, A. K. Rao, S. K. Agrawal, and A. K. Lalwani, “Balance and gait in the elderly: A contemporary review,” *Laryngoscope Investig. Otolaryngol.*, vol. 4, no. 1, pp. 143–153, Feb. 2019, doi: 10.1002/lio2.252.
[98] N. Amiez *et al.*, “Effects of balance shoes on balance and postural stability in the elderly: A crossover, controlled, randomized single-blind study,” *Healthcare*, vol. 9, no. 2, p. 179, Feb. 2021, doi: 10.3390/healthcare9020179.

Appendix A

Table A-1 outlines the model parameters that were added to the primary elderly model for the forward dynamics simulations to create the secondary elderly model.

Table A-1.Model components for the secondary elderly model used in the forward dynamics simulations.

Component	Parameters	Value
Contact Half Space	Provide the simulation with a platform ground object that can interact with contact geometry on the model.	N/A
Contact Geometry	Heel radius	2 cm
	1st metatarsal head radius	2 cm
	5th metatarsal head radius	2 cm
Hunt–Crossley Force parameters	Transition Velocity (m/s)	0.2
	Stiffness (MPa/m)	50
	Dissipation (s/m)	5
	Coefficient of Static Friction	0.9
	Coefficient of Dynamics Friction	0.9
	Coefficient of Viscous Friction	0.6
Torque Actuators	Used to apply various magnitudes of assistive hip abduction/adduction torque from the exoskeleton device.	0.15 N·m/kg
		0.30 N·m/kg
		0.45 N·m/kg
		0.60 N·m/kg
		0.75 N·m/kg
Controllers	Defines the force-generating ability and activation of the Torque Actuators in the model.	Step function
Disturbance (Perturbation) Force	A force applied laterally at the pelvis to simulate a perturbation applied to the model. Various magnitudes of disturbance are characterized and applied at the pelvis.	5%, 10% and 15% Body Weight

Figures A-1, A-2 and A-3, describe the model-settling simulation from simulation set A.

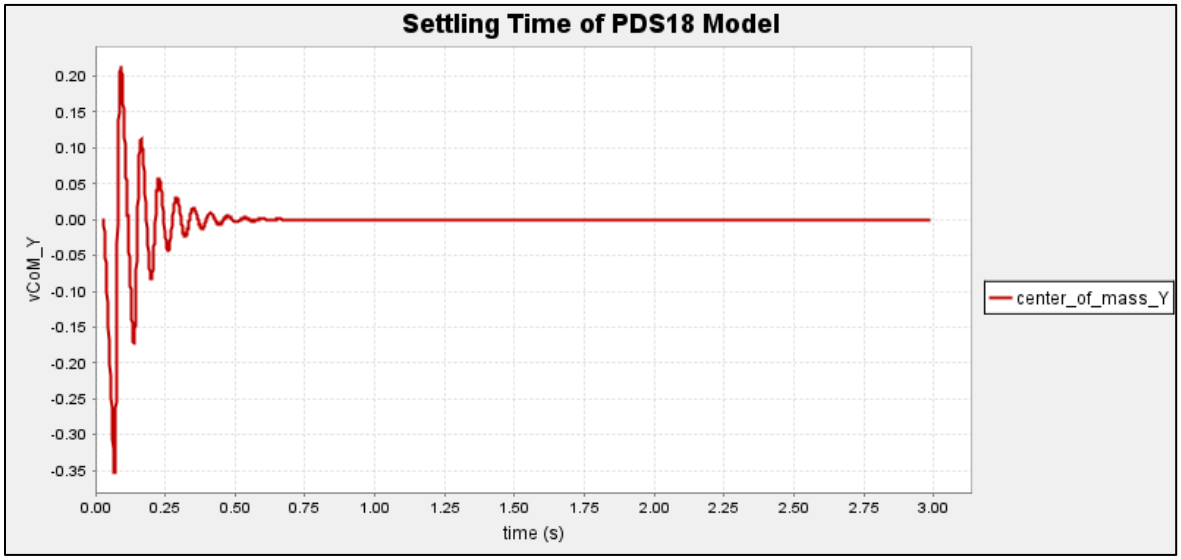

Figure A-1. Determination of the settling time for the forward dynamics simulations of the PDS18 subject.

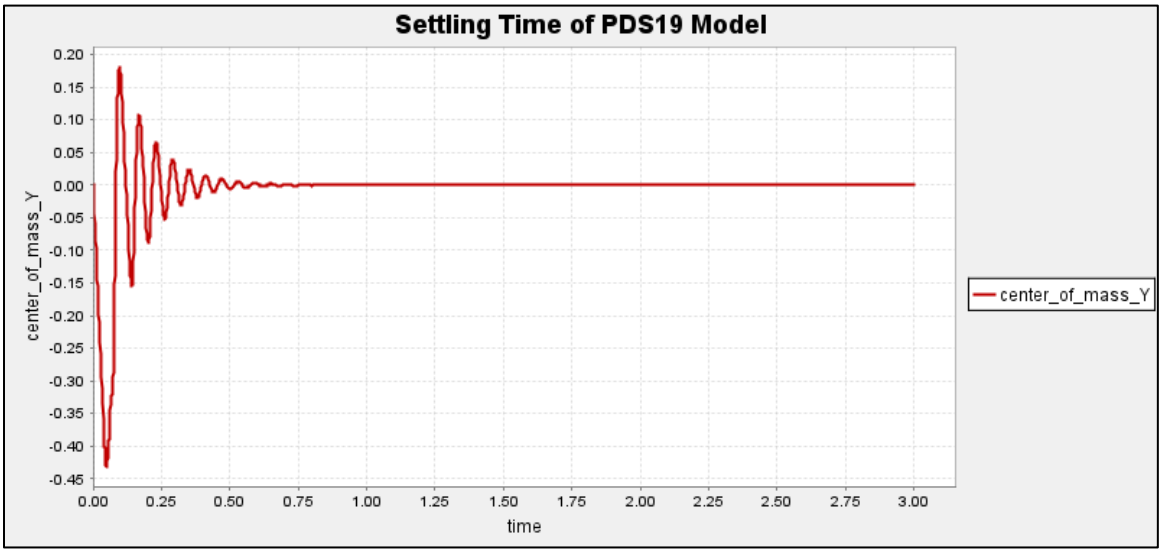

Figure A-2. Determination of the settling time for the forward dynamics simulations of the PDS19 subject.

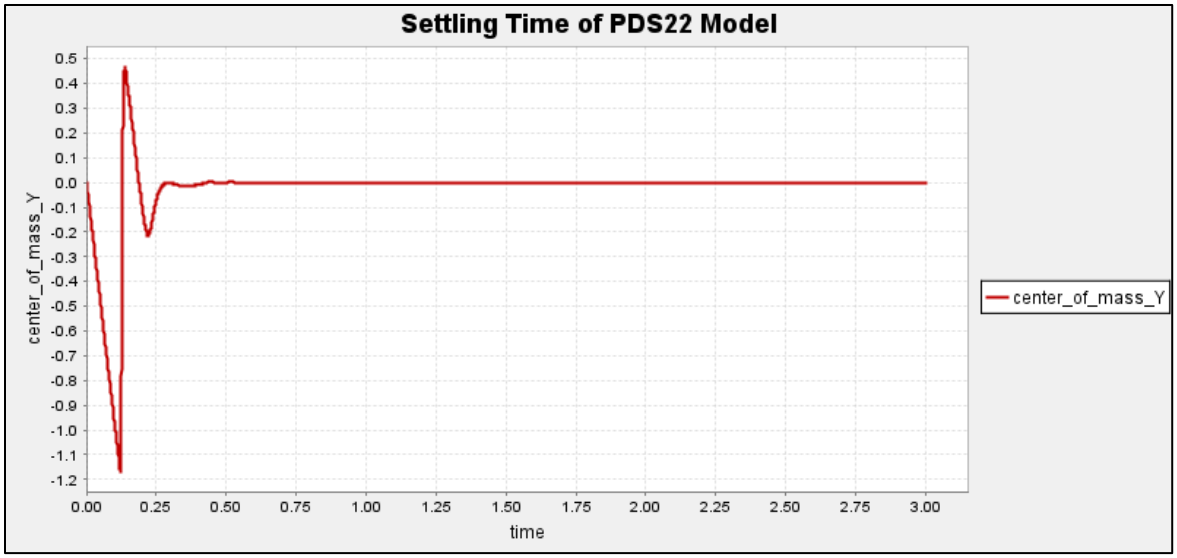

Figure A-3. Determination of the settling time for the forward dynamics simulations of the PDS22 subject.

Figures A-4, A-5 and A-6 show examples of the lateral perturbation force profiles for the PDS13 subject that were applied to the pelvis body of the model throughout simulation sets B and C of the forward dynamics simulations.

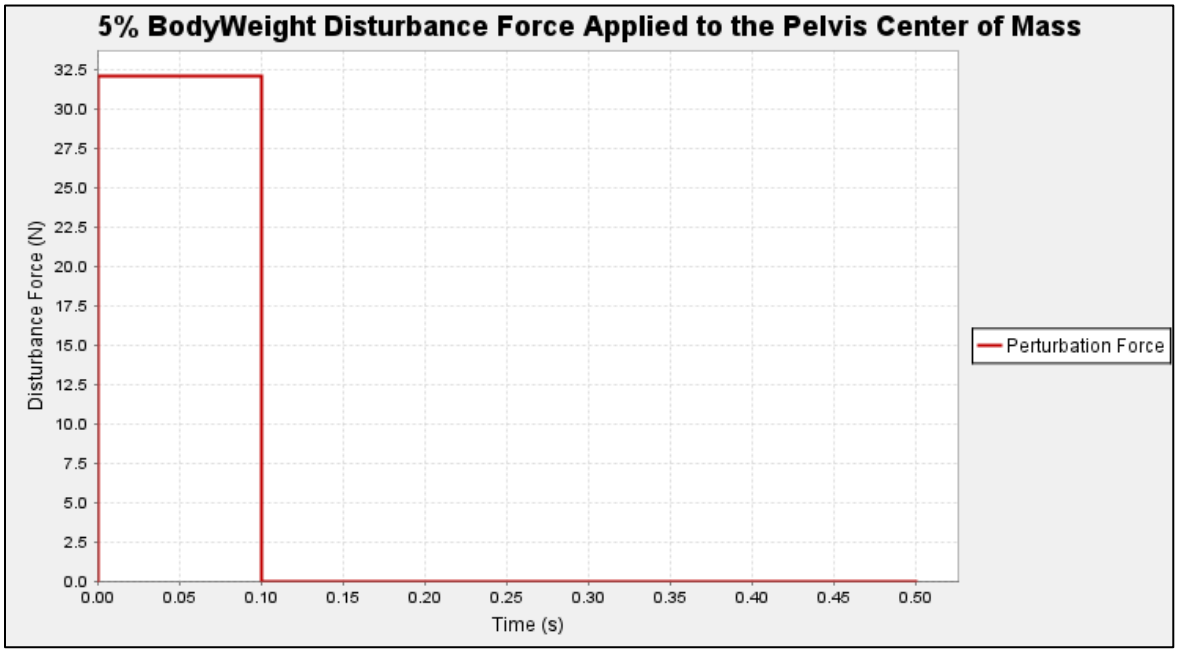

Figure A-4. The 5% body weight lateral perturbation applied to the pelvis for the PDS13 subject

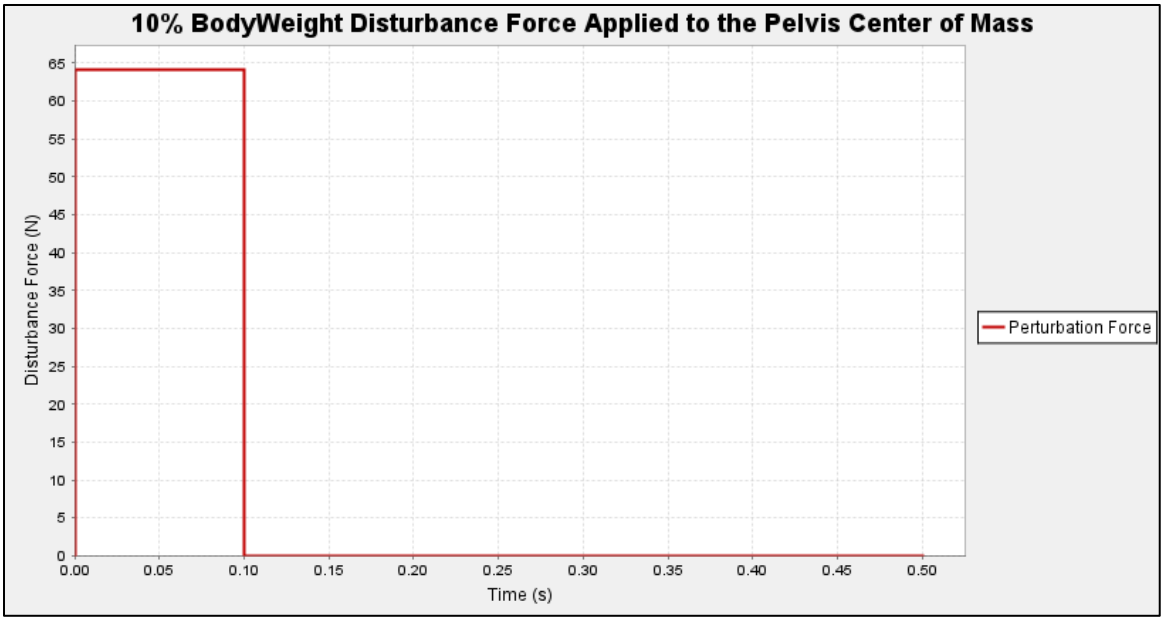

Figure A-5. The 10% body weight lateral perturbation applied to the pelvis for the PDS13 subject

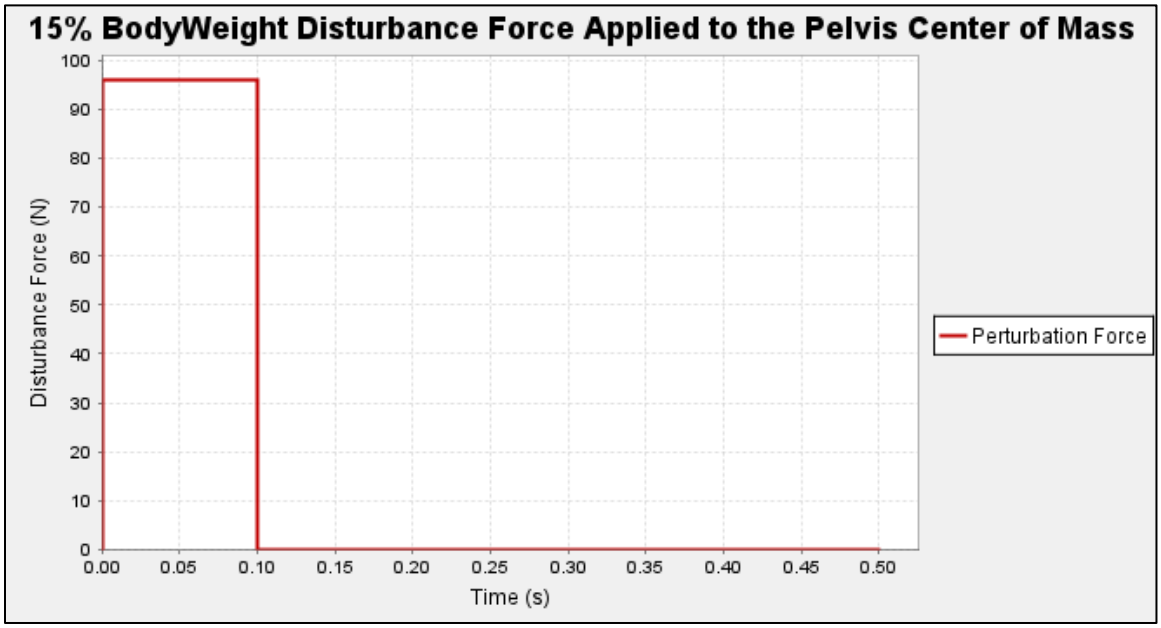

Figure A-6. The 15% body weight lateral perturbation applied to the pelvis for the PDS13 subject

The applied perturbations and torque tables for each subject during the simulations in set C.1 are described in Tables A-2, A-3 and A-4.

Table A-2. Conditions for the contralateral hip abduction assistance, ipsilateral hip adduction and bilateral simulations for subject PDS18 (C.1).

Subject	Lateral Perturbation Magnitude (% BW)	Lateral Perturbation Magnitude (N)	Contralateral Assistance Magnitude (N·m)	Ipsilateral Assistance Magnitude (N·m)	Bilateral Assistance Magnitude (N·m per hip)	Assistance Activation Time (s)
PDS18	5	34.58	10.58	10.58	5.29	0.124
			21.17	21.17	10.59	
			31.75	31.75	15.88	
			42.33	42.33	21.17	
			52.91	52.91	26.46	
	10	69.21	10.58	10.58	5.29	0.124
			21.17	21.17	10.59	
			31.75	31.75	15.88	
			42.33	42.33	21.17	
			52.91	52.91	26.46	
	15	103.74	10.58	10.58	5.29	0.124
			21.17	21.17	10.59	
			31.75	31.75	15.88	
			42.33	42.33	21.17	
			52.91	52.91	26.46	

Table A-3. Conditions for the contralateral hip abduction assistance, ipsilateral hip adduction assistance and bilateral assistance simulations for subject PDS19 (C.1).

Subject	Lateral Perturbation Magnitude (% BW)	Lateral Perturbation Magnitude (N)	Contralateral Assistance Magnitude (N·m)	Ipsilateral Assistance Magnitude (N·m)	Bilateral Assistance Magnitude (N·m per hip)	Assistance Activation Time (s)
PDS19	5	35.44	10.84	10.84	5.43	0.124
			21.68	21.68	10.84	
			32.51	32.51	16.23	
			43.35	43.35	21.68	
			54.19	54.19	27.10	
	10	70.88	10.84	10.84	5.43	0.124
			21.68	21.68	10.84	
			32.51	32.51	16.23	
			43.35	43.35	21.68	
			54.19	54.19	27.10	
	15	106.32	10.84	10.84	5.43	0.124
			21.68	21.68	10.84	
			32.51	32.51	16.23	
			43.35	43.35	21.68	
			54.19	54.19	27.10	

Table A-4. Conditions for the contralateral hip abduction assistance, ipsilateral hip adduction and bilateral simulations for subject PDS22 (C.1).

Subject	Lateral Perturbation Magnitude (% BW)	Lateral Perturbation Magnitude (N)	Contralateral Assistance Magnitude (N·m)	Ipsilateral Assistance Magnitude (N·m)	Bilateral Assistance Magnitude (N·m per hip)	Assistance Activation Time (s)
PDS22	5	34.58	10.58	10.58	5.29	0.124
			21.15	21.15	10.58	
			31.73	31.73	15.87	
			42.3	42.3	21.15	
			52.88	52.88	26.44	
	10	69.16	10.58	10.58	5.29	0.124
			21.15	21.15	10.58	
			31.73	31.73	15.87	
			42.3	42.3	21.15	
			52.88	52.88	26.44	
	15	103.74	10.58	10.58	5.29	0.124
			21.15	21.15	10.58	
			31.73	31.73	15.87	
			42.3	42.3	21.15	
			52.88	52.88	26.44	

Appendix B

In this section, the results that were omitted in chapter 4 will be presented, including all actuator torque magnitudes. Figure B-1, Figure B-2 and Figure B-3 show the results of the 5%, 10% and 15% BW perturbation conditions, respectively, with HAA assistance.

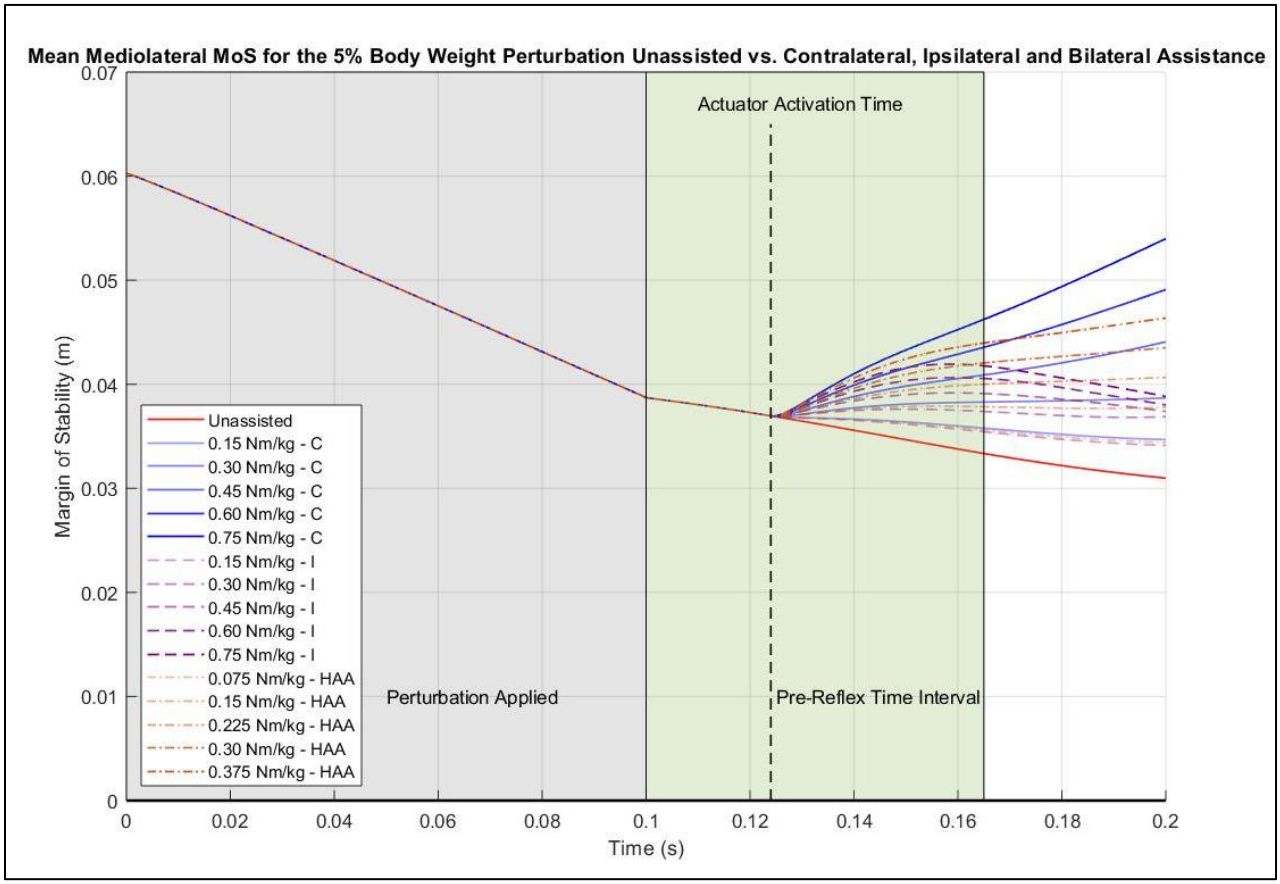

Figure B-1. Mean ML MoS for the 5% BW perturbation condition showing the unassisted condition and the contralateral, ipsilateral and bilateral assistance strategies. Unassisted (red line); contralateral hip abduction assistance (blue solid lines, "C"); ipsilateral hip adduction assistance strategy (purple dashed lines, "I"); bilateral HAA assistance strategy (orange dash-dotted lines, "HAA"). The grey area indicates the time during which the lateral perturbation was applied to the model. The green area indicates the time during which muscle reflexes would not have a substantial effect on the model's motion. The vertical dashed line represents the time at which the exoskeleton begins applying assistive torques.

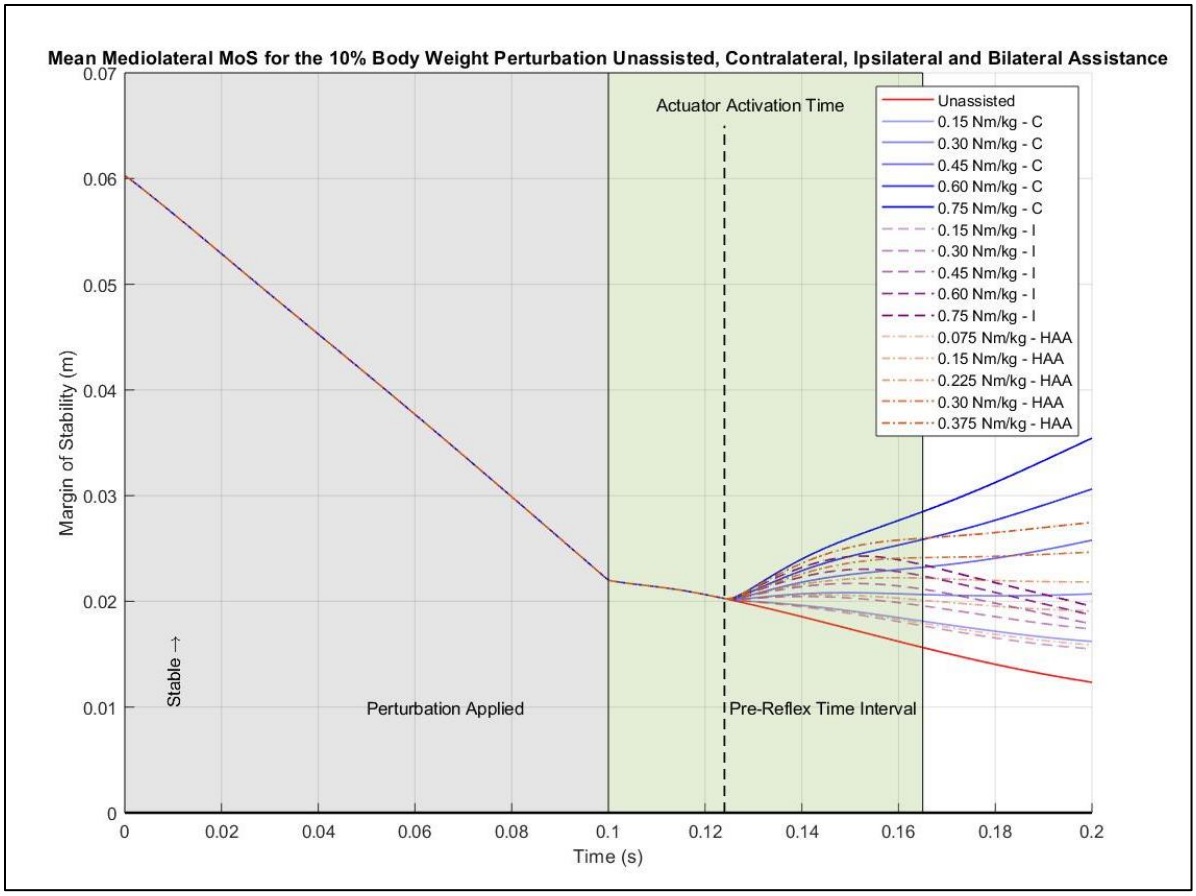

Figure B-2. Mean ML MoS for the 10% BW perturbation condition showing the unassisted condition and the contralateral, ipsilateral and bilateral assistance strategies. Unassisted (red line); contralateral hip abduction assistance (blue solid lines, "C"); ipsilateral hip adduction assistance strategy (purple dashed lines, "I"); bilateral HAA assistance strategy (orange dash-dotted lines, "HAA"). The grey area indicates the time during which the lateral perturbation was applied to the model. The green area indicates the time during which muscle reflexes would not have a substantial effect on the model's motion. The vertical dashed line represents the time at which the exoskeleton begins applying assistive torques.

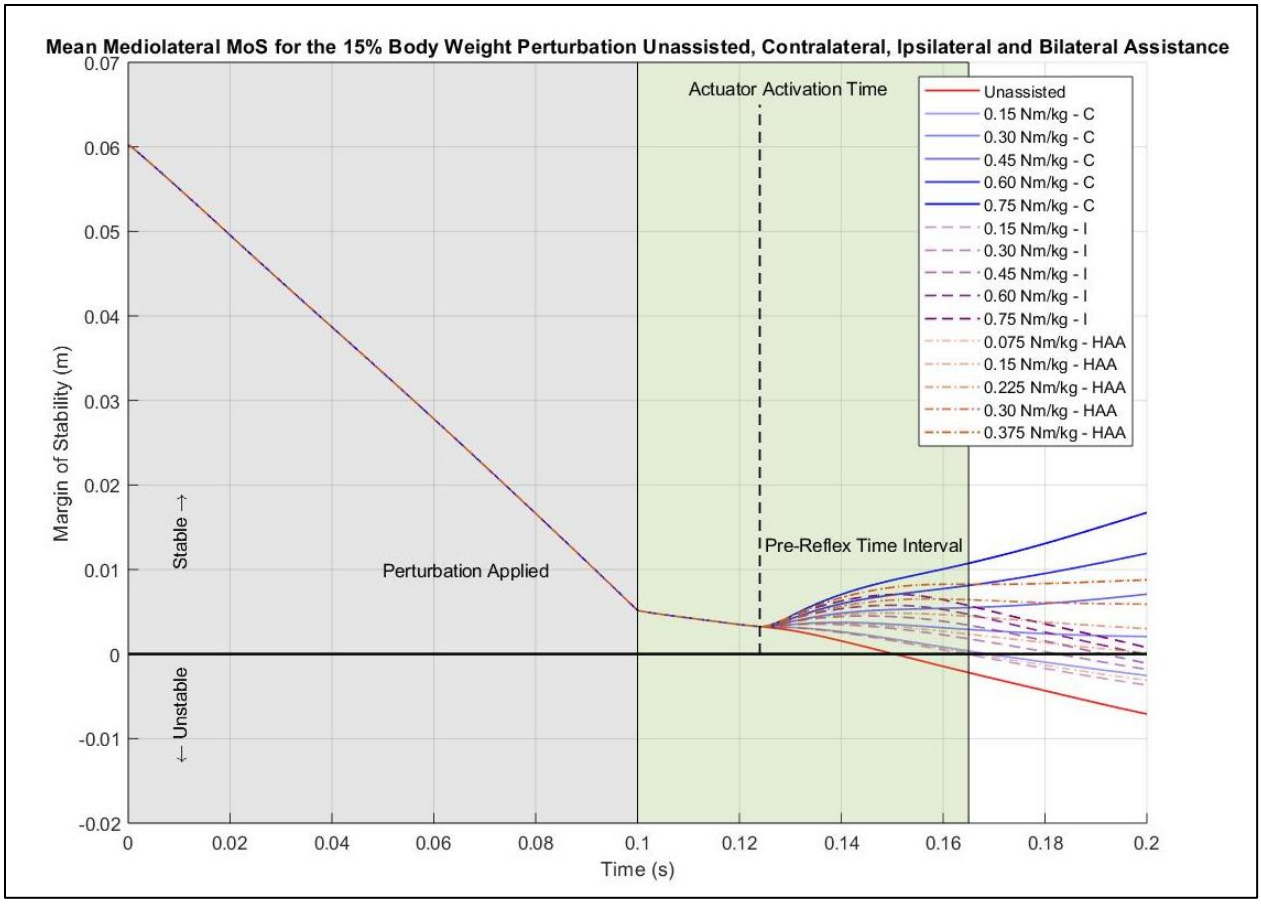

Figure B-3. Mean ML MoS for the 15% BW perturbation condition showing the unassisted condition and the contralateral, ipsilateral and bilateral assistance strategies. Unassisted (red line); contralateral hip abduction assistance (blue solid lines, "C"); ipsilateral hip adduction assistance strategy (purple dashed lines, "I"); bilateral HAA assistance strategy (orange dash-dotted lines, "HAA"). The grey area indicates the time during which the lateral perturbation was applied to the model. The green area indicates the time during which muscle reflexes would not have a substantial effect on the model's motion. The vertical dashed line represents the time at which the exoskeleton begins applying assistive torques.